PhD degree in Systems Medicine

(curriculum in Molecular Oncology)
European School of Molecular Medicine (SEMM),

University of Milan and University of Naples "Federico II"

Settore disciplinare: MED/4

Tumor suppressor activity of the Polycomb Group Ring Finger protein Pcgf6 in Myc-induced lymphomagenesis

Nina Tanaskovic

IEO, Milan

Matricola n. R11472

Supervisor: Dr. Bruno Amati,

European Institute of Oncology (IEO), Milan

Added Supervisor: Dr. Andrea Bisso,

European Institute of Oncology (IEO), Milan

Anno accademico 2018-2019

TABLE OF CONTENTS

1 . List of Abbreviations 4

2 . FIGURE INDEX 7

3 . LIST OF TABLES 8

4 . ABSTRACT 9

5 . INTRODUCTION 11

5 . 1 Myc 11

5 . 1 . 1 Myc protein family 11

5 . 1 . 2 Biological functions of Myc 12

5 . 1 . 3 Structure of Myc protein 16

5 . 1 . 4 Regulation of Myc expression and activity 19

5 . 1 . 5 Myc as a transcription factor 21

5 . 1 . 6 Selective transcription model versus general transcriptional amplification model 24

5 . 1 . 7 Myc as an oncogene 26

5 . 1 . 8 Myc in B-cell development 28

5 . 1 . 9 *Eμ-myc* and other Myc-driven mouse models of B-cell lymphomas 31

5 . 1 . 1 0 The Max and MXD network 33

5 . 2 Polycomb group proteins 37

5 . 2 . 1 Canonical and non-canonical PRC1 complex 41

5 . 2 . 2 Polycomb Repressive Complex in hematopoiesis and B-cell-lymphomagenesis 44

5 . 2 . 3 Polycomb Repressive Complex 1.6 46

5 . 2 . 4 Polycomb Group Ring Finger Protein 6 48

5 . 3 Aim of the project 51

6 . MATERIALS AND METHODS 52

6.1 Mice 52

6.2 *In vivo* transplantation of lymphomas 53

6.3 *Ex vivo* single-cell suspension isolation 53

6.4 Cell lines 53

6.5 Growth curve and cell viability assay 54

6.6 Western Blot 55

6.7 Antibodies 56

6.8 Cloning of shRNAs 56

6.9 Genomic DNA extraction and recombination control 57

6.10 Isolation of mouse B-cells 57

6.11 Flow cytometric analysis 58

6.12 RNA extraction and gene expression analysis 59

6.13 Chromatin Immunoprecipitation 59

6.14 List of primers used 61

6.15 Computational analysis 62

6.15.1 ChIP-seq data analysis 62

6.15.2 RNA-seq analysis 63

6.16 Statistical analysis. 64

7. RESULTS 65

7.1 Pcgf6 loss accelerates Myc-induced lymphomagenesis 65

7.2 Pcgf6 is not required for B-cell development 70

7.3 Pcgf6 is not required for Myc binding to chromatin 74

7.4 Silencing of Pcgf6 in *Eμ-myc* lymphomas does not alter Myc binding 79

7.5 Loss of Mga does not impair Myc-induced lymphomagenesis 84

7.6 Loss of Mga dissociates Pcgf6 but not Myc from chromatin 86

7.7 Loss of Pcgf6 does not affect Myc-dependent transcription 90

7.8 Analysis of cellular infiltrates in lymphomas 100

8. DISCUSSION 105

9. REFERENCE 113

1 . List of Abbreviations

Aa = amino acid

AML = Acute Myelocytic leukemia

APC = Antigen presenting cells

bHLH-LZ = basic helix-loop-helix leucine zipper

BM = bone marrow

Cbx = Chromobox

ChIP-seq = Chromatin Immunoprecipitation coupled with high throughput sequencing

CLL = Chronic Lymphocytic Leukemia

CLPs = Common lymphoid progenitors

Cont = control

cPRC1 = canonical Polycomb Repressive Complex 1

DC = dendritic cells

DEG = differentially expressed genes

DLBCL = Diffuse large B-cell lymphoma

DNA = deoxyribonucleic acid

Dpc = days post coitus

E-box = Enhancer box

FC = fold change

FL = Follicular lymphoma

FO = Follicular Zone B-cells

GC = germinal center

GO = Gene Ontology

GSEA = Gene Set Enrichment Analysis

HSCs = hematopoietic stem cells

KD = knock down

KO = knock out

Ly = lymphoma

MB = Myc box

MEFs = mouse embryonic fibroblasts

mESCs = mouse embryonic stem cells

MZ = Marginal Zone B-cells

ncPRC1 = non-canonical Polycomb Repressive Complex 1

NK = natural killer

NKT = natural killer T-cells

P6 = Pcgf6

PC = Pheochromocytoma

PcG = Polycom group of proteins

Pcgf = Polycomb Group Ring Finger Protein

PRC = Polycomb Repressive Complex

PRC2 = Polycomb Repressive Complex 2

preT = pre-tumoral

rDNA = ribosomal DNA

Ren = *Renilla Luciferase*

Ring = Really Interesting New Gene

RNA = ribonucleic acid

RPKM = reads per kilo base per million mapped reads

rRNA = ribosomal RNA

Rybp = RING1 and YY1-binding protein

SCLC = Small Cell Lung Cancer

sh = short hairpin

T = tumor

T1 = Transitional Type 1 B-cells

T2 = Transitional Type 2 B-cells

T3 = Transitional Type 3 B-cells

TAD = transactivation domain

UTR = untranslated region

VDJ recombination = Variable, diversity, and joining recombination

WT = wild type

2. FIGURE INDEX

Figure 5.1 Examples of Myc-dependent genes and cellular processes (Kress et al., 2015). 13

Figure 5.2 Structure of Myc protein family. 16

Figure 5.3 Schematic representation of Myc domains and some of its cofactors. 18

Figure 5.4 Schematic representation of B-cell development. 30

Figure 5.5 Domain organization of Max network. 34

Figure 5.6 Max interacting network of transcription factors. 36

Figure 5.7 Mutation profiles of small cell lung cancer and non-small cell lung cancer patients. 37

Figure 5.8 Polycomb Repressive Complex and its components. 39

Figure 5.9 Recruitment of the PRC complex to the chromatin. 41

Figure 5.10 Polycomb Group Ring Finger family members and their structure. 42

Figure 5.11 Biochemical structure of different PRC1 complexes. 43

Figure 5.12 Scheme of PRC1.6 binding to chromatin. 48

Figure 7.1 Schematic representation of *Pcgf6 allele.* 65

Figure 7.2 *Pcgf6* deletion accelerate *Eμ-myc* lymphomagenesis. 67

Figure 7.3 Distribution of either naïve or immature B-cell *CD19-Cre/*Eμ-*myc/Pcgf6$^{f/f}$* tumors is balanced. 68

Figure 7.4 *CD19-Cre/Eμ-myc/P6$^{f/f}$* tumors are monoclonal based on VDJ recombination. 69

Figure 7.5 *Pcgf6* deletion does not alter BM-derived B-cell fractions. 72

Figure 7.6 *Pcgf6* deletion does not alter splenic B-cell fractions 73

Figure 7.7 *Pcgf6* is recombined upon exposure to CD19-*Cre* recombinase. 73

Figure 7.8 LyP6KO does not express Pcgf6 protein or mRNA levels, and is of the same origin as LyWT.. 75

Figure 7.9 Peak density heatmap of Myc, Pcgf6, Max and histone marks in LyWT and LyP6KO. 77

Figure 7.10 Vast majority of Myc and Max bound peaks are specific for LyP6KO. 78

Figure 7.11 Pcgf6 knockdown in LyWT cells. 80

Figure 7.12 Distribution of Myc and Max binding sites does not change upon KD of Pcgf6. 82

Figure 7.13 Peak density heatmap of Myc, Pcgf6, Max and histone marks in LyWT upon knockdown of Pcgf6 83

Figure 7.14 Conditional- mutated *Mga* allele is hypomorphic. 85

Figure 7.15 Loss of Mga does not accelerate Myc-induced lymphomagenesis. 86

Figure 7.16 Pcgf6-bound peaks are lost in LyMgaKO, even though protein is still present 88

Figure 7.17 Peak density heatmap of Myc, Pcgf6, Max and histone marks in LyWT and LyMgaKO. 89

Figure 7.18 Pcgf6 is efficiently deleted at the pre-tumoral stage. 90

Figure 7.19 Pre-tumoral samples are highly correlated based on the presence/absence of *Eμ-myc* transgene. 92

Figure 7.20 Pcgf6 does not affect transcriptional profiles in the pre-tumoral B-cells, on top of Myc. 93

Figure 7.21 DEGs called in preT_P6KO and preT_Myc compared to cont_WT are enriching for the same categories and show high overlap. 94

Figure 7.22 Tumor samples are highly correlated between each other. 96

Figure 7.23 Genes expressed in T_LyP6KO when compared T_LyWT showed downregulation of inflammatory pathways and immune system response. 97

Figure 7.24 Gene Ontology analysis of DEGs specifically identified in T_LyP6KO experimental group. ... 99

Figure 7.25 Analysis of myeloid and lymphoid lineages in tumors isolated from transplanted mice. 101

Figure 7.26 Analysis of T-cells of tumors isolated from transplanted mice. 102

3 . LIST OF TABLES

Table 1. Primary antibodies used in Western Blot and/or ChIP experiments. 56

Table 2. Antibodies used for Flow Cytometric Analysis 58

Table 3. List of primers for RT-PCR and PCR 61

Table 4. Frequency of different genotypes obtained by crossing *Eμ-myc/P6*$^{wt/fl}$ and *CD19-Cre/P6*$^{wt/fl}$ mice. 66

4. ABSTRACT

The Myc oncoprotein is a bHLH-LZ transcription factor that heterodimerizes with another bHLH-LZ protein, Max, in order to bind DNA and activate transcription. Max also dimerizes with alternative bHLH-LZ partners, including Mxd1-4, Mnt and Mga: these proteins act as transcriptional repressors, are thought to counteract Myc activity at common target genes, and may thus conceivably act as tumor suppressors. Consistent with this concept, Small Cell Lung Cancer (SCLC) shows sporadic loss of either *Max* or *Mga*, as well as *Myc* amplification: all of these events are mutually exclusive, pointing to a common functional consequence. At the molecular level, Max and Mga are also part of a variant of the Polycomb Repressive Complex (PRC1.6), the function of which – if any – in tumorigenesis remains to be characterized.

Based on the above observations, we hypothesized that Mga/Max dimers may recruit the PRC1.6 complex to chromatin, thereby antagonizing Myc/Max function. We further speculated that this may endow Mga and/or Pcgf6 with widespread tumor suppressor activity, possibly extending to tumor types other than SCLC.

Here, we addressed the roles of Pcgf6 and Mga in *Eμ-myc* transgenic mice, a well-characterized model of Myc-induced lymphomagenesis. Remarkably, B-cell specific deletion of *Pcgf6* – but not *Mga* – led to a marked acceleration in lymphoma onset. As assessed by ChIP- and RNA-seq profiling, loss of Mga or Pcgf6 affected neither DNA-binding by Myc/Max, nor Myc-regulated transcription. Nonetheless, while having no impact tumor onset, deletion of Mga led to a near-complete loss of Pcgf6 recruitment to chromatin, implying that Pcgf6 suppressed lymphomagenesis through an alternative mechanism. Close inspection of mRNA profiles indicated that Pcgf6-null lymphomas were associated with a mild downregulation of genes involved in immune surveillance pathways. Immunophenotypic

profiling of infiltrating cells in transplanted lymphomas pointed to a reduction in infiltrating T-cells, and in particular of effector $CD8^+$ and $CD4^+$ T-cells in Pcgf6-null tumors.

Altogether, we have shown that Pcgf6 acts as a tumor suppressor in a model of Myc-induced B-cell lymphoma, but does so in a Mga- and PRC1.6-independent manner. While cell-autonomous Pcgf6-dependent effects in lymphoma B-cells remain to be addressed, our data point to a possible non-cell autonomous function of Pcgf6 in T-cell recruitment and/or activation, and thus possibly in tumor rejection.

5 . INTRODUCTION

5 . 1 Myc

5 . 1 . 1 Myc protein family

The *MYC* proto-oncogene (or c-*myc*), originally identified as the cellular homolog of the avian retroviral oncogene v-*myc* (Roussel et al., 1979; Vennstrom et al., 1982), is the founding member of a family of three related genes that also includes N- and L-*myc* (or *MYCN* and *MYCL*). Myc family members are largely expressed during development, with c-*myc* expressed in all the tissues of new-born mice, while N-*myc* is restricted to brain, kidney, intestine and lungs and L-*myc* only in brain, kidney and lungs (Zimmerman et al., 1986). Moreover, c-*myc* is expressed mostly in dividing cells (Zimmerman et al., 1986). The importance of Myc family members in early embryonic development has been investigated by generating homozygous null mice for either c-*myc*, N-*myc* or L-*myc*: embryos lacking c-*myc* die between 9.5 and 10.5 days post coitus (dpc) due to abnormal heart, neural tube and yolk sac development (Davis et al., 1993). Knockout of N-*myc* also causes embryonic lethality around mid-gestation, with its deletion in neural stem and precursors cells leading to severe disruption of murine brain growth, specifically of cerebellum (Charron et al., 1992; Stanton et al., 1992), while L-*myc* null mice did not show any congenital defects and a life span comparable to that of WT siblings (Hatton et al., 1996), possibly owing to compensation by c-*myc* and N-*myc*, which have been detected in all L-*myc* expressing tissues (Hatton et al., 1996). Moreover, substitution of c-*myc* alleles with the N-*myc* coding region supports the survival of viable offspring (Malynn et al., 2000), supporting the idea of functional redundancy among Myc family proteins. Most noteworthy here, mice carrying a hypomorphic

c-*myc* allele are smaller than the wild type, due to decreased overall cell numbers (Trumpp et al., 2001).

5.1.2 Biological functions of Myc

The *MYC* protein product, MYC (or Myc), is a transcription factor characterized by the presence of a an amino-terminal transactivation domain (TAD) and a carboxy-terminal basic helix-loop-helix-leucine zipper (bHLH-LZ) domain, both features being shared by the related proteins N- and L-Myc (Dang, 2012). Myc proteins have to dimerize with another bHLH-LZ factor, Max (Myc Associated factor X) to bind to DNA, with a preference for the E-box ("Enhancer box") consensus motif CACGTG, or variants thereof (Blackwell and Weintraub, 1990; Blackwood and Eisenman, 1991; Eilers and Eisenman, 2008; Park et al., 2004). Dimerization with Max is also required for Myc role in transcription activation (Amati et al., 1992) as well as induction of cell proliferation, apoptosis and transformation (Amati et al., 1993a; Amati et al., 1993b).

In normal cells, c-*myc* expression is exquisitely dependent upon the exposure of cells to mitogenic stimuli, and in turn, leads to variety of transcriptional changes that foster cell growth and proliferation, mainly regulating key components of biosynthetic and metabolic processes necessary to maintain cellular growth (a small fraction of the Myc-regulated pathways are schematically summarized in Figure 5.1, and will be discussed in more details in the following sections) (Dang, 2013; de Alboran et al., 2001; Kress et al., 2015; Perna et al., 2012; Tesi et al., 2019; Wang et al., 2011). For example, in both B- and T-cells, Myc is a direct sensor of activating signals that is required for several steps of cellular activation, such as metabolic reprograming, ATP synthesis, ATP-dependent chromatin decompaction, RNA

accumulation and cell growth (de Alboran et al., 2004; Kieffer-Kwon et al., 2017; Murn et al., 2009; Wang et al., 2011).

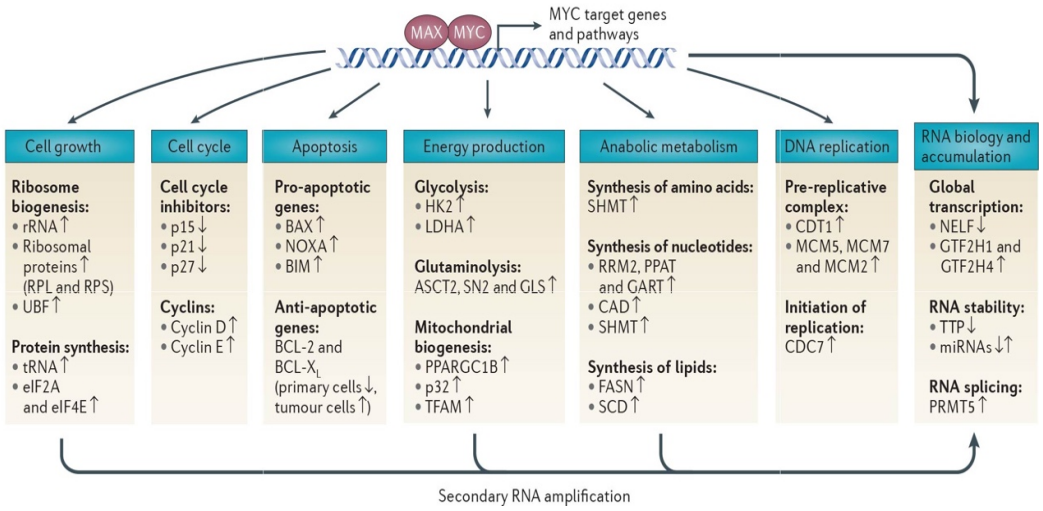

Figure 5.1 Examples of Myc-dependent genes and cellular processes (Kress et al., 2015).

Unfortunately, its central role in the cellular circuity also endows *MYC* with potent oncogenic activity when aberrantly expressed: indeed over-expression of this gene is as a hallmark of many different human cancers (Meyer and Penn, 2008; Tansey, 2014). Oncogenic activation of *MYC* can happen through translocation or gene amplification (Ciriello et al., 2013; Gabay et al., 2014) or, in the absence of direct oncogenic lesions, through aberrant activation of upstream signaling pathways, such as Wnt/β-catenin (He et al., 1998; Sansom et al., 2007), Notch (Palomero et al., 2006; Sharma et al., 2006), or JAK/STAT (Bromberg et al., 1999; Kiuchi et al., 1999). Altogether, Myc overexpression occurs in up to 70% of human tumors (Dang, 2012).

5.1.2.1 Proliferation and apoptosis

In somatic cells, main function of Myc is regulation of proliferation, which is tightly controlled. Myc can promote the cell division in two ways: either by upregulating genes that

are involved in cell cycle entry, such as *cyclin D* (Perez-Roger et al., 1999; Yu et al., 2005) and *cyclin E* (Beier et al., 2000), by repressing the cell cycle inhibitor *p21* or $p15^{INK4b}$ (Gartel et al., 2001; Seoane et al., 2001), or by bypassing the cell cycle arrest through cyclin-dependent kinase inhibitors, such as $p27^{KiPl}$ and $p16^{INK4a}$ (Alevizopoulos et al., 1997; Vlach et al., 1996). One of the alternative ways how Myc can influence proliferation of the cells is by regulating the biological processes needed to support cell proliferation, such as energy production. In order to provide the energy required for the cycling cell, Myc is upregulating genes implicated in different metabolic processes, such as mitochondrial biogenesis and glycolysis (Dejure and Eilers, 2017; Kim et al., 2007; Li et al., 2005; Zhang et al., 2007).

It is believed that the ability of Myc to tightly control proliferation on one side, and to trigger cell death on the other, is a safeguard mechanism to prevent uncontrolled cell divisions due to Myc deregulation. Indeed, In the absence of survival signals, such as growth hormones or cytokines, deregulated Myc expression can induce apoptosis (Bissonnette et al., 1992; Evan et al., 1992) in both p53-dependent and p53-independet ways. First, Myc deregulation leads to the increase in the ARF protein expression (Zindy et al., 1998), which inhibits the negative regulator of p53, known as Mdm2 (Weber et al., 1999). On the other side, disruption of the equilibrium between pro-apoptotic and anti-apoptotic proteins by Myc-dependent mechanisms is another way how Myc induces apoptosis (Eischen et al., 2001; Mitchell et al., 2000; Oster et al., 2002). For example, activation of p53 can increase Puma and Noxa levels that further downregulate anti-apoptotic factors - Bcl2 and Bcl-X_L (Eischen et al., 2001; Maclean et al., 2003; Oda et al., 2000). p53 can also activate pro-apoptotic protein Bax which subsequently causes permeabilization of the mitochondrial outer membrane that leads to induction of cell death (Chipuk et al., 2004).

5.1.2.2 DNA and RNA biology

DNA replication is one of the key cellular processes in which Myc has an important role (Dominguez-Sola and Gautier, 2014). Different studies demonstrated protein-protein interaction between Myc and factors of pre-replication complex, such as the Origin Replication Complex 1 and 2 (ORC1, ORC2) (Dominguez-Sola et al., 2007; Takayama et al., 2000b), Mcm 2-7 proteins (Dominguez-Sola et al., 2007), Cdc6 (Takayama et al., 2000a) and Cdt1 (Dominguez-Sola et al., 2012). *Cdt1* gene has also been characterized as one of the Myc target genes (Valovka et al., 2013). Moreover, Myc interacts with Cdc7 and Cdc45, which are essential for the initiation step of DNA replication (Dominguez-Sola et al., 2007; Kwan et al., 2015).

In RNA biology, Myc is important in controlling the expression of other transcription factors and co-factors, including the general transcription factors such as GTF2H1 and GTF2H4 (Sabò et al., 2014b), AP4 (Chou et al., 2014) and E2F (Leone et al., 2001). Myc-dependent regulation of ribosomal biogenesis and mRNA translation is a highly regulated process. First, Myc can regulate multiple stages of ribosomal biogenesis by regulating the transcription of ribosomal RNA (rRNA) trough chromatin remodeling of ribosomal DNA (rDNA) loci and recruitment of RNA polymerase I (RNAPolI) co-factors (Arabi et al., 2005; Poortinga et al., 2004; Shiue et al., 2009), RNA polymerase II (RNAPolII)-dependent transcription of ribosomal protein genes and factors for rRNA processing, as well as ribosomal subunit transport (Maggi et al., 2008; Wu et al., 2008; Zeller et al., 2001). Additionally, in order to obtain mature rRNAs, these rRNAs need to be processed and modified post-transcriptionally. Some of the Myc-regulated genes are important for the pre-processing of rRNAs into 18S, 5.8S and 28S rRNA, such as Nucleolin, nucleoplasmin, Nop56 and many more (Schlosser et al., 2003). Therefore, Myc not only controls the transcription of component of the translation

machinery, but it is also an important factor in assuring their proper maturation. One of the recent examples how *MYC* can control translation of important genes is by altering the translation of the mRNA encoding immune checkpoint proteins, such as PD-L1, which leads to more aggressive cancers (Xu et al., 2019).

5 . 1 . 3 Structure of Myc protein

Myc-family proteins (c-, N- and L-Myc) are composed by two major regions (Figure 5.2): an N-terminal transcriptional activation domain (TAD) (Amati et al., 1992; Kato et al., 1990) and the C-terminal bHLH-LZ domain, required for dimerization and DNA binding, transcriptional activation and Myc oncogenic activity (Conacci-Sorrell et al., 2014; Reddy et al., 1992; Tansey, 2014) (Figure 5.2). At the level of their primary sequence, these proteins show six highly conserved regions, termed Myc boxes (MBs), spread through TAD region and central portion of Myc protein, followed by bHLH-LZ at the C-terminus (Meyer and Penn, 2008).

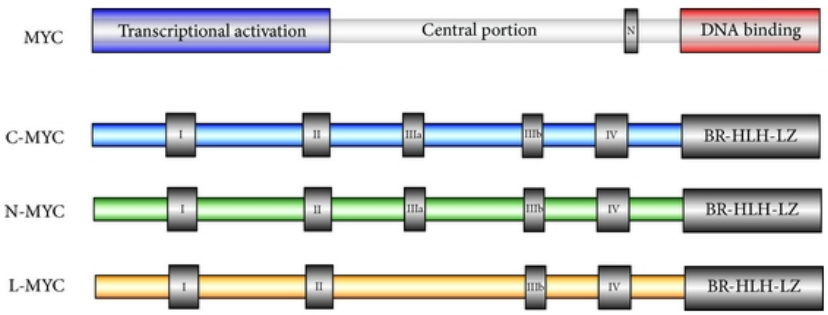

Figure 5.2 Structure of Myc protein family.
The main structural domains of Myc are shown at the top of the figure. Transcriptional activation, central portion, canonical nuclear localization sequence 'N' and region of DNA binding via interaction with Max are reported. A representation of the different family members (c, N and L-Myc) is shown. Modified from (Tansey, 2014).

The TAD (aa 1-143) of Myc, is sufficient for transcriptional activation when fused with a DNA binding domain, (Kato et al., 1990) and is characterized by the presence of two MBs, MBI (aa 43-63) and MBII (aa 128-143), which are highly conserved among Myc family

members (Figure 5.2). MBI is important for the interaction with p-TEFb (Rahl and Young, 2014), the cyclin-CDK complex important for phosphorylation of RNAPolII that stimulates transcription elongation. Besides its role in gene activation, MBI is also important for ubiquitin/proteasomal degradation of Myc: this region is characterized by the presence of Threonine 58 (T58) and Serine 62 (S62) residues that are phosphorylated in order to regulate the activity and stability of Myc (Pulverer et al., 1994; Sears et al., 2000). Stabilization of Myc happens via phosphorylation of S62, which in turn primes T58 for phosphorylation (Sears et al., 2000); on the other hand, T58 triggers the dephosphorylation of the stabilizing phosphate group S62 (Arnold and Sears, 2006; Yeh et al., 2004). MBI is a hot spot for a point mutation that leads to Myc transactivation often occurring in Burkitt's lymphoma. Point mutation in this region also impacts the transformation and apoptotic activities of Myc (Bhatia et al., 1993; Hemann et al., 2005).

MBII is a key domain important for binding of Myc coactivators, such as TRAPP, Tip60, p400, STAGA complex (Figure 5.3) and it has been showed that MBII is important for Myc transformation activity *in vivo* and *in vitro* and for gene activation (Kalkat et al., 2018; Oster et al., 2002). Recent publication of comprehensive phenotypic analyses revealed that MBII is essential for Myc-dependent tumor initiation, by enabling histone acetylation through its interaction with TRAPP-HAT complex (Kalkat et al., 2018).

The central portion of the Myc protein is its least studied part. The key element of this region is a nuclear localization sequence composed by two short peptides: the M1 (PAAKRVKLD, aa 320-328) and the M2 (RQRRNELKRSP, aa 364-374); the first one induces complete nuclear localization, while the latter determines only a partial nuclear localization (Dang and Lee, 1988). In this region there are three other MBs, MBIIIa, MBIIIb and MBIV. MBIIIa (aa 180-199) is the only MB that is not conserved inside the Myc family members, since it is lost

in L-Myc paralog (Figure 5.2). It has been reported that this region is important for the pro-apoptotic activity of Myc, hence, has a role in both *in vitro* and *in vivo* transformation (Herbst et al., 2005). MBIIIb (aa 259-270) is poorly understood and characterized region of Myc. Recent paper showed that MBIIIb can interact directly with WD repeat-containing protein 5 (WDR5), which is part of various chromatin remodeling complexes such H3K4 methyltransferases and could facilitate Myc recruitment to open chromatin (Thomas et al., 2015b). Finally, MBIV (aa 304-324) has been reported to be involved in different Myc functions: its deletion impairs Myc-induced apoptosis and partially reduces its transforming potential, but it does not have any effects on cellular proliferation (Cowling et al., 2006).

The discovery of Max as the heterodimerization partner of Myc (Blackwood and Eisenman, 1991) gave rise to multiple studies addressing the function of Myc/Max dimes. The fact that Myc homodimers are never detected at physiological levels (Dang et al., 1991; Smith et al., 1990), highlights the importance of Max presence for Myc activity. In particular, early studies showed that Myc requires Max for its proper folding and biological activities, such as regulation of gene expression, proliferation, transformation and apoptosis (Amati et al., 1992; Amati et al., 1993b). Both Myc and Max contain bHLH-LZ that mediate their heterodimerization, with each bHLH domain (either in Myc or Max) containing two α helixes connected by a random coil loop; together these helixes form a stable four-helix bundle which binds to DNA through recognition of E-box sequences (Luscher and Larsson, 1999).

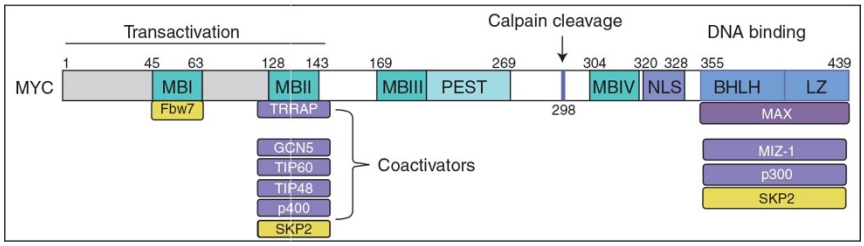

Figure 5.3 Schematic representation of Myc domains and some of its cofactors.
In yellow are depicted major ligases responsible for Myc turnover and in violet are transcriptional binding partners of Myc. Modified from (Conacci-Sorrell et al., 2014).

5 . 1 . 4 Regulation of Myc expression and activity

The abundance and activities of Myc are tightly regulated by a complex signaling network that may act at different biological steps.

- Transcriptional control. The first step of the Myc regulation is the control of its own gene transcription. As an example, Myc expression levels are very low in quiescent cells, and rapidly induced upon mitogenic stimuli, classifying it as an immediate early gene (Kelly et al., 1983). After stimulation, *Myc* levels needs to be lowered again to avoid uncontrolled proliferationa and that can be done both by reducing the rate of transcriptional initiation or by blocking the nascent mRNA elongation (Bentley and Groudine, 1986; Eick and Bornkamm, 1986; Krystal et al., 1988; Xu et al., 1991).

- Post-transcriptional control. Upon transcription of *Myc* mRNA, its export to the cytoplasm is controlled by the translation initiation factor eIF4E (Culjkovic et al., 2006), which is activated upon mitogenic stimuli. The half-life of *Myc* mRNA is very short (Dani et al., 1984), with its expression controlled by a number of miRNAs as well as many RNA binding proteins (RBP), such as TIAR, AUF1 and HuR (Kim et al., 2009b; Liao et al., 2007).

- Translational control. In eukaryotes, the assembly of ribonucleoprotein complex is a fundamental step for initiation of translation, and mRNAs with long and complex 5'UTR, such as the one encoding for Myc, are impaired in translation initiation (Kozak, 1989). It has been shown that down-stream target of mTORC1 (mammalian target of rapamycin 1 complex) complex effector S6 Kinase 1 (S6K1) enhances Myc translation efficiency by modulating the phosphorylation of eIF4B factor, critical for unwinding of 5' UTR of *Myc* (Csibi et al., 2014). In addition, in the *Myc* mRNA, the presence of a ribosome internal entry site (IRES) can lead to the cap-dependent initiation of translation (Stoneley et al., 1998). Moreover, mutations in IRES has been shown to result in the increase of Myc protein amount in multiple myeloma

cells (Chappell et al., 2000; Paulin et al., 1998), and in Bloom's syndrome patients derived cells, a cancer prone disorder (West et al., 1995).

Synthesis of Myc protein can be halted in response to stress stimuli, where consequent DNA damage and oncogenic mutations lead to the association of TIAR protein with 3' UTR of many key regulators of different cellular processes, including *Myc*, which ultimately results in suppression of their translation (Mazan-Mamczarz et al., 2006).

-Post-translational control. The Myc protein undergoes many different post-translational modifications, such as phosphorylation, acetylation, ubiquitination and sumoylation, that have a role in Myc stabilization and degradation (Rabellino et al., 2016; Sabò et al., 2014a; Vervoorts et al., 2006). The main route for controlling Myc protein levels is trough ubiquitin-proteasome system (UPS) (Farrell and Sears, 2014; Thomas and Tansey, 2011), one of the most characterized Ub-ligase that control Myc levels is SCF^{Fwb7}, which is part of SCF-type Ub-ligase complex (Deshaies, 1999). The regulation of the stability of Myc protein depends on the phosphorylation of two residues on the N-terminus: Threonine 58 and Serine 62, and it is mediate by Fwb7 (see chapter 5.1.2) (Welcker et al., 2004; Yada et al., 2004). Myc stabilization via phosphorylation of S62 is a consequence of cell growth stimulation, but at the same times it leads to priming for T58 phosphorylation which is a signal for protein degradation (Sears et al., 2000). Indeed, T58 is recognized by SCF^{Fwb7} that than leads to Myc ubiquitination and proteasome-mediated degradation. SCF^{Fwb7} is not the only enzyme involved in Myc ubiquitination: Skp2 (S-phase kinase-associated protein 2) promotes poly-ubiquitination independently of phosphorylation (Kim et al., 2003). On the contrary, ubiquitination by b-TrCP increases Myc protein stability (Popov et al., 2010). Recently, the importance of post-translational control of Myc levels in both normal and tumor tissues was highlighted by demonstrating that S62 phosphorylation and Pin1-mediated isomerization of

Myc control its spatial localization in the nucleus and further allow for optimal regulation of gene expression in response to extinct signals (Su et al., 2018).

Taking into account that Myc can be also acetylated and that acetylation occurs on the Lysine residues, it has been hypothesized that such modification competes with ubiquitination process for the lysine residues. Indeed, it has been shown that Myc increases its protein stability upon acetylation and it is negatively correlated with ubiquitination (Faiola et al., 2005; Vervoorts et al., 2003). Moreover, Myc can be a substrate for addition of small ubiquitin-like modifier (SUMO) proteins (Gonzalez-Prieto et al., 2015; Sabò et al., 2014a). SUMOylation also occurs on the lysine residues, thus it might compete with both phosphorylation and acetylation. In c-Myc, mass spectrometry analysis identified several SUMO acceptor lysines, K52, K148, K157, K317, K323, K326, K389, K392, K398 and K430 (Gonzalez-Prieto et al., 2015). However, in N-Myc only Lysine 349 has been reported to be modified by SUMOylation (Sabo et al., 2014). Both c-Myc and N-Myc SUMOylation can have a role in quality control of Myc protein, e.g. multiple SUMO monomers have been associated with ubiquitin-proteasome pathway (Gonzalez-Prieto et al., 2015), while Myc phosphorylation and dephosphorylation of S62 and T58 could be SUMO-dependent process (Rabellino et al., 2016).

5 . 1 . 5 Myc as a transcription factor

The formation of Myc/Max heterodimer is fundamental for the biological activities of Myc such as DNA binding to the E-box (Blackwood and Eisenman, 1991; Prendergast et al., 1991), transcriptional activation (Amati et al., 1992; Crouch et al., 1993; Kretzner et al., 1992; Reddy et al., 1992), cell proliferation, apoptosis and transformation (Amati et al., 1993a; Amati et al., 1993b), and Myc-dependent gene regulation (Mao et al., 2003).

A recent publication dissected functional interplay between c-Myc and Max in B lymphocytic differentiation by using either *c-myc* KO, *Max* KO or double KO mice, where it was shown that Myc requires Max in primary B lymphocytes in order to exert its function, while cell differentiation, and DNA replication can be initiated without the formation of Myc/Max heterodimers. However, Myc/Max heterodimer is required for the maintenance, amplification or fine-tuning of these functions upon their initial activation (Perez-Olivares et al., 2018).

Another recent publication confirmed importance of Max by demonstrating that loss of Max in B-cells abrogates lymphomagenesis in the *Eμ-myc* mouse model. These results suggested that loss of Max leads to downregulation of numerous transcriptional targets of Myc/Max, confirming the importance of Max presence in Myc-driven gene regulation (Mathsyaraja et al., 2019).

Early DNA binding and gene expression profiles suggested that Myc binds to and potentially regulates transcription of around ~15% of the genome (Fernandez et al., 2003; Zeller et al., 2006). Genomic regions found to be enriched at Myc binding sites were CpG island (Luscher and Vervoorts, 2012; Zeller et al., 2006), and more in general chromatin regions enriched for epigenetic marks of open and active chromatin, such as tri- and di-methylation of lysine 4 as well as acetylation of lysine 27 of the histone H3 (H3K4me3, H3K4me2, H3K27ac respectively) (Fernandez et al., 2003; Guccione et al., 2006; Sabò and Amati, 2014). So far, it has not been reported that Myc can bind to heterochromatin, even though the E-boxes could be present in those regions (Lin et al., 2012; Sabò et al., 2014b). Hence, chromatin has to be open prior to Myc binding to its target sites.

Apart from being marked by H3K4me3, regions that are bound by Myc can also be pre-bound by transcriptional regulators such as WDR5 (see in chapter 5.1.3) (Carugo et al., 2016; Thomas et al., 2015a; Thomas et al., 2015b), to which Myc binds and in turn recruits a number

of transcription co-factors that lack sequence specificity, such as TRAAP (McMahon et al., 2000), HDACs (Matsuoka et al., 2008), Tip60 or Gcn5 (Frank et al., 2003; McMahon et al., 2000). Moreover, Myc can interact with general transcription factors, such as p-TEFb (cyclin-CDK complex) which mediates RNAPolII CTD phosphorylation, and such interaction has been proposed to lead to the stimulation of transcriptional elongation (Bouchard et al., 2004; Eberhardy and Farnham, 2002; Lin et al., 2012; Rahl et al., 2010). In addition, Myc can associate with the H3K4me3 demethylases Jarid1A/Kdm5a and Jarid1B/Kdm5b and different subunits of ATP-dependent chromatin remodeling complexes such as SWI/SNF (Cheng et al., 1999; Pal et al., 2003; Park et al., 2002; Secombe and Eisenman, 2007).

Myc can interact also with other proteins through its C-terminal domain (CTD), which leads to Myc-dependent repression, which is thought to occur mainly through blockage of the activating action of other transcription factors, such as Miz1 (Staller et al., 2001; Walz et al., 2014). An example of Myc/Miz1 mediated repressed gene is $p21^{Cip1}$: upon UV radiation in mammalian cells, Miz1 promotes transcription of $p21^{Cip}$ in order to trigger the DNA damage-induced cell cycle arrest; on the other hand, Myc antagonize Miz1 activity and facilitate recovery of proliferation after the arrest (Herold et al., 2002). Since both Myc and Miz1 are transcriptional activators, but together form a repressive complex, it has been proposed that the ratio of Myc/Miz1 bound to promoters correlates with the direction of response: in case of Myc upregulated genes this ratio is bigger than 1, while for Myc-repressed genes is close to 1 (Walz et al.2014). However, an integrative analysis of genomic and transcriptomic data from different *in vitro* and *in vivo* systems revealed that the relative Myc abundance at the promoters is an alternative and more accurate predictor of gene transcriptional outcome, while Myc/Miz1 ratio contribution has been shown to be restricted only to some cell lines (de Pretis et al., 2017).

5.1.6 Selective transcription model versus general transcriptional amplification model

Traditionally, it has been thought that Myc-dependent transcriptional activation occurs upon its direct binding to a target sequence on the promoter DNA (Kress et al., 2015; Sabò and Amati, 2014), while Myc-dependent repression in most cases is a result of its indirect DNA binding through other transcription factors of whom Myc would antagonize the function, as previously explained (see chapter 5.1.5) (Staller et al., 2001). In 2012, two studies challenged this view proposing that Myc act as a general amplifier of transcription of all the expressed genes (Lin et al., 2012; Nie et al., 2012). The observation that in cancer cells, Myc overexpression leads to its widespread binding to basically all accessible regions of the genome (active promoters and enhancers) is often coupled with an increase in global RNA levels, an event called "RNA amplification". This phenomenon was explained by the model where Myc binds broadly trough the genome and provides non-specific amplification of already expressed genes, mainly through enhancement of transcription elongation via its interaction with the p-Tefb complex (Lin et al., 2012; Nie et al., 2012).

However, the transcriptional amplification model failed to consider a fundamental aspect: Myc can trigger a series of cellular processes which dramatically impact cell physiology, thus, may in turn foster a general increase in transcription. One of the ways how RNA amplification phenomenon can be explained is by a variety of metabolic changes that rely on Myc and, in turn, impact the global RNA synthesis and turnover (Kress et al., 2015). For example, it has been known for decades that differences in total RNA content may be used as a discriminating marker for cycling and quiescent cells in yeast (Darzynkiewicz et al., 1980) and changes in Myc levels often co-occur with changes in the proliferative state of the cells, e.g. tumor versus normal tissue (Sabò et al., 2014b), or quiescent B-cells versus LPS-stimulated cells (Nie et al., 2012; Sabò et al., 2014b; Tesi et al., 2019; Zeller et al., 2006). Moreover, Myc invasion and

RNA amplification are distinct events that can occur independently: in serum-stimulated fibroblasts, increased RNA levels are observed in cells transitioning from G0/G1 to S-phase, while Myc does not completely invade the open chromatin (Sabò et al., 2014b). On the contrary, overexpressed Myc occupies all the active chromatin in already proliferating fibroblast, without triggering RNA amplification (Kress et al., 2015; Sabò et al., 2014b).

Another indication of the specificity of the action of Myc as a transcription factor comes from recent published work (Muhar et al., 2018), that showed that upon acute degradation of the Myc protein, only few hundreds genes were transcriptionally silenced, in contrast to the general effect that was scored after degradation of a general transcription cofactor, such as Brd4 (Muhar et al., 2018). Another example of a specific Myc-dependent transcriptional program has been recently described in the context of B-cell activation (Tesi et al., 2019).

In this context, different models were proposed to explain the complexity of Myc-dependent transcription. One of the models suggested that occupancy of Myc at different genomic sites controls the quantity of how much a genomic locus responds to the increase of Myc levels in tumors. The higher is the physiological occupancy of Myc on the promoter, the lower will be its response to the additional Myc levels present in cancer cells (Lorenzin et al., 2016). Another model suggested that what better predicts the transcriptional output of increased Myc binding at one locus is the relative increase occurring at that locus compared to all the others to which Myc is bound in that cell (the so-called “Myc share”). Myc-activated promoters can bind Myc at the highest levels, and show enhanced RNAPolII recruitment, while the opposite being true in the case of down-regulated genes (de Pretis et al., 2017).

5.1.7 Myc as an oncogene

Since the discovery of Myc, a vast amount of research has outlined its central role in cellular and tissue homeostasis, where it is regulated both at the transcriptional and post-transcriptional levels (Kress et al., 2015). Therefore, deregulation of Myc can have serious consequences that may eventually lead to the tumor formation.

Myc overexpression was shown to directly contribute to malignant transformation in multiple cell types and it is a hallmark of many human cancers (Ciriello et al., 2013; Gabay et al., 2014). Oncogenic activity of Myc can be reached through chromosomal abnormalities, such as translocation, which for example is a recurrent event in Burkitt's B-cell lymphomas (Kuppers and Dalla-Favera, 2001). Besides Burkitt's B-cell lymphoma, Myc translocation has been reported in different human B-cell lymphomas, such as follicular B-cell lymphoma (FL), diffuse large B-cell lymphoma (DLBCL), and chronic lymphocytic leukemia (CLL), as well in multiple myeloma (Bisso et al., 2019; Grande et al., 2019; Huh et al., 2008; Pasqualucci and Dalla-Favera, 2018; Pasqualucci et al., 2014; Shou et al., 2000). In all of these cancers, Myc deregulation correlates with a more aggressive phenotype and poor prognosis (Bisso et al., 2019; Gabay et al., 2014; Pasqualucci and Dalla-Favera, 2018). Apart from translocation, oncogenic potential of Myc can be achieved through amplification of its locus, which is observed in different solid tumors (Beroukhim et al., 2010). These genetic rearrangements induce a direct Myc overexpression, without affecting the protein coding sequence. This is one of the reasons why Myc differs from other proto-oncogenes, where changes in protein sequence are necessary for their oncogenic activation. Most frequently, Myc becomes activated indirectly, and its overexpression is triggered by the aberrant activation of the upstream signalling pathways (e.g. Wnt (He et al., 1998; Sansom et al., 2007), Notch (Palomero et al., 2006; Weng et al., 2006) or JAK-STAT signalling (Bromberg et al., 1999;

Kiuchi et al., 1999)). For example, mutations in Wnt pathway can lead to enhanced TCF-mediated transcriptional activation of Myc in human colon cancer (He et al., 1998), and deregulation of Notch pathway may induce Myc expression in T-cell leukemia (Palomero et al., 2006). Myc is known to induce cell growth and proliferation in normal cells, while in cancer, oncogenic Myc can also increase the number of divisions in cycling cells and the size of cells (Iritani and Eisenman, 1999). Myc overexpression in normal cells can cause the proliferative arrest (Felsher et al., 2000) and cellular senescence (Grandori et al., 2003), thus its deregulation alone cannot lead to tumor transformations. When Myc overexpression is in cooperation with other oncogenic event, e.g. overexpression of Bcl-2, it eventually leads to transformation of the cells and tumor initiation (Clegg et al., 2011; DeoCampo et al., 2000; Welm et al., 2005).

When oncogenic Myc is switched off in already established tumors, it causes tumor involution, based on either growth arrest, apoptosis, block in differentiation or systemic repression, suggesting that tumors are addicted to continuous Myc overexpression (Felsher and Bishop, 1999; Gabay et al., 2014; Kress et al., 2016; Shachaf et al., 2004). Even in the tumors that are not Myc-driven, e.g $Kras^{G12D}$ or SV40 viral antigen, inhibition of Myc leads to tumor regression (Soucek et al., 2013), implying that Myc is generally required for tumor maintenance. Consistent with these observation, many mouse models of Myc-driven tumors has shown that malignant cells became addicted to its overexpression, where upon its inhibition tumor growth arrest and normal cell differentiation continues (Felsher and Bishop, 1999; Jain et al., 2002).

5 . 1 . 8 Myc in B-cell development

B-cells play a central function in humoral immunity and as part of the adaptive immune system, have a protective effect against a variety of pathogens. Production of B-cells is a life-long process which starts in the fetal liver during embryonic development and continues in postnatal life in the bone marrow (BM) from multipotent hematopoietic stem cells (HSC) (Figure 5.4) (Era et al., 1991; Hardy et al., 1991; Hardy and Hayakawa, 1991; Matthias and Rolink, 2005). B-cells (and T-cells) originate from common lymphoid progenitors (CLPs) and during their differentiation undergo rearrangements of their genetic material in order to establish a plethora of antigen receptors which is necessary for their protective immune function. Indeed, each B-cell is characterized by the expression of a B-cell receptor (BCR) composed of membrane-bound immunoglobulin and the Igα/Igβ heterodimer and has been shown to form tetrameric structure. B- receptors contain a variable region which is responsible for the recognition of foreign antigens and a constant region responsible for the function of the receptor. Variable region of each receptor is generated by a gene rearrangement process called VDJ recombination, which joins together a unique variable (V), diversity (D) and joining (J) gene segment (only V and J segments for the Ig light chain (IgL) of the BCR) in lymphoid precursors. In BM CLPs differentiate in Pre/Pro-B-cells ($B220^{+}IgM^{-}CD43^{+}CD25^{-}CD19^{-}$), which is the first B-cell precursors that rearrange their IgH locus. These cells further differentiate into Pro-B cells ($B220^{+}IgM^{-}CD43^{+}CD25^{-}$). Functional IgH chain expression interrupts the VDJ rearrangement of the second IgH locus, a process called allelic exclusion (Cedar and Bergman, 2008). When IgH chain is paired to the IgL, forming a pre-BCR, the clonal expansion of pre-B cells ($B220^{+}IgM^{-}CD43^{-}CD25^{+}$) is triggered, cells exit from the cell cycle and complete IgL rearrangement. This newly generated Pre-B cells express non-autoreactive BCRs, which are BCRs that do not auto-react with B-cells, while paring of

functional IgH and IgL chains leads to generation of surface BCR expressed at immature B-cell stage. These cells further migrate from BM to secondary lymphoid organs such as spleen and lymph nodes where they exert their immunological function.

Transitional B cells are the first immature B cells to exit from the BM and they contain a fraction of self-reactive B cells committed to death, known as T1 ($B220^{lo}IgM^{+}CD23^{-}$) cells (Carsetti et al., 1995; Pillai et al., 2004). T2 cells ($B220^{lo}IgM^{high}CD23^{+}$) are derived from T1 cells and are direct precursors of the long-lived mature B-cells. Moreover, the three major mature B-cell subsets are follicular (FO) ($B220^{+}CD21^{int}CD23^{+}$), marginal zone (MZ) ($B220^{+}CD21^{high}CD23^{lo}$) and B1 B-cells ($B220^{+}CD21^{low}CD23^{low}$). B1 B-cells are subclass of B-cells that are not part of the adaptive immune response since they do not have memory, while usually present in the periphery sites, but less common in blood. MZ and B1 B-cells have an important role in the production of natural antibodies and they respond fast to T-cell independent antigens by differentiating into low-affinity antibodies secreting plasma cells (Song and Cerny, 2003). On the other hand, FO B-cells are the main players in T-cell dependent antigen responses. Once FO B-cells are exposed to a T-cell dependent antigen, they form germinal centers (GCs). GCs are micro-anatomy structures in which B-cells prone to produce high affinity antibodies are selected and further expanded (Basso and Dalla-Favera, 2015). The so-called “GC reaction” is characterized by increased B-cell proliferation, Ig gene mutations (“Somatic hypermutation”), selection of high-affinity Ig mutants and finally their differentiation into memory B-cells and plasma cells (Dal Porto et al., 2002). The scope of GC reaction is to select B-cells able to produce high-affinity Ig for the encountered antigen (Basso and Dalla-Favera, 2015; De Silva and Klein, 2015; Rajewsky, 1996).

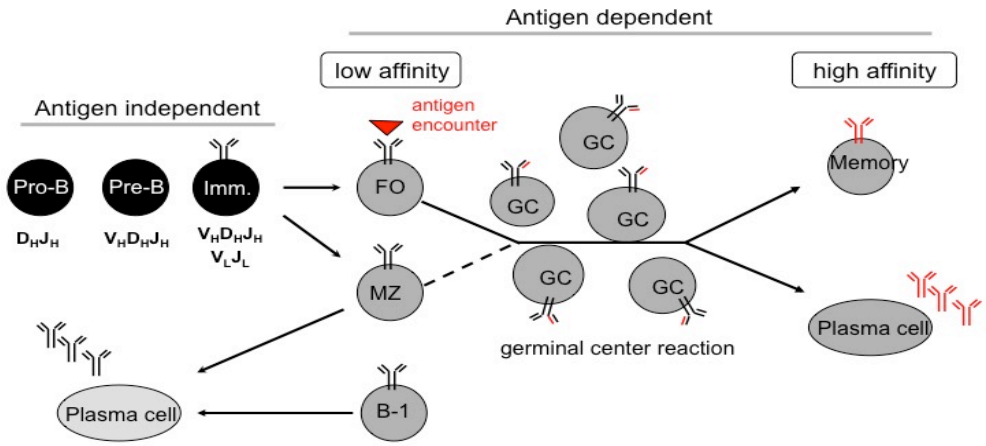

Figure 5.4 Schematic representation of B-cell development.
Graphical representation of the different stages of B-cell development. FO – Follicular zone B-cells; MZ – Marginal Zone B-cells; GC – Germinal Center B-cells.

B-cell development is a highly ordered pathway, controlled by different transcriptional pathways and checkpoints (Matthias and Rolink, 2005). Myc is known to have an important role in this process, since it is involved in B-cell proliferation, differentiation and apoptosis (Meyer and Penn, 2008). Studies in different mouse models demonstrated that Myc is essential for the survival, proliferation and proper differentiation from Pre-B cells into immature B-cells (de Alboran et al., 2001; Vallespinos et al., 2011). Indeed Myc induces the expression of early B-cell factor 1 (Ebf-1), important for Pro/Pre-B cell development (Lin and Grosschedl, 1995). Besides, Myc null B-cells led to impaired cell cycle re-entry of B-cells, increased resistance to CD95-induced apoptosis, and impaired mitogenic response upon stimulation with IL-4 and CD40L (de Alboran et al., 2004; de Alboran et al., 2001). Moreover, Myc has a crucial role during the GC reaction, demonstrated by the absence of GCs upon its specific deletion in GC B-cells (Calado et al., 2012). Recently, Myc has been characterized as a timer of B-cell proliferation, by its involvement in regulating the levels of its protein production. However, cell division is blocked when the amount of Myc protein falls below critical levels (Heinzel et al., 2017). The role of Myc as a timer of B-cell proliferation was also recently confirmed in

GC B-cells: deregulation of Myc was shown to trigger B-cell lymphomagenesis (Finkin et al., 2019). The aforementioned discoveries allow to conclude that Myc expression and function are necessary for B-cell differentiation and maturation (Eilers and Eisenman, 2008; Wang et al., 2011).

5.1.9 *Eμ-myc* and other Myc-driven mouse models of B-cell lymphomas

Altered c-*myc* expression has been implicated in different lymphoid neoplasia. For example, in human Burkitt's B-cell lymphomas, c-*myc* is activated as a result of t(8;14) translocation to immunoglobulin heavy (IgH)-chain locus upstream of c-*myc* exon 1. Such translocation preserves an intact c-*myc* coding region but promotes high c-*myc* expression, that is now regulated by the enhancer controlling the expression of the IgH, thus converting Myc into a potent leukemogenic agent (Cory, 1986). Adams and colleagues created a transgenic mouse model in which expression of the c-*myc* gene is regulated by lymphoid-specific IgH enhancer (*Eμ*), thus recapitulating the translocation hallmark of Burkitt's lymphoma (Adams et al., 1985). The activation of the *Eμ* enhancer causes overexpression of Myc in B-cells and the expansion of Pro/Pre-B cell compartment which eventually leads to a block in B-cell differentiation (Langdon et al., 1986) and development of tumors of B-cell origin at around 4 months of age (Adams et al., 1985). These lymphomas massively infiltrate lymph nodes and spleen (that invariably shows splenomegaly), and frequently also the thymus. They are usually mono/oligoclonal, based on VDJ rearrangement analyses, indicating that the clonal expansion of B-cells is needed for development of *Eμ-myc* lymphomas (Adams et al., 1985). During the period of latency that precedes the development of full-blown lymphomas ("pre-tumoral stage"), B-cells that overexpress Myc experience massive proliferation (Langdon et al., 1986), restrained by the activation of cellular checkpoints that lead to cell death (Bissonnette et al.,

1992; Evan et al., 1992), which has been linked to the activation of p53 as tumor suppressor (Zindy et al., 1998), and cellular oncogene-induced senescence (Campaner et al., 2010). During this pre-tumoral stage B-cells usually acquire second mutations that are positively select for their cooperation with Myc (that is not sufficient *per se* for neoplasia development) in promoting lymphoma development (Adams et al., 1985; Alexander et al., 1987).

Eμ-myc tumors can be of different cell-of-origin, such as mainly of Pre-B cell, B-cell or mixed origin, while human diseases are often characterized by GC B-cell or plasma cell origin. In the past, other transgenic mouse models that develop lymphomas with striking similarities to human Burkitt's lymphoma have been generated. One of those is the *λ-Myc* transgenic mouse model, where c-*myc* is under the control of a reconstructed immunoglobulin-light chain Igλ locus, has occurs in a subset of Burkitt's lymphoma where c-Myc is translocated in the Igλ locus (Kovalchuk et al., 2000). These mice showed lymphadenopathy, with minimal splenomegaly and median onset of tumors around 150 days. Another model was generated by Sander and colleagues (Cγ1-Cre,R26Stop^{FL}MYC,R26Stop^{FL}P110* mouse model) (Sander et al., 2012), where Myc is overexpressed in GC B-cells together with a constitutively active form of PI3K, a known effector of BCR signaling. In these mice, PI3K is able to block Myc pro-apoptotic response and cooperates with Myc for the onset of lymphoma, which almost fully phenocopies human Burkitt lymphoma.

Although human B-cell lymphomas differ from the one developed in *Eμ-myc* mouse model, this transgene remains a unique tool to study Myc-driven lymphomagenesis for a variety of reasons. First, in this model disease progression can be easily monitored by palpation of lymph nodes and analyses of peripheral blood counts. Second, isolated primary tumors can be easily infected with suitable retroviral vector to modulate the expression of genes of interest and study their functions in this context. Besides *Eμ-myc* derived lymphomas can be studied

either *in vitro* or expanded *in vivo* in immune-competent mice, preserving the same histological characteristics as the original primary tumors (Langdon et al., 1986). Moreover, the presence of a pre-tumoral stage provides the opportunity to follow Myc-dependent proliferation, apoptosis and genomic and transcriptional programs prior of the onset of the "second hit" mutation. This also allows the study of the effect of a gene of interest on these Myc-induced phenotypes and ultimately in Myc-driven lymphomagenesis, such as the landmark studies of the cooperation between Myc overexpression and the knock-out of the tumor suppressors p53 or p19ARF (Eischen et al., 1999).

Altogether, this model allows for a unique opportunity to understand how cancer cell can bypass cellular checkpoint activated by Myc oncogenic activities, which will ultimately open the door for novel therapeutic opportunities against aggressive Myc-induced lymphoma.

5.1.10 The Max and MXD network

Besides heterodimerizing with Myc family members, Max can form heterodimers with other bHLH-LZ transcription factors, such as members of Max dimerization protein family (Mxd) (Mxd1-4), Mnt (Max Network Transcriptional Repressor) and Mga (Max Gene Associate protein) (Ayer et al., 1993; Hurlin et al., 1997; Hurlin et al., 1995; Meroni et al., 1997; Zervos et al., 1993), forming the so-called Max/Mxd network (Diolaiti et al., 2015; Hurlin and Huang, 2006).

Mxd1 and Mxd2 (previously known as Mad and Mxi1) were the first proteins identified as interactors able to form heterodimers with Max (Ayer et al., 1993; Zervos et al., 1993). They show 43% of conserved sequence between themselves, and apart from containing bHLH-LZ domain, they do not possess other domains similar to the ones found in Myc. Although, Mxd1 and Mxd2 are not able to homodimerize *in vitro*, they efficiently compete with Myc for Max

binding. When in heterodimer with Max, Mxd1 and Mxd2 are binding to the E-box and act as transcriptional repressors (Ayer et al., 1993).

After the discovery of Mxd1 and Mxd2, four other Mxd-like protein (Mxd3, Mxd4, Mnt and Mga) were described (Hurlin et al., 1997; Hurlin et al., 1995; Hurlin et al., 1999): while Mxd3 and Mxd4 are highly similar to previously discovered Mxd1 and Mxd2, Mnt and Mga were structurally different (see below) (Figure 5.5).

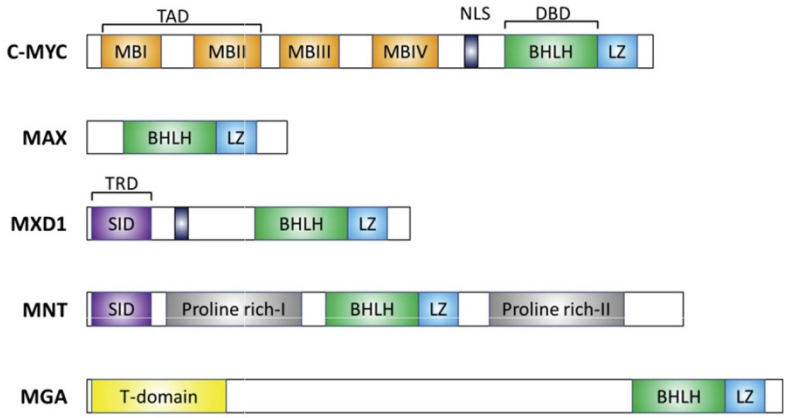

Figure 5.5 Domain organization of Max network.
MBI-IV, Myc box domains; NLS, nuclear localization signal; BHLH, Basic helix loop helix; LZ, leucine zipper; SID, SIN3-interacting domain; TAD, transcriptional activation domain; TRD, transcriptional repression domain; T-domain, T box domain. Modified from (Diolaiti et al., 2015).

All the members of the Max-interacting network (Figure 5.5) can act as transcriptional repressors and may block Myc-dependent cell transformation *in vitro* (Ayer et al., 1993; Foley et al., 1998; Hurlin et al., 1997; Hurlin et al., 1995; Hurlin et al., 1999; Zervos et al., 1993).

Indeed, Mnt (previously known as Rox) and Mxd1-4 at the N-terminus domain contain Sin3-interacting domain (SID) which is responsible for the interaction with Sin3a and Sin3b (Ayer et al., 1995; Schreiber-Agus et al., 1995), the two corepressors that can interact with different proteins, as the histone deacetylases (HDAC) Hdac1 and Hdac2 (reviewed in (Ayer, 1999)). HDACs can modify chromatin that becomes less accessible to the transcription machinery by removing acetyl groups from histones H3 and H4, thus generating more closed and

inaccessible chromatin environment (Hassig et al., 1997; Laherty et al., 1997; Zhang et al., 1997). By recruiting mSin3-HDAC co-repressor complex, Mxd/Mnt proteins appear to antagonize or reverse the transcriptional activity of Myc (McMahon et al., 2000; Popov et al., 2005). Studies examining the relationship between Mxd1-4, Mnt and Myc proteins suggest that Mnt plays a general role as Myc antagonist, while Mxd proteins function as more specialized Myc antagonists. These conclusions were based on the research done on the knock-out mice for each Mxd member: mice lacking Mxd1, Mxd2 and Mxd3 are viable and fertile (Foley et al., 1998; Queva et al., 2001; Schreiber-Agus et al., 1998), while mice where Mnt is not expressed typically die within 24 hours of birth (Toyo-oka et al., 2004). Conditional deletion of Mnt in breast epithelium or other cells is known to lead to tumor formation, suggesting a role of Mnt as a negative regulator of Myc functions associated with cell proliferation and tumorigenesis (Hurlin et al., 2003). Moreover, studies on the effect of Mxd1 deletion or its overexpression *in vivo* suggested its involvement in suppression of key Myc-associated activities, such as proliferation, cell growth and apoptosis. Altogether, these studies implied that the interplay between Mnt and Mxd1-4 is crucial for fine-tuning Myc activity for cell-cycle entry and exit, proliferation rate and apoptosis.

Mga differs from the other members of the Max/Mxd network: besides the bHLH domain it contains also another DNA-binding domain, the T-box domain (Hurlin et al., 1999). It is different from other Mxd members due to its large size: contains more than 3000 residues, which makes Mga ~ 14 fold bigger than the Mxd family, and ~ 5 fold larger than Mnt (Hurlin et al., 1999). Mga requires heterodimerization with Max in order to bind to E-box binding site, however, it is also able to bind alone to T-box binding elements (TBEs) (Hurlin et al., 1999). Moreover, Mga, unlike other Mxd family members, is essential for early embryonic development and has a role in embryonic patterning and maintenance of pluripotency by

regulating the transcription of *Odc1* (Sun et al., 2014; Washkowitz et al., 2015). Surprisingly, Mga and Max were found to be part of non-canonical PRC1.6 complex, which is implicated in transcriptional repression (see below 1.2.3) (Gao et al., 2012; Ogawa et al., 2002). Of note, genomic alterations affect Mga locus in variety of tumors, with a much higher frequency respect to Mxd/Mnt family members. A subset of these alterations are predicted to inactivate Mga bHLH-LZ domain close to its C-terminus, such as alterations occurring in chronic lymphocytic leukemia (CLL), acute lymphocytic leukemia (AML) and Small Cell Lung Cancer (SCLC) (Chigrinova et al., 2013; De Paoli et al., 2013; Edelmann et al., 2012; Lee et al., 2018; Romero et al., 2014). For example, loss of Mga occurs in a subset of SCLC and these alterations are mutually exclusive to other genomic alterations, such as loss of Max and overexpression of Myc (Romero et al., 2014). Frequency of potentially inactivating mutations, along with the potential antagonistic effect of Mga on Myc transforming activity, strongly suggest a possible role of Mga as a tumor suppressor.

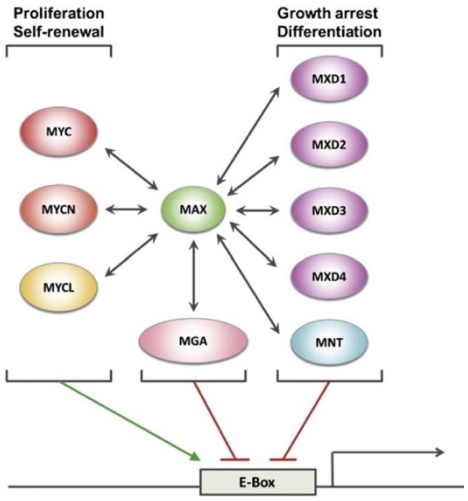

Figure 5.6 Max interacting network of transcription factors.
Schematic representation of Max interactome. On the left side are present Myc protein family members that are acting as activators of transcription, while on the right are Mxd1-4, Mnt and Mga as partners of Max that act as repressors of the same target genes. Modified from (Diolaiti et al., 2015)

Loss of Max-Mxd network balance may play important roles in tumor formation. Absence of Max leads to early post-implantation lethality (Mathsyaraja et al., 2019; Suzuki et al., 2016), while inactivating mutations or deletions of Max can result in tumor development. The initial discovery of Max deletion in tumors was made in neuroendocrine carcinomas, specifically in Pheochromacytoma (PC) (Comino-Mendez et al., 2011). This was followed by the same discovery in SCLC a couple of years later, where ~ 6% of human SCLC were shown loss of Max. Of note, this oncogenic event is found to be mutually exclusive with loss of Mga or Myc overexpression (Romero et al., 2014) (Figure 5.7): these observations suggested that, in the case of SCLC, tumor development may be associated with a selective pressure to either gain Myc/Max or lose Mga/Max activity, with both of these events that may have similar consequences on the expression of the downstream common target genes.

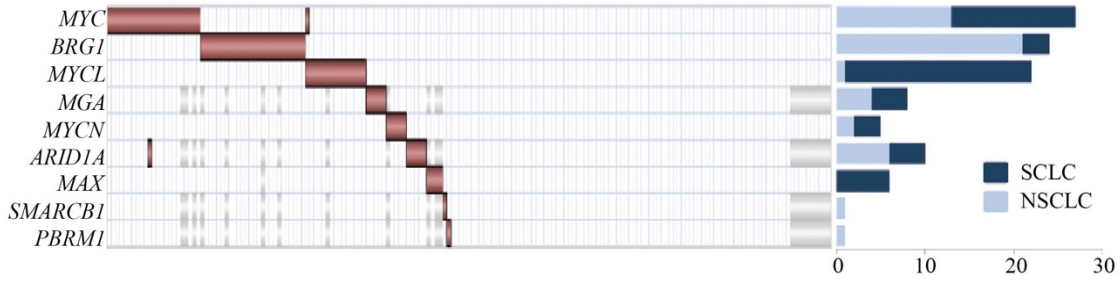

Figure 5.7 Mutation profiles of small cell lung cancer and non-small cell lung cancer patients.
Schematic representation of the co-occurrence analysis of indicated gene alteration in a panel of 180 lung cancer cell lines, either Small Cell Lung Cancer (SCLC) in dark blue or Non-Small Cell Lung Cancer (NSCLC) in light blue. Modified from (Romero et al., 2014).

5.2 Polycomb group proteins

Polycomb group proteins (PcGs) are group of chromatin-modifying factors that participate in the establishment and maintenance of cell fates, mainly by repressing transcription and closing the chromatin state. PcGs were first identified in *Drosophila melanogaster* as regulators of

anterior-posterior body pattering through repression of *Hox* genes (Johansson et al., 1978). Since their discovery, they were characterized from protozas to metazoas where they play crucial roles during development, as well in a variety of biological processes including cell cycle progression, cell fate transitions, tissue homeostasis and tumorigenesis (Bracken and Helin, 2009). They are required for cell fate determination and exert such function through Polycomb-mediated repression, in which PcG complexes are redistributed during differentiation to specific genomic locations (Sauvageau and Sauvageau, 2010). PcG proteins are epigenetic transcriptional silencers of gene expression, which establish post-transcriptional modification (PMT) on the histone tails, e.g. trimethylation on the lysine 27 of histone H3 (H3K27me3) or histone H2A at lysine 119 (H2AK119Ub). These modifications lead to compaction of the chromatin and consecutive silencing of the gene expression. The importance of PcG proteins is highlighted by early embryonic lethality of several PcG mutant mice such as: Eed (embryonic ectoderm development), Ezh2 (enhancer of zeste homolog 2), Suz12 (suppressor of zeste 12 homolog) and Rnf2 (ring finger protein 2; Ring1b) (Faust et al., 1995; O'Carroll et al., 2001; Voncken et al., 2003).

PcG proteins are usually part of two distinct multi-protein complexes, the Polycomb repressive complex-1 (PRC1) and -2 (PRC2), that are recruited to target sites in sequential manner (Figure 5.8) (Margueron and Reinberg, 2011; Simon and Kingston, 2009).

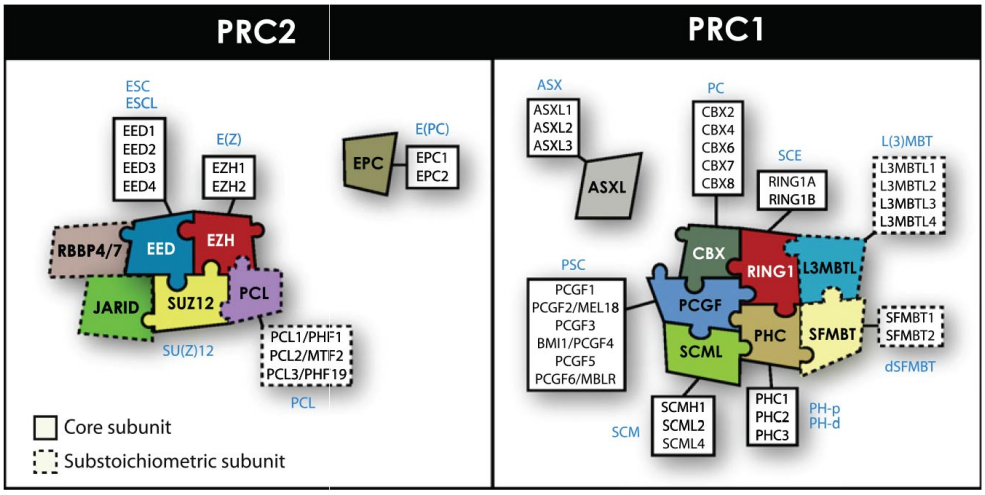

Figure 5.8 Polycomb Repressive Complex and its components.
Modified from review (Sauvageau and Sauvageau, 2010).

A central function of PRC2 is to methylate histone H3 on K27, establishing H3K27me3 which is widely viewed as operative chromatin mark that accompanies PcG silencing. PRC2 can deposit each of the three successive methyl groups that ultimately yield K27me3.

PRC2 complex is formed by four main subunits: Suz12, Eed, retinoblastoma binding protein 46 and 48 (Rbbp4/7) and Ezh1/2. The methyltransferase activity of PRC2 resides in Su(var)3-9, Enhancer-of-zeste, Trithorax (SET) domain of two mutually exclusive proteins, Ezh1 and Ezh2 (Cao et al., 2002). Ezh1 and Ezh2 retain distinct enzymatic proprieties *in vitro*: cell type specific expression patterns and chromatin binding capabilities (Margueron et al., 2008). While loss of Ezh1 is dispensable for embryogenesis and mice viability (Ezhkova et al., 2011), lack of Ezh2 results in early embryonic lethality during gastrulation period and cannot be compensated by Ezh1 (O'Carroll et al., 2001). This notwithstanding, the presence of all core proteins is essential for the enzymatic Ezh1/2 activity both *in vitro* and *in vivo* (Cao et al., 2002; Ketel et al., 2005). This is consistent with the comparable developmental block observed in Eed, Suz12 or Ezh2 knockout mice and in line with the involvement of PRC2 in transcriptional repression of genes involved in cell differentiation and lineage specification

(Faust et al., 1995; O'Carroll et al., 2001; Pasini et al., 2004). PRC2 complex also contains several other, often sub-stoichiometric, PRC2-associated factors with cell-type-specific expression patterns, such as PCL family of proteins (Phf9 and Pcl2/Mtf2) that bind K36-methylated histone H3 through TUDOR domain (Sarma et al., 2008; Zhang et al., 2011), the RNA and histone binding Jumonji protein Jarid2 (Li et al., 2010; Pasini et al., 2010), and the zinc-finger-containing Aebp2 (Cao et al., 2002; Kim et al., 2009a), which support the recruitment of PRC2 to the chromatin.

PRC1 complex was first identified in *Drosophila* and contained Pc (Polycomb, a chromodomain-containing protein with affinity for H3K27me3), dRing (catalyze H2A ubiquitination), Psc (Posterior sex combs, important in chromatin compaction) and Ph (Polyhomeotic) (Shao et al., 1999). Mammalian PRC1 complex contains various chromodomain homologs to Pc (Cbx 2/4/6/7/8), two ubiquitin ligase (Really Interesting New Gene - Ring1a/b) homolog to dRing, six Psc homologs called Polycomb group RING Finger proteins (Pcgf1-6), and three PHC family members (homologs to Ph) (Levine et al., 2002). PRC1 complexes can be divided in two different groups – canonical (cPRC1) and non-canonical (ncPRC1) PRC1 complexes. The cPRC1 contains chromobox (Cbx) protein important for recognition of H3K27me3, while ncPRC1, instead of Cbx protein, has Rybp (RING1 and YY1-binding protein) (Gao et al., 2012). In mammalian cells, PRC1 catalyzes H2AK119Ub and promotes chromatin compactions. Details of each PRC1 subunit will be discussed in the following chapter.

PRC1 and PRC2 typically colocalize at the same target sites throughout the genome. A hierarchical model of PRC recruitment suggests that PRC2 establishes *de novo* H3K27me3 by Ezh1/2 (Margueron et al., 2008; Shen et al., 2008), which is than recognized by Cbx of canonical PRC1 (cPRC1) and followed by its establishment of H2AK119Ub. On the other

hand, an alternative model has been proposed, where the initial event is marked by binding of the non-canonical PRC1 through Rybp subunit to chromatin. Hence, PRC1 catalyzes the formation of H2AK119Ub, independently of PCR2. Consecutively, this modification promotes the recruitment of PRC2 (Figure 5.9) (Blackledge et al., 2015). However, several reports challenged this model since it has been shown that PRC1 can exert gene repression in the absence of PRC2 recruitment (Schoeftner et al., 2006). Yet, the majority of PcG targets require action of both PRC2 and PRC1 to allow stable gene repression.

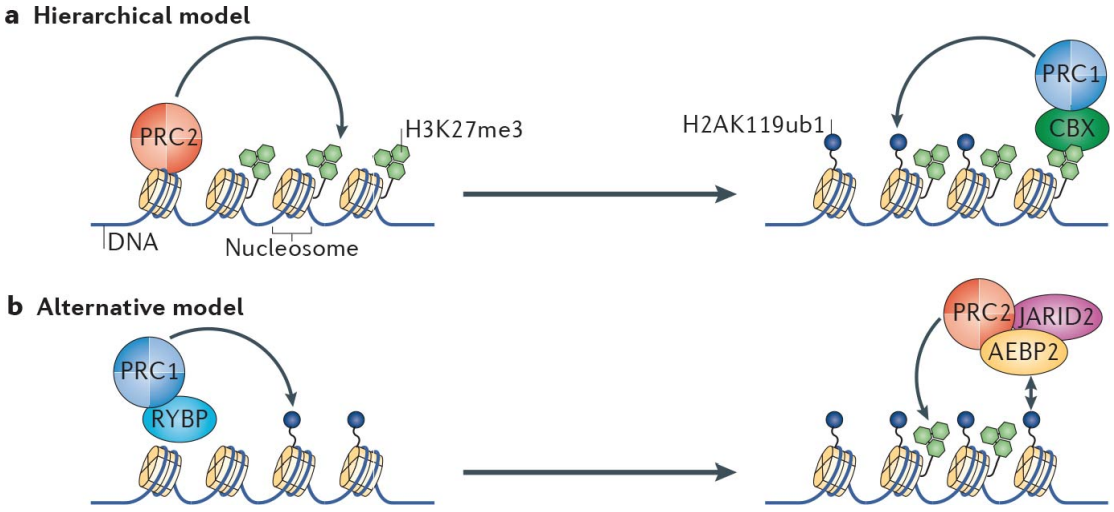

Figure 5.9 Recruitment of the PRC complex to the chromatin.
A. Hierarchical model - PRC2 first binds to chromatin and establish H3K27me3 epigenetic mark. This mark is recognized by chromobox proteins (Cbx), which are a subunit of canonical PRC1 complexes, thereby allowing PRC1 to bind to H2AK119Ub. **B.** Alternative model - the ncPRC1 complexes (which contain Rybp instead of CBX) is bound to chromatin. PRC1 then catalyses the formation of H2AK119Ub, which is then promoting the recruitment of PRC2, and following with establishing of H3K27me3 epigenetic mark. Modified from review (Blackledge et al., 2015).

5.2.1 Canonical and non-canonical PRC1 complex

PRC1 is the complex with the largest number of reported subunits which can form six biochemically distinct subcomplexes (Gao et al., 2012). These are distinguished by the presence of a different member of the Pcgf protein family that dictates the recruitment of

specific ancillary subunits with diverse properties (Di Croce and Helin, 2013; Scelfo et al., 2015). Six different PRC1 sub-complexes (PRC1.1-.6) have been identified. In general all the members fo the Pcgf protein family contain a RING finger domain in their central region (Figure 5.10), that mediates the interaction with the catalytic subunit Ring1a/b which is responsible for the E3-ligase activity for H2AK119Ub (Akasaka et al., 2002). Another domain share among all Pcgf proteins is the WD40-associated ubiquitin-like domain (RAWUL). It has been shown that both RING and RAWUL domains are important in determining the identity of the specific PRC1 subcomplex (Sanchez-Pulido et al., 2008).

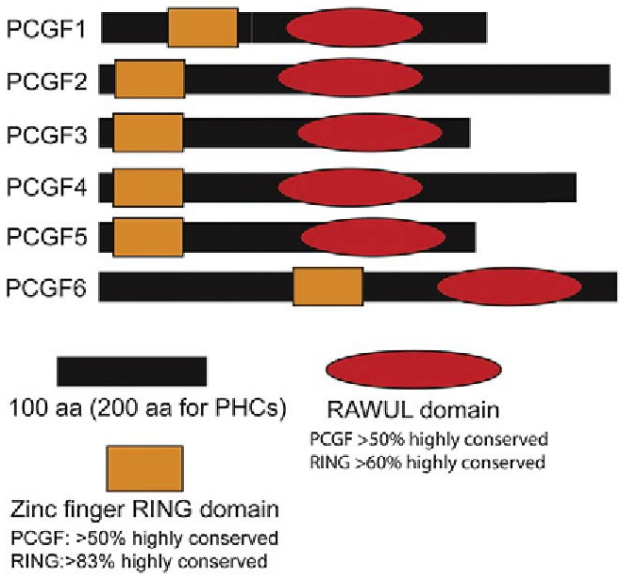

Figure 5.10 Polycomb Group Ring Finger family members and their structure.
Conserved domains are depicted in order to visualize similarities and differences among paralogs. Modified from review (Connelly and Dykhuizen, 2017).

The core elements of all PRC1 complexes, both cPRC1 and ncPRC1, are the E3-ligase Ring1a and Ring1b that catalyze mono-ubiquitination of the lysin 119 at histone H2A (Figure 5.11). Ring1a and Ring1b-ubiquitin ligase activity requires stable interaction with one of the Pcgfs, both *in vitro* and *in vivo* (Cao et al., 2005; Elderkin et al., 2007). Importantly, Pcgf2 and

Pcgf4, or Pcgf3 and Pcgf5 can assemble independently biochemically identical complexes with redundant biological functions (Gao et al., 2012).

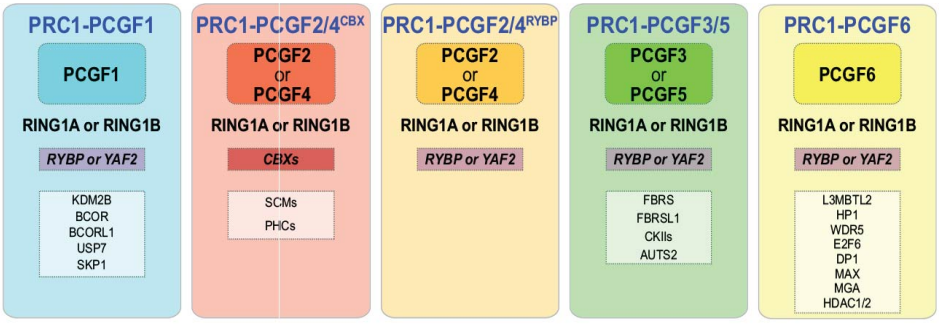

Figure 5.11 Biochemical structure of different PRC1 complexes.
Schematic depiction of PRC1 family complex. Specific PCGF proteins, in association with either CBX or RYBP or YAF2, define the different PRC1 subcomplexes. Modified from review (Scelfo et al., 2015).

cPRC1 complex, known as PRC1.2/PRC1.4, is defined by the presence of Pcgf2 or Pcgf4 (previously known as Bmi-1 and Mel-18) and by their association with subunits like Phc and Cbx. Notably, the Cbx subunit is not present in any other PRC1 subcomplex rather than cPRC1 (also known as Cbx-containing PRC1) (Gao et al., 2012). This complex is recruited to chromatin through Cbx ability to bind to H3K27me3 deposited by PRC2 (Min et al., 2003; Wang et al., 2004). Moreover, PRC1.2/PRC1.4 complex can also interact with Rybp/Yaf subunit, with apparently no additional associated proteins, suggesting that this PRC1.2/PRC1.4-Rybp/Yafp complex might correspond to transient products before specific canonical and noncanonical PRC1 holocomplex assembly (Hauri et al., 2016).

On the contrary, non-canonical PRC1 (ncPRC1), instead of Cbx, contains Rybp/Yaf subunit and can be classified in different sub-complexes based on the presence of a different Pcgf: PRC1.1, PRC1.3/PRC1.5 and PRC1.6 (Gao et al., 2012; Hauri et al., 2016). Apart from the presence of Ring1a/b E3-ligases and Rybp/Yaf, each of these complexes has distinct associated proteins (Blackledge et al., 2015). For example, Kdm2b is a JumonjiC-containing

histone demethylase important for the recruitment of PRC1.1 to the CpG island, and it is present only in this complex (Gao et al., 2012). ncPRC1 is targeted to the chromatin through H3K27me3-independent mechanism. It is responsible for the H2AK119Ub which leads to the recruitment of PRC2 and downstream H3K27me3 deposition (Blackledge et al., 2014). Recent work in mouse embryonic stem cells (mESC) showed that silencing of Pcgf2 and Pcgf4 of cPRC1 (PRC1.2/PRC1.4) plays a central role in Ring1a/b occupancy, while cPRC1 is not required for the H2AK119Ub deposition and may only slightly contribute to the Polycomb target gene repression (Fursova et al., 2019; Scelfo et al., 2019). Therefore, H2AK119Ub deposition occurs via synergy between variant ncPRC1 complexes and it is required for Polycomb-mediated gene repression (Fursova et al., 2019; Scelfo et al., 2019; Scelfo et al., 2015). Different Pcgf proteins with their corresponding PRC1 occupy distinct genomic loci, preferably promoters of their target genes (Scelfo et al., 2019). Specifically, it has been shown that PRC1.1 and PRC1.2/PRC1.4 are functionally compensating for one another without any evident competition, since they act redundantly and enzymatically engage the same target sites (Scelfo et al., 2019). Moreover, PRC1.3 and PRC1.6 complex were shown to have high target specificity and they moderately cross-talk with other PRC1 complexes (Scelfo et al., 2019).

5.2.2 Polycomb Repressive Complex in hematopoiesis and B-cell-lymphomagenesis

The essential role of PcG genes of PRC complexes in hematopoiesis has been documented by different hematological defects observed in mouse mutants: for example Pcgf4 mutant mice display a block in maturation of both B- and T-cell development (reviewed in detail in (Di Carlo et al., 2019; Vidal and Starowicz, 2017)).

Regarding the PRC2 complex, Ezh2 and Suz12 are highly expressed in both fetal and adult bone marrow, while Ezh1 is preferentially expressed in adult HSCs (Xie et al., 2014). Moreover, it has been shown that Ezh1 null mice do not have any defects in primitive HSCs, however, the impaired B-cell development is observed in the adults (Konuma et al., 2010). On the contrary, Ezh2 null mice display embryonic lethality, while its inactivation in the adult HSCs lead to an early block of B-cell differentiation (at the Pro-B cell stage) and T-cell differentiation (Su et al., 2003; Su et al., 2005). Furthermore, constitutive deletion of Ezh2 facilitates lymphomagenesis by dysregulation of the GC reaction through silencing of p21/p27 and Blimp1 loci (Caganova et al., 2013). Constitutive expression of Bcl6, a transcriptional repressor involved in GC reaction, as well as somatic mutation in Exh2 can lead to recruitment of PRC1.1 which leads to gene repression, thus stopping the GC formation which results in lymphoma development (Beguelin et al., 2016; Hatzi and Melnick, 2014). Moreover, loss of PRC2 lead to acceleration of *Eμ-myc* lymphomagenesis, as observed upon deletion of Suz12 or by short hairpin RNA-mediated knockdown of Suz12 and Ezh2 (Lee et al., 2013).

PRC1 subunits are highly expressed in HSCs and, not surprisingly, their loss is critical for the HSC (Osawa et al., 1996). For example, Pcgf4 null newborn mice are characterized by a severe bone marrow hypoplasia (Lessard and Sauvageau, 2003). Pcgf4 (also known as Bmi-1) heterozygous deletion was shown to accelerate Myc-driven lymphomagenesis through repression of Ink4a/Arf gene locus, suggesting its role as a tumor suppressor (Jacobs et al., 1999). Moreover, ectopic expression of Pcgf4 in the lymphoid compartment is sufficient to perturb normal lymphomagenesis, giving rise to B- and T-cell lymphomas in mice (Alkema et al., 1997).

In Pcgf2 null mice, it was noticed that the B-cell compartment is completely diminished *in vivo* (Akasaka et al., 1997), while the mice with constitutive loss of Ring1a/b exhibited hypoplasia of bone marrow cells and increase in myeloid linage cells (Cales et al., 2008).
Altogether, these evidences point out to the importance of PRC1 and PRC2 subunits in normal hematopoiesis, since their gain- or loss-of-function lead to aberrant hematopoiesis, and ultimately, to hematological malignancies.

5.2.3 Polycomb Repressive Complex 1.6

PRC1.6 complex, also known as E2f6-PRC1 or Pcgf6-PRC1 complex, is one of the ncPRC1 complex, defined by the presence of Pcgf6 protein (Ogawa et al., 2002). In fact, it is similar - if not identical - to the L3mbtl2-containing complex and the E2f6 repressive complex which have a role in chromatin compaction and gene repression (Endoh et al., 2017; Qin et al., 2012; Trojer et al., 2011). Apart from the presence of Ring1a/b as catalytical core of the PRC1.6 complex, the PRC1.6 complex is also characterized by the presence of specific proteins, such as Pcgf6, Mga, E2f6, Heterochromatin protein 1-gamma (HP1γ) and Lethal (3) Malignant Brain Tumor-like 2 (L3mbtl2) (Gao et al., 2012). Recent papers showed that the H2AK119Ub-mediated repression is achieved via combinatorial control of all ncPRC1, including PRC1.6 (Fursova et al., 2019; Scelfo et al., 2019).
L3mbtl2 belongs to the group of proteins with C2/C2-type zinc finger followed by four malignant brain tumor (MBT) domains necessary for its chromatin compaction in a histone methylated-dependent manner (Guo et al., 2009; Wang et al., 2003). L3mbtl2 has a role in germ cell formation and cell cycle progression (Trojer and Reinberg, 2008): mice lacking L3mbtl2 display embryonic lethality soon after the implantation due to desynchronized cell divisions, causing mitotic arrest and eventually to oogenesis defects (Qin et al., 2012). In

PRC1.6, L3mbtl2 facilitates PRC1.6 recruitment and establishes the interaction of Mga/Max with E- or T-box-containing promoters (Stielow et al., 2018).

HP1γ (known as Chromobox 3 - Cbx3) is conserved chromosomal protein that participates in chromosomal compaction and gene silencing (Eissenberg and Elgin, 2000) and it can bind to the chromatin through recognition of H3K27me3 (Fischle et al., 2003). Hovewer, at least in embryonic stem cells (ESCs), HP1γ has a marginal role in the repression of PRC1.6 targets, since its deletion did not result in any increase of the expression of PRC1.6 target genes (Endoh et al., 2017).

Mga was found to be essential for binding of the PRC1.6 to the chromatin: genome-wide binding of E2f6, L3mbtl2 and Pcgf6 was lost in Mga-depleted ESCs (Endoh et al., 2017; Scelfo et al., 2019; Stielow et al., 2018). In particular Mga acts as a sequence-specific DNA-binding factor, mediating recruitment of PRC1.6 to E-box and T- box containing promoters (Scelfo et al., 2019; Stielow et al., 2018).

E2f6 transcription factor is another sequence specific DNA-binding protein found in the PRC1.6 complex (Ogawa et al., 2002). In order to bind to the chromatin, it is necessary the presence of transcription factors Dp1 or Dp2 and together they are forming homo- or heterodimers. E2f6/Dp1-2 are major regulators of genes involved in cell cycle progression and proliferation and specifically, they act as transcriptional repressors (Trimarchi et al., 1998). Presence of both E2f6 and its binding partners Dp1 or Dp2 in PRC1.6 complex demonstrated that PRC1.6 could also be recruited to the E2f recognition sequences *in vitro* (Ogawa et al., 2002; Stielow et al., 2018). Together, they recognize the E2f-binding site (GCGGGAA) (Stielow et al., 2018).

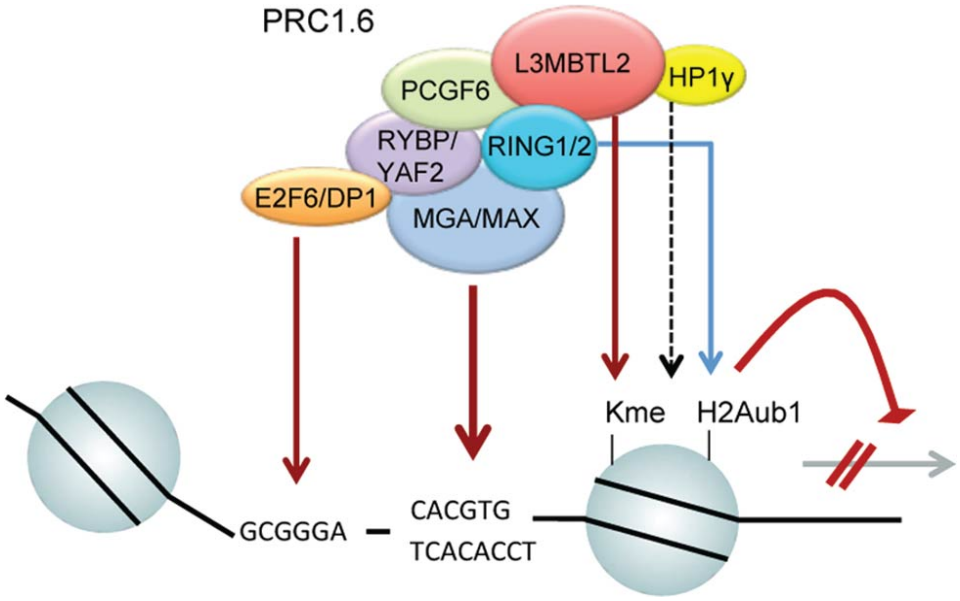

Figure 5.12 Scheme of PRC1.6 binding to chromatin.
PRC1.6 is recruited to the chromatin by cooperative binding to E2f6 and E-box elements. The complex is recruited to the E-box and T-box domains thought Mga/Max complex. Mga also acts as a scaffold tethering E2F6 that in turns mediates PRC1.6 binding to the E2f6-binding sites. L3mbtl2 could also contribute to the recruitment to the specific target loci. Modified from (Stielow et al., 2018).

Presence of sequence specific DNA binding proteins Mga/Max and E2f6/Dp1-2, and the histone-interacting protein L3mbtl2 in PRC1.6 complex implied their crucial role in locus-specific recruitment of the PRC1.6 (Figure 5.12). Indeed, in ESCs it has been showed that each subunit of PRC1.6 and their locus-specific enrolment are necessary for PRC1.6 recruitment to the chromatin (Huang et al., 2018).

5.2.4 Polycomb Group Ring Finger Protein 6

Polycomb Group Ring Finger Protein 6 (Pcgf6), also known as Mel18 and Bmi-like RING finger protein (MBLR), is a member of transcription factor family and it is a subunit specific for PRC1.6 complex (Gao et al., 2012). In ESCs, Pcgf6 was identified as an essential self-renewal gene via a genome-wide RNAi screen (Hu et al., 2009). Of note, in the same screen, Mga was characterized as another gene with an analogous role in self-renewal (Hu et al., 2009). In adults, Pcgf6 is expressed in multiple human and mouse tissues, with preferentially

higher expression in mouse male testis (Akasaka et al., 2002; Yang et al., 2016) where it was shown to modulate mouse male germ cell differentiation (Sun et al., 2015). Pcgf6 has an important role in embryonic development, specifically in pre- and peri-implantation mouse development, since its loss lead to pleiotropic defects *in vivo*, including aberrant axial development and impaired placenta formation (Endoh et al., 2017).

Pcgf6 is the only paralog of the Pcgf family that is highly expressed in undifferentiated ESCs, while its expression declines upon differentiation (Zdzieblo et al., 2014). However, the role of Pcgf6 in maintaining ESCs identity is controversial, since several reports suggest different roles of Pcgf6: one implies that Pcgf6 has repressive function on mesodermal-specific (Zdzieblo et al., 2014) and on endodermal lineage genes (Zhao et al., 2017), while the third report proposes a PRC1.6-independent direct activator Pcgf6 function on core ESC regulators such as *Oct4*, *Sox2* and *Nanog*. Moreover, Pcgf6 overexpression prevents the downregulations of these factors and impairs differentiation (Yang et al., 2016).

Pcgf6 has an important role in PRC1.6-dependent transcriptional repression, since studies on its loss-of-function demonstrated the clear de-expression of the Pcgf6 unique targets in such setting (Scelfo et al., 2019). Although the mechanism of its transcriptional activity still remains unknown, most likely the recruitment of Pcgf6 to actively transcribed genes can lead to the distinct biological activities of the rest of Pcgf paralogs (Scelfo et al., 2019). Pcgf6-associated genes were clustered as part of genes involved in spermatogenesis and homologous chromosome segregation which denote distinct functional properties of Pcgf6 (Scelfo et al., 2019).

Apart from its role in the PRC1.6 complex, Pcgf6 has been also reported to have PRC1-independent functions. Indeed, Pcgf6 associates with H3K4 demethylase Jarid1d, a Jmjc-domain-containing protein capable of demethylating di- and trimethylated H3K4, which is

associated with promoter regions and leads to the increase of transcription (Lee et al., 2007). The physical and functional association between these two proteins showed that Pcgf6 can slightly modulate demethylase activity of Jarid1d and pointed out PRC1.6-independent Pcgf6 function, since this interaction does not require presence of Ring1a/b catalytic unit of PRC1.6 (Lee et al., 2007). Another Jmjc-containing protein Jarid1c has been recently reported to associate with Pcgf6 in dendritic cells (DCs) and together they negatively regulate the DCs activation and function by actively suppressing H3K4me3 levels of genes important for DCs activation, which ultimately promote DC quiescence (Boukhaled et al., 2016). These findings suggest that Pcgf6 may have a Ring1a/b and PRC1.6-independent role in transcriptional repression.

5.3 Aim of the project

The genetics of Max and Mga in PC and SCLC (Figure 5.7) and their presence within the Polycomb repressive complex PRC1.6 (Figure 5.11) led us to hypothesize that Mga/Max dimers may act as an antagonist of Myc/Max on a common set of downstream target genes, and may do so - at least in part - through recruitment of the PRC1.6 complex to the same loci. This may endow Mga, Max, and PRC1.6 with widespread tumor suppressive activity, possibly extending to tumor types other than PC and SCLC.

While the multiple roles of Max as partner of Myc, Mga and other proteins of the network (Figure 5.6) might confound genetic analysis, this complication should not apply to Mga or PRC1.6-restricted subunits, such as Pcgf6. On this basis, the general aim of our project was to determine whether down-regulation of Mga and/or Pcgf6 activity may potentiate Myc-induced tumorigenesis.

In order to investigate this scenario, we took advantage of the *Eμ-myc* mouse model of lymphomagenesis and of conditional knock-out alleles of *Mga* and *Pcgf6*.

The specific aims of the project were the following:

i) to address the role of Pcgf6 and Mga as tumor suppressors in B-cell lymphomagenesis;

ii) to characterize the genomic distribution of Myc, Max, Pcgf6 and Mga in lymphomas and normal B-cells;

iii) to address the impact of Pcgf6 and Mga deletion on Myc-driven transcriptional programs.

6. MATERIALS AND METHODS

6.1 Mice

CD19-Cre (Rickert et al., 1997), *Eμ-myc* (Adams et al., 1985), *Pcgf6*$^{f/f}$ (Endoh et al., 2017) and *Mga*$^{f/f}$ (Washkowitz et al., 2015) mice were used for generation of either *CD19-Cre/Eμ-myc/Pcgf6*$^{f/f}$ and *CD19-Cre/Eμ-myc/Mga*$^{f/f}$. Mice were monitored 2-3 times a week for tumor-free survival by peripheral lymph node palpation and were sacrificed as soon as they showed signs of lymphoma development (i.e. enlarged lymph nodes) (Adams et al., 1985). In all experiments, gender and age-matched mice (both females and males) were used without randomization or blinding.

Genomic DNA (gDNA) for purpose of genotyping was extracted from tail biopsies by overnight digestion in lysis buffer (100 mM TrisHCl pH 8.5, 5 mM EDTA pH 8, 0,2% SDS, 0,2 M NaCl and freshly added Proteinase K 0,1 mg/ml) at 55°C, followed by heat inactivation (5 minutes at 95°C), followed by ten times dilution with water. Genotypes of offspring were performed by semi-quantitative PCR (GoTaq® G2 Hot Start Polymerase, M7408). Primers used for each genotyping are listed in Table 3.

For pre-tumoral analysis CD19-*Cre*/Eμ-*myc*/Pcgf6$^{f/f}$ mice were collected at 4-6 weeks of age. Spleen and bone marrow were dissected and processed for the molecular analysis as previously described (Gorrini et al., 2007).

Experiments involving animals were done in accordance with the Italian Laws (D.lgs. 26/2014), which enforces Dir. 2010/63/EU (Directive 2010/63/EU of the European Parliament and of the Council of 22 September 2010 on the protection of animals used for scientific purposes) and authorized by the Italian Minister of Health with projects 391/2018-PR.

6.2 *In vivo* transplantation of lymphomas

0.5-1 x 10^6 lymphoma cells were resuspended in 0.3 ml of PBS and were injected intravenously in C57/Bl6 mice (purchased from Charles River Laboratories). Animals were monitored by lymph node palpation twice a week, and sacrificed and analyzed when the first enlarged lymph nodes were detected.

6.3 *Ex vivo* single-cell suspension isolation

Infiltrated lymph nodes, spleen and bone marrow of the mice were collected and smashed in PBS separately. Cell suspension was filtered through a Falcon® 70 µm Cell Strainer (Corning, #352350) three times, centrifuged at 2000 rpm for 5 minutes and then resuspended in 10 ml of Erythrocytes Lysis buffer (150 mM NH_4Cl, 10 mM $KHCO_3$, 0,1 mM EDTA). After a centrifugation step at 2000 rpm for 5 minutes, cells were resuspended in 10 ml of MACS buffer (PBS, 2mM EDTA, 0.5% BSA) and this single cell suspension is then used in subsequent experiments.

6.4 Cell lines

Part of the single cell suspension isolated from infiltrated lymph nodes was grown *in vitro* in B cell medium (BCM), composed of DMEM medium (Dulbecco's Modified Eagle Medium, Euroclone, ECM0103L) and IMDM medium (Iscove's Modified Dulbecco's Medium, Sigma, I3390) in ratio 1:1, 10% fetal calf serum (FCS) (Globefarm Ltd, Cranleigh, UK), 2 mM L-glutamine (Invitrogen Life Technologies, Paisley, UK), 1% of non-essential amino acids (NEAA), 1% penicillin/streptomycin and 25 uM β-mercaptoethanol.

Phoenix Ecotropic packaging cells were used for production of the retrovirus. These cells were transfected overnight with 5 µg of Turbo-miR-E-GFP (TUMIPU) retroviral vector,

further mixed in a solution of 240 mM $CaCl_2$ and HBS (25 mM HEPES, pH 7.0, 5 mM KCl, 6 mM dextrose, 140 mM NaCl, 0.750 mM NA_2PO_4). The next day the medium was replaced and after 48 hours, supernatant of transfected Phoenix packaging cells was collected, filtered through Falcon® 0.40 μm filter (Corning, #431750) and supplemented with polybrene (2 μg/ml). Stabilized lymphoma cells were then resuspended at $1x10^6$ cell per ml of medium-containing retrovirus and centrifuged at 2300 rpm for 1 hour at room temperature, followed by 3 hours recovery at 37°C. Medium was then replaced with fresh BCM medium diluting cells at a concentration of $0,3x10^6$ cell/ml. 24 hours later cells were selected with 1 μg/ml of puromycin for 72 hours, after which were either used for Western Blot analysis, gDNA or RNA extraction (explained below) or were plated for growth curve assay.

6.5 Growth curve and cell viability assay

Growth curve assays of stabilized lymphomas were performed as follows: cells were plated in triplicated in tissue culture treated 6-well plates at the concentration of $0,3*10^{\wedge 6}$ cells/ml and were counted by MACSQuant® every 48 hours for the period of at least 7 days. In order to measure number of viable cells, ATP levels of cells were evaluated by CellTiter-Glo® Luminescent Cell Viability Assay (Promega, G7570). CellTiter-Glo® Reagent was added at 1:1 ratio directly to the cells cultured in serum-supplemented medium every 48 hours for the period of at least 7 days and luminescence was then measured by GloMax® Discover Microplate Reader (Promega, GM3000).

6.6 Western Blot

Protein extraction was performed resuspending cells in Lysis buffer (300 mM NaCl, 1% NP-40, 50 mM Tris-HCl pH 8.0, 1 mM EDTA) with freshly added protease inhibitors (cOmplete™ Mini Protease Inhibitor Cocktail, #11836153001 Roche-Merck) and phosphates inhibitors (PhosSTOP™, #4906845001, Roche-Merck). Cell lysates were then sonicated for 10 seconds, cleared by centrifugation at 13000 rpm for 20 minutes at 4°C and quantified by Bradford assay (Bio-Rad Protein Assay, #5000006). Upon addition of 6X Laemmli buffer (375 mM Tris-HCl, 9% SDS, 50% glycerol, 9% β-mercaptoethanol and 0.03% bromophenol blue), lysates were boiled 5 minutes at 100°C and then analysed on 4-15% gradient pre-casted polyacrylamide gel (Bio-Rad, #5678084). Proteins were then transferred to a methylcellulose membrane (Bio-Rad, #1704271) for 30 min at 0.3 A with a Trans-Blot® SD Semi-Dry Transfer apparatus (BioRad, #1704150). Membranes were then washed in TBS-T (10 mM Tris-HCl, 100 mM NaCl, 0.1% Tween at pH7.4) and blocked with 5% milk in TBS-T for 30 minutes, and incubated over-night at 4°C with the indicated primary antibodies (see Table 1). Next day membranes were washed three times for 5 minutes with TBS-T and then incubated at room temperature for 1 hour with the proper secondary antibodies. After three washes in TBS-T, chemiluminescence was detected using a CCD camera (ChemiDoc XRS+ System, Bio-Rad) using Calrity™ Wester ECL substrate (Bio-Rad, #1705060).

6.7 Antibodies

The antibodies used in this thesis were:

Antibody	Company	Host	Application	Dilution/µg used
Myc Y69	Abcam (ab32072)	rabbit	WB	1:2000
Vinculin	Sigma-aldrich (V9264)	mouse	WB	1:10000
Max	Bethyl (A302-866A)	rabbit	WB/ChIP	1:1000 / 5 µg
Pcgf6	(Scelfo et al., 2019)	rabbit	WB/ChIP	1:1000 / 5 µg
Hsp90	Santa Cruz (sc-13119)	mouse	WB	1:10000
Myc N262	Santa Cruz (sc-764)	rabbit	ChIP	5 µg
H3K4me3	Active Motif (#39159)	rabbit	ChIP	5 µg
H3K4me1	Abcam (ab8895)	rabbit	ChIP	5 µg
H3K27ac	Abcam (ab4729)	rabbit	ChIP	5 µg
H3K27me3	Cell Signaling (#9733)	rabbit	ChIP	5 µg
IgG	Santa Cruz (sc-2027)	rabbit	ChIP	5 µg

Table 1. Primary antibodies used in Western Blot and/or ChIP experiments.

6.8 Cloning of shRNAs

To generate shRNAs targeting Pcgf6 or Renilla Luciferase (used as a control), 97-mer oligonucleotide were designed with SplashRNA software (Pelossof et al., 2017). The 97-mer served as a template for a PCR reaction performed using primers miR-E-Xho-fw and miR-E-EcoOligo-rev (sequences of primers are indicated in Table 3). Amplified 125 bp-long PCR products containing the sequence for each specific shRNA inserted in the context of a miR-E backbone (Fellmann et al., 2013), were digested overnight at 37°C with XhoI (NEB, R0146S) and EcoRI (NEB, R0101S) restriction enzymes. Digested PCR products were then ligated in the TUMIPU (turboGFP-miR-E-puro, see below) vector digested with the same restriction enzymes. TUMIPU retroviral vector was designed and cloned in our laboratory, and features a

turbo-GFP reported which is transcribed from the same MSCV LTR promoter of the miR-E shRNA. It also contains a cassette for puromycin resistance. Upon ligation of 1 hour on room temperature with T4 DNA ligase (NEB, M0202S), ligation product was used to transform competent Stable-3 bacteria cells on the agar plate overnight containing 100 µl/ml of ampicillin for selection. The following day bacteria colonies were analyzed by Sanger sequence to control for the presence of the correct insert. Sequences of primers and 97-mer oligonucleotides are indicated in Table 3.

6.9 Genomic DNA extraction and recombination control

Genomic DNA was extracted from either mouse tail or single cell suspension of $CD19^+$ sorted cell isolated from tumors with the Nucleospin® tissue kit (Macherey-Nagel, 740952.250), and eluted in 50 µl of BE buffer (5 mM Tris/HCl, pH 8.5). The analysis of the *Pcgf6* recombination efficiency was performed on gDNA isolated from CD19+ sorted cell from enlarged lymphnodes using qPCR. 10 ng of gDNA were used as template for each real-time PCR reaction. gDNA was detected by fast SyberGreen Master Mix (Applied Biosystems, #4385614) on CFX96 Touch™ Real-Time PCR Detection System (Biorad). Data were normalized to the amplicon of internal region of Utp6 gene. Primer are listed in Table 3.

6.10 Isolation of mouse B-cells

Mouse B-cells were isolated from the spleens or lymph nodes of 4-6 weeks old mice by using magnetic columns (Myltenil Biotech, #130-042-401) and positive selection of $CD19^+$ B-cells with anti-mouse CD19 microbeads (Mylteni Biotech, Cat, No.130-121-301), following manufacturer's protocol.

6.11 Flow cytometric analysis

All the cells used for FACS analysis were stained at least 1 hour at 4°C in the dark. Staining was performed in MACS buffer (PBS 1x, 2 mM EDTA, 0.5% BSA) mixed with specific for fluorochrome-conjugated antibodies, used at the dilution indicated in Table 2 below and analysed with a FACSCelesta™ cytofluorimeter. Results were then further processed and analysed with FlowJo Version 10.4.0 software.

Antibody	Conjugate	Company	Clone	Species	Dilution used
B220	PE	BD Pharmingen (#553089)	RA3-6B2	mouse	1:200
B220	efluor 450	eBioScience (48-0452-82)	RA3-6B2	mouse	1:200
CD19	PE-Cy7	BD Pharmigen (552854)	1D3	mouse	1:400
CD21	PE	eBioScience (12-0211-82)	8D9	mouse	1:800
CD23	AlexaFluor 647	BioLegende (101612)	B3B4	mouse	1:100
CD25	APC	eBioScience (17-0251-82)	PC61.5	mouse	1:100
CD43	FITC	eBioScience (11-0431-85)	R2/60	mouse	1:200
IgD	BV510	BD Pharmigen (#563110)	11-26C.2A	mouse	1:200
IgM	APC	eBioScience (47-5790-82)	II/41	mouse	1:200
IgM	APC-Cy7	BioLegend (406516)	RMM-1	mouse	1:200
CD45	BV786	BD Pharmingen (#564225)	30-F11	mouse	1:100
CD4	PE	BD Pharmingen (#553049)	RM4-5	mouse	1:200
CD8	BB515	BD Pharmingen (#564459)	53-6.7	mouse	1:200
CD44	APC-R700	BD Pharmingen (#565480)	IM7	mouse	1:400
CD3	BB700	BD Pharmingen (#566495)	145-2C11	mouse	1:25
CD62L	BV605	BD Pharmingen (#563252)	MEL-14	mouse	1:400
MHCII	BV605	BD Pharmingen (#563413)	M5/114.15.2	mouse	1:100
Ly6G	PE	BD Pharmingen (#551461)	1A8	mouse	1:200
Ly6C	BV421	BD Pharmingen (#562727)	AL-21	mouse	1:200
CD11b	BB515	BD Pharmingen (#564454)	M1/70	mouse	1:200
CD11c	APC-R700	BD Pharmingen (#565872)	N418	mouse	1:200
F4/80	PECF594	BD Pharmingen (#565613)	T45-234	mouse	1:200
NK1.1	APC	BD Pharmingen (#550627)	PK136	mouse	1:100

Table 2. Antibodies used for Flow Cytometric Analysis

6.1.2 RNA extraction and gene expression analysis

Total RNA was purified onto Quick-RNA columns (Zymo, R1054) and treated on-column with DNaseI (Zymo, R1504). Complementary DNA (cDNA) was obtained by using ImProm-II™ reverse transcription kit (Promega, A3800) and 10 ng of cDNA were used as template for each quantitative PCR reaction. cDNA amplification was performed with Fast SyberGreen Master Mix (Applied Biosystem, 4385614) on CFX96 Touch™ Real-Time PCR Detection System (Biorad). Sequences of the PCR primers are reported in Table 3.

For RNA-seq experiments, total RNA was purified as above. RNA quality was checked with the Agilent 2100 Bioanalyzer (Agilent Technologies). 0.5-1 μg of extracted RNA were used to prepare libraries for RNA-Seq with the TruSeq stranded total RNA Sample Prep Kit (Illumina, #20020596) following manufacturer instruction. RNA-seq libraries were then run on the Agilent 2100 Bioanalyzer (Agilent Technologies) for quantification and quality control and then sequenced on Illumina NovaSeq 6000.

6.1.3 Chromatin Immunoprecipitation

In vitro stabilized lymphoma cell lines (LyWT, LyP6KO, LyMgaKO and LyWT infected with shP6 #1, shP6 #2 and shRen) were fixed with 1% formaldehyde in PBS addition for 10 minutes at room temperature. The reaction was stopped by adding 0.125 M glycine and incubation for 5 minutes at room temperature. Cells were washed twice with cold PBS and resuspended in SDS buffer (100 mM NaCl, 50 mM Tris-HClpH8.0, 5 mM EDTA, 0.5% SDS, protease inhibitors). After centrifugation the cell pellet was resuspended in 4 ml of cold IP-buffer (100 mM Tris pH8.6, 0.3% SDS, 1.7% Triton X-100, and 5 mM EDTA) and the chromatin was sonicated to an average length of 300-500 bp and used for the immunoprecipitation.

1% of each sample was collected and saved as input, while the remaining sample was used for the overnight incubation with 5 µg of primary antibody at 4°C. Immunoprecipitation of Myc, Max and Pcgf6 was performed on 500 µg of fixed chromatin, while for the histone marks H3K4me3, H3K4me1, H3K27ac, H3K27me3 and H2Ak119Ub 250 µg of fixed chromatin were used. Chromatin was quantified by Bradford quantitative assay. List of the specific antibodies used is in Table 1.

The following day, 40 µl of protein A sepharose beads were added to each sample and incubated for 3 hours in agitation at 4°C and then washed three times with 1 ml of mixed micelle buffer (150 mM NaCl, 20 mM Tris-HClpH8.1, 25 mM EDTA, 0.1% NaN3, 5% Triton-X 100, 1% SDS, 26% sucrose), twice with buffer 500 (0.1% DOC, 1mM EDTA, 50 nM HEPES, 500 mM NaCl, 1% Triton-X 100, 0.2% NaN3), twice with LiCl-detergent buffer (0.5% DOC, 1 mM EDTA, 250 mM LiCl, 0.5% NP-40, 10 mM Tris-HClpH8, 0.2% NaN3) and once with TE. Pcgf6 and histone marks IPs were washed with milder detergents: three times with 150mM Wash Buffer (150 mM NaCl, 20 mM Tris-HClpH8.0, 2 mM EDTA, 1% Triton-X 100) and once with buffer 500 (Scelfo et al., 2019). To elute the protein-DNA complex and reverse the crosslink, the beads and the inputs were resuspended in 200 µl of 2% SDS in TE and incubated overnight at 65°C. DNA was then purified by Qiagen columns (Qiagen, #28104) and quantified using Qubit™ dsDNA Assay kit (Invitrogen, Q32854).

1.5-2 ng of recovered DNA was used to generate the ChIP-Seq libraries according to the Illumina protocol and then sequenced with Illumina NovaSeq 6000.

6.14 List of primers used

	species	Amplicon	Forward sequence	Reverse sequence
Expression	mouse	Pcgf6	CTTCTCTCTGCGTCTGGAGTC	TCAGCTCGACAAGGTTTATCAG
		c-Myc	TTTTTGTCTATTTGGGGACAGTG	CATCGTCGTGGCTGTCTG
		Max	CCTGGGCCGTAGGAAATGAG	CAGCCGCAGATTGAAACCTC
		Mga	AAATCTTTAACTGCTGCCAAGAA	CTGCAACCTGAATCATTTGTGGT
Recombination	mouse	Pcgf6	CCACCAGACTCAGCCTCTTT	CCCCAACTGCACAATGTCAA
		Mga^{wt}	ATTCCTGTAGGCCCTGGAAG	GGGAGGATTGGGAAGACAAT
		Mga^{null}	ATTCCTGTAGGCCCTGGAAG	CAGGACAACCTGACACCTCTG
ChIP	mouse	Ncl	GGCGTGGTGACTCCACGT	CGAAATCACCTCTTAAAGCAGCA
		Utp6	AGCTAGGCAGCAGTCACCAT	CAGTTGCGCAATAGTGTCGT
Cloning	mouse	Xho/Eco	TGAACTCGAGAAGGTATATTGCTGTTG ACAGTGAGCG	TCTCGAATTCTAGCCCCTTGAAGTCCG AGGCAGTAGGC
	mouse	shRen713	TGCTGTTGACAGTGAGCGCAGGAATTATAATGCTTATCTATAGTGAAGCCACAGA TGTATAGATAAGCATTATAAT TCCTATGCCTACTGCCTCGGA	
	mouse	shP6 #1	TGCTGTTGACAGTGAGCGATGAGACATTTTTACTATAGTATAGTGAAGCCACAGAT GTATACTATAGTAAAAATGTCTCACTGCCTACTGCCTCGGA	
	mouse	shP6 #2	TGCTGTTGACAGTGAGCGCTGCACCAAAGATTCTCACAAATAGTGAAGCCACAGA TGTATTTGTGAGAATCTTTGGTGCAATGCCTACTGCCTCGGA	
Genotyping	mouse	$CD19^{wt}$	CCAGACTAGATACAGACCAG	AACCAGTCAACACCCTTCC
		$CD19^{-}$	CCAGACTAGATACAGACCAG	TCAGCTACACCAGAGACGG
		Eμ-myc	GGTTTAATGAATTTGAAGTTGCCA	TTCTTGCCCTGCGTATATCAGTC
		Mga^{wt}	CAGGACAACCTGACACCTCTG	GGTATGGTTGTAATGATCAGCTTTC
		Mga^{Inv}	CAGGACAACCTGACACCTCTG	GCTGGGGCTCGATCCTCTAG
		$Pcgf6^{wt}$	TTAATTGCTGCGTTCCATCTC	ATGTCAGAGAACTGGGACCGC
		$Pcgf6^{fl}$	TTAATTGCTGCGTTCCATCTC	GGCTAGATCTGCTGGAGACTT

Table 3. List of primers for RT-PCR and PCR

6.1.5 Computational analysis

RNA-seq and ChIP-seq reads were filtered with the fastq_quality_trimmer and fastq_masker tools of the FASTX-Toolkit suite (http://hannonlab.cshl.edu/fastx_toolkit/) and their quality was assessed with the FastQC (www.bioinformatics.babraham.ac.uk/projects/fastqc/) application. The reads were analyzed with our own pipeline HTS flow (Bianchi et al., 2016). The HTS flow pipeline allows primary analysis, consisting of the quality control of the raw reads followed by filtering and the alignment to a reference genome, and secondary analysis, consisting in the differential gene expression and peak calling.

6.1.5.1 ChIP-seq data analysis

The HTS-flow pipeline aligned the ChIP-seq reads to the mouse reference genome (mm9) through the BWA aligner using default settings (Bianchi et al., 2016). Later, the MACS software (Zhang et al., 2008) was used for the peak calling, using a cut-off parameter q value<1e-5. The read counts found inside the genomic region were normalized considering the total number of aligned reads in that sample (library size).

The enrichment of a peak was defined considering the library size-normalized reads of the ChIP falling in the peak region (ChIPw) minus the library size-normalized reads of the input in the same region (inputw) as a logarithmic value, $\log_2$ (ChIPw - inputw).

Peaks were mapped and annotated as either promoter, intragenic or gene body according to the genomic position of the peak midpoint. More in details:

- promoter: the peak positioned within the genomic region of -2Kb and +1Kb from the annotated refgene start coordinate or transcriptional start site (TSS).

- gene body: the peak is located inside an annotated refgene (in a region different between > 1Kb from the TSS to its 3' end).

- intergenic region: the peak position does not match any of the aforementioned criteria.

Qualitative and quantitative heatmaps of ChIP-seq enrichment were generated using R with Bioconductor and compEpiTools packages, tools for computational epigenomics (Gentleman et al., 2004; Kishore et al., 2015).

6.1.5.2 RNA-seq analysis

RNA-Seq Next Generation Sequencing reads were aligned to the mm9 mouse reference genome using the TopHat aligner (version 2.0.8) with default parameters (Kim et al., 2013). RNA-seq duplicates were eliminated using rmdup function from the suite samtools (http://samtools.sourceforge.net/). Read counts were associated to each gene (based on UCSC-derived mm9 GTF gene annotations), using the featureCounts software (http://bioinf.wehi.edu.au/featureCounts/) setting the options -T 2 -p -P (Liao et al., 2014). Absolute gene expression was defined determining reads per kilobase per million mapped reads (RPKM) defining total library size as the number of reads mapping to exons only. DESeq2 was used to analyze RNA-seq data, as genes with q value > 0.05 (Love et al., 2014). Genes were hierarchically clustered with the R function hclust. Functional annotation was performed using the Gene Ontology categories of the bioinformatics tool Gene Set Enrichment Analysis (GSEA) by using default parameters of GSEA platform (Subramanian et al., 2005). In case of tumors, ΔDEG of tumors used for GSEA analysis was calculated as following: $\Delta DEG = \log_2FC(LyP6KO) - \log_2FC(LyWT)$. Only ΔDEG with $p_{adj}<0.05$ and $\Delta DEG > |0.5|$ were used for these analyses.

6.16 Statistical analysis.

All the experiments were performed at least in biological triplicates, apart from ChIP-seq analysis where only one biological replicate was used. Sample size was not predetermined but is reported in the respective figure legends. Two-tailed Student's t-test was used to compare between two groups and expressed as p-values. In the figures: *$p < 0.05$, **$p < 0.01$, ***$p < 0.001$, ****$p<0.0001$.

7. RESULTS

7.1 Pcgf6 loss accelerates Myc-induced lymphomagenesis

In order to understand if Pcgf6 can act as a tumor suppressor in Myc-driven lymphomagenesis, we took advantage of the *Eμ-myc* transgene (Adams et al., 1985) and of a recently published *Pcgf6*$^{fl/fl}$ conditional knock-out allele (hereafter *P6*$^{f/f}$) (Endoh et al., 2017) (Figure 7.1), in which the second and third exons of *Pcgf6* are flanked by LoxP sites, leading to their complete deletion and loss of Pcgf6 expression upon exposure to Cre recombinase. B-cell specific deletion of *Pcgf6*$^{fl/fl}$ was achieved with the *CD19-Cre* transgene (Rickert et al., 1997).

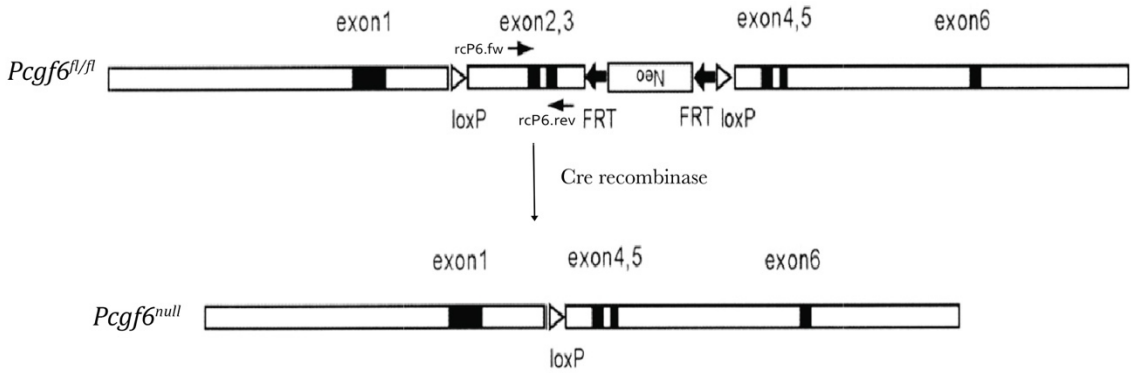

Figure 7.1 Schematic representation of *Pcgf6 allele.*
The second and the third exon of mouse *Pcgf6* are flanked by the two LoxP sites (open triangles). Upon exposure to a Cre recombinase, the exons 2 and 3 are completely removed, as indicated. The arrows are depicting the position of the primers used for qPRC in order to check the recombination of *Pcgf6* allele (Endoh et al., 2017).

We first derived compound CD19-Cre/P6wt/fl and Eμ-myc/P6wt/fl mice and crossed them to generate a cohort of CD19-Cre/Eμ-myc/P6fl/fl animals. In line with the presence of both the Pcgf6 locus (http://www.informatics.jax.org/marker/MGI:1918291) and the Eμ-myc transgene (Lefebure et al., 2017) on mouse chromosome 19, the co-occurrence of the recombinant

alleles was sub-mendelian (Table 4). The same was true for *Eμ-myc/P6*$^{wt/fl}$ mice in the absence of *CD19-Cre* (data not shown). Of note, the Mendelian ratio observed in *CD19-Cre/P6*$^{wt/fl}$ and *CD19-Cre/P6*$^{fl/fl}$ mice (i.e. in the absence of *Eμ-myc*) did not show any significant imbalance.

	Expected frequency	Observed frequency
CD19-Cre/P6$^{wt/wt}$	12.50%	12.14%
CD19-Cre/P6$^{wt/fl}$	25%	30.06%
CD19-Cre/P6$^{fl/fl}$	12.50%	17.34%
CD19-Cre/Eμ-myc/P6$^{wt/wt}$	12.50%	20.81%
CD19-Cre/Eμ-myc/P6$^{wt/fl}$	25%	16.76%
CD19-Cre/Eμ-myc/P6$^{fl/fl}$	12.50%	2.89%

Table 4. Frequency of different genotypes obtained by crossing *Eμ-myc/P6*$^{wt/fl}$ and *CD19-Cre/P6*$^{wt/fl}$ mice.
Genotype prevalence was calculated taking into account that *CD19-Cre* allele can only be heterozygous since crossing strategy was set up as following: *CD19-Cre* homozygous mice with a wild type mice; *Eμ-myc* could be either transgenic or non-transgenic; *Pcgf6* can be either wild type, heterozygous or homozygous from the crossing of *P6*$^{wt/fl}$ with *P6*$^{wt/fl}$

In order to generate sizeable cohorts of *CD19-Cre/Eμ-myc/P6*$^{wt/fl}$ and *CD19-Cre/Eμ-myc/P6*$^{fl/fl}$ animals, we set up further breedings between *CD19-Cre/P6*$^{fl/fl}$ and *Eμ-myc/P6*$^{fl/fl}$ animals. All the mice, either wild type, heterozygous or homozygous for the *Pcgf6*^{fl} allele, and bearing - or not - the *Eμ-myc* transgene, were monitored over a period of one year for lymphoma development. As expected, *Eμ-myc* mice developed aggressive lymphomas at about 4-5 months of age (Figure 7.2A, grey line), with characteristic enlargement of axillary, cervical and/or inguinal lymph nodes, and splenomegaly (Adams et al., 1985; Langdon et al., 1986). Remarkably, *Eμ-myc*-dependent lymphomagenesis was accelerated and became fully penetrant upon homozygous deletion of *Pcgf6* in B-cells (Figure 7.2A, red line), with

intermediate latency in heterozygous mice (Figure 7.2A, blue line), while no lymphomas arose in the absence of *Eμ-myc* regardless of the *Pcgf6* status. The lymphomas that developed in *CD19-Cre/Eμ-myc/P6*$^{wt/wt}$, *CD19-Cre/Eμ-myc/P6*$^{wt/fl}$ and *CD19-Cre/Eμ-myc/P6*$^{fl/fl}$ mice showed similar symptoms and distribution. Thus, consistent with our initial hypothesis, a reduced or null *Pcgf6* gene dosage led to disease acceleration in *Eμ-myc* mice.

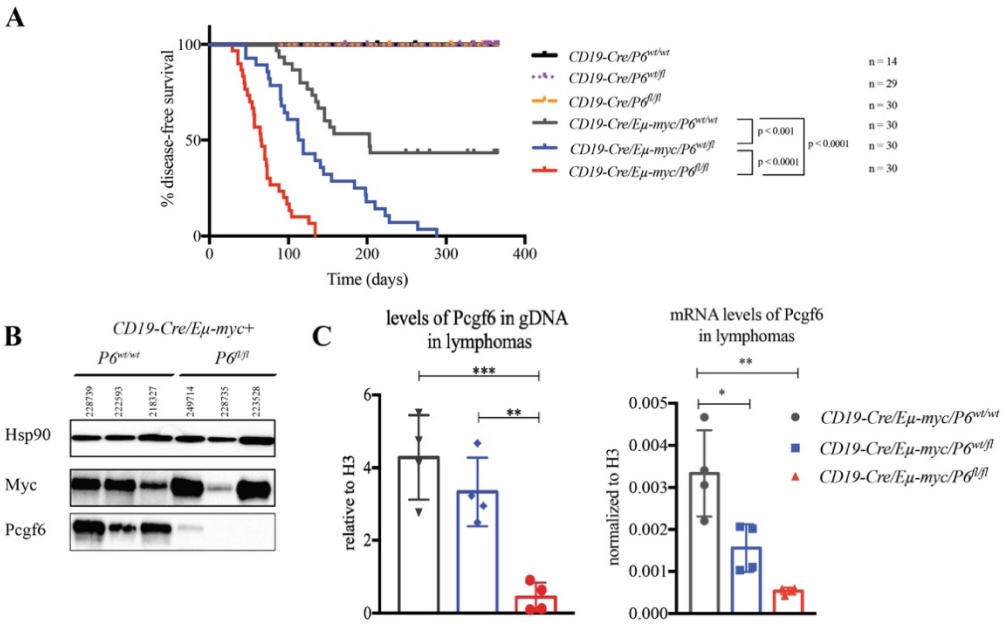

Figure 7.2 *Pcgf6* deletion accelerate *Eμ-myc* lymphomagenesis.
A. Kaplan-Meier survival curve of *CD19-Cre/Eμ-myc/P6*$^{f/f}$ mice. Group of mice with absence of *Eμ-myc* showed disease-free survival. Mice were scored as disease-positive and sacrificed when tumor masses became detectable by palpation in either the inguinal, cervical or axillary lymph nodes. The numbers represent number of animals in each group. The median tumor onset for these groups were as following: *CD19-Cre/Eμ-myc/P6*$^{wt/wt}$ 180; *CD19-Cre/Eμ-myc/P6*$^{wt/fl}$ 118; *CD19-Cre/Eμ-myc/P6*$^{fl/fl}$ 66 days. **B.** Western blot analysis of Pcgf6 and Myc in primary *CD19-Cre/Eμ-myc/Pcgf6*$^{f/f}$ tumors. Hsp90 was used as a loading control. **C.** Quantification of the RT-qPCR of wild type *Pcgf6* allele performed on the gDNA extracted from the sorted CD19^{+} B-cell population of primary infiltrated lymph nodes. Samples were normalized to H3 genes. **D.** qPCR performed on the mRNA extracted from sorted CD19+ B-cells from infiltrated lymph nodes of *CD19-Cre/Eμ-myc/Pcgf6*$^{f/f}$ mice. Numbers above pictures of gel indicate the unique ID number for each mouse analyzed. * p <0.05, ** p < 0.005, **** p < 0.0001.

Western Blot analysis of infiltrated lymph nodes showed that lymphomas expressed high levels of Myc, albeit with significant variability. Hence, addressing whether Pcgf6 loss has any systematic impact on Myc protein levels, though unlikely at this stage, would require further analysis with higher numbers of lymphomas. As expected, Pcgf6 expression was lost

upon homozygous deletion of the gene – trace amounts in occasional samples being most likely due to the presence of non-B-cells that do not express Cre (Figure 7.2B). Pcgf6 deletion was also measured by analyzing genomic DNA (Figure 7.2C) and mRNA levels (Figure 7.2D), confirming a recombination efficiency of ~ 90%. In the *Eμ-myc* mouse model, lymphomas can derive from either naïve mature B-cells ($B220^{+}IgM^{+}$) or B-cell precursors ($B220^{+}$ IgM^{-}) (Langdon et al., 1986). The profiling of B220 and IgM in multiple primary lymphomas showed similar proportions naïve vs. immature tumors in all of our experimental groups, in line with previously observed frequencies in the *Eμ-myc* model (Adams et al., 1985; Campaner et al., 2010; Gorrini et al., 2007), excluding a role for Pcgf6 on determining a different cell of origin of the observed lymphomas (Figure 7.3).

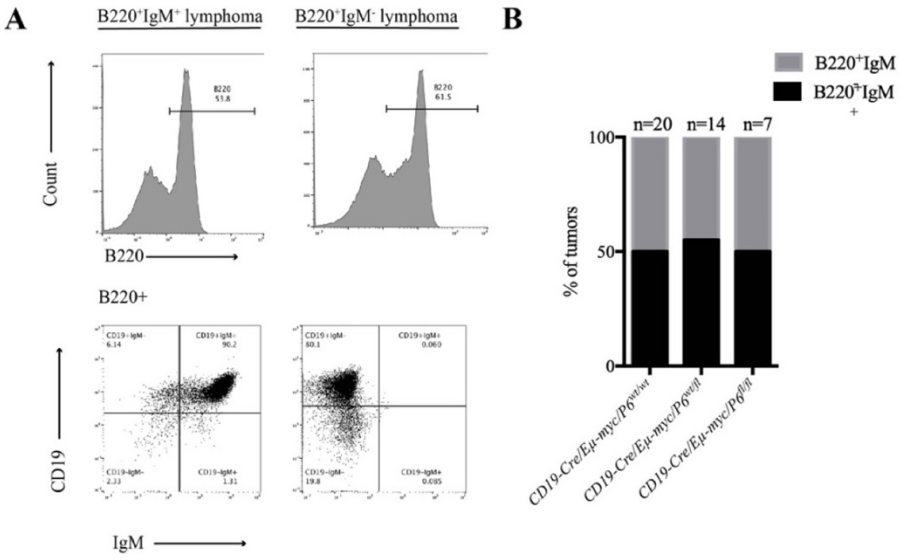

Figure 7.3 Distribution of either naïve or immature B-cell *CD19-Cre/*Eμ*-myc/Pcgf6$^{f/f}$* tumors is balanced.
A. FACS profiles of two different tumors, either of immature B-cell ($B220^{+}IgM^{-}$) or naïve B-cell origin ($B220^{+}IgM^{+}$). Number indicated the percentage of lymphoma cells in each gate, relative to the total infiltrated cells (top panel) or to the population in the gate indicated above the plot (bottom panel). **B.** Graph represent quantification of the FACS analysis according to the status of B220 and IgM. Numbers above each bar plot represent number of mice analyzed for each genotype.

The *Eμ-myc* model is characterized by an initial polyclonal expansion of B-cells, followed by the emergence of monoclonal tumors (Adams et al., 1985). In this setting, mutations that accelerate lymphomagenesis may either enlarge the pre-tumoral pool, thus enhancing the emergence of a monoclonal malignancy, or may allow the development of multiple tumor clones (Adams et al., 1985). In order to address the clonal composition of our lymphomas, we sorted $CD19^+$ B-cells from tumor samples, extracted genomic DNA, and used PCR to analyze VDJ rearrangements at the Igh locus: the results showed that both *CD19-Cre/Eμ-myc/P6*$^{wt/wt}$ and *CD19-Cre/Eμ-myc/P6*$^{fl/fl}$ lymphomas were mainly of monoclonal origin (with 1/6 and 2/6 oligoclonal tumors, respectively), as judged by the prevalence of a V_H7183 to J_H-D_H recombination (Figure 7.4). We infer that Pcgf6 deletion does not impair VDJ recombination. Altogether, the above data show that loss of *Pcgf6* accelerates B-cell lymphomagenesis in *Eμ-myc* mice, without altering the gross pathological and cellular features of the resulting tumors.

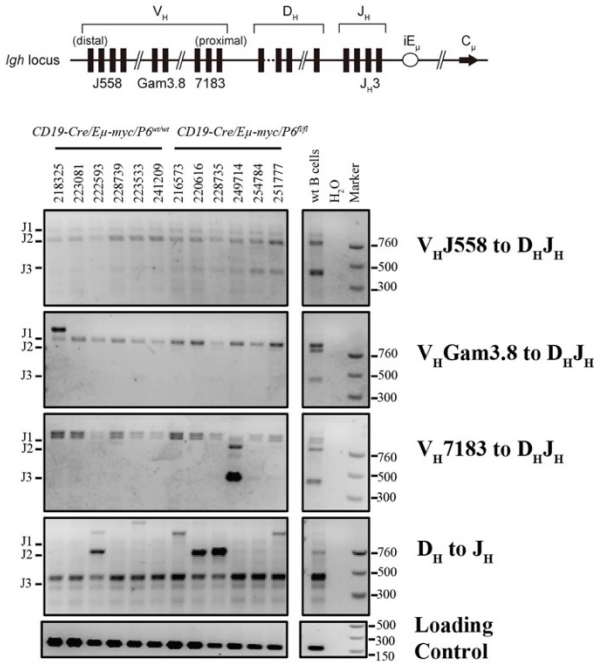

Figure 7.4 *CD19-Cre/Eμ-myc/P6*$^{f/f}$ tumors are monoclonal based on VDJ recombination.
Top - Schematic representation of the germline *Igh* locus (Inoue et al., 2015). Bottom - PCR analysis of D_H-J_H and V_H-D_HJ_H rearrangements performed on the genomic DNA from sorted $CD19^+$ B-cells of *CD19-Cre/Eμ-myc/P6*$^{wt/wt}$ and *CD19-Cre/Eμ-myc/P6*$^{fl/fl}$ mice (6 mice per group). Numbers above pictures of gel indicated unique ID number for each mouse analyzed.

7.2 Pcgf6 is not required for B-cell development

The aforementioned effects of Pcgf6 deletion on Myc-induced lymphomagenesis called for a careful examination of its consequences on normal B-cell development, in the absence of the oncogene. In this regard, it is noteworthy that the *CD19-Cre* transgene is expressed from the very onset of B-cell ontogeny. Indeed, CD19 itself is a hallmark of the B-cell lineage, expressed from pro-B-cell stage in the bone marrow and throughout B-cell development and differentiation (Krop et al., 1996). At the functional level, CD19 is a transmembrane protein with a dual role, acting either as an adaptor to recruit cytoplasmic proteins to the membrane, or in complex with CD21 to establish intrinsic B-cell signaling threshold modulating both BCR-dependent and independent signaling (Zhou et al., 1992). It plays a role in both antigen-independent development as well as activation of B-cells mediated by immunoglobulins.

Composite *CD19-Cre/P6$^{f/f}$* animals were analyzed to determine a possible interference of Pcgf6 loss with B-cell differentiation in two major lymphoid organs, bone marrow (BM) and spleen. As shown in Figure 7.5, flow cytometric analysis of BM cell suspensions revealed no significant changes in the percentage of B220^{+} cells between *CD19-Cre/P6$^{wt/wt}$*, *CD19-Cre/P6$^{wt/fl}$* and *CD19-Cre/P6$^{fl/fl}$* mice. A series of additional markers (B220, IgM, CD43, CD25 and CD19), revealed no alterations in the Pre-B, Pro-B, Pre-Pro B, early and late Pro-B cell compartments, neither as percentage or total cell number of each subset (Figure 7.5A, B, C). The same was true for either mature (B220^{+}IgM^{+}) or recirculating mature B-cell populations (B220^{hi}IgM^{int}).

In order to analyze the splenic B-cell compartment in the same mice, we performed immune-staining followed by flow cytometry of total splenic B-cells, such as follicular zone (FO), marginal zone (MZ), transitional type 1 (T1), type 2 (T2) or type 3 (T3) markers (Carsetti et al., 1995). In line with the results obtained in the BM, no major differences in the different B-

cell fractions in spleen were observed between the experimental groups (Figure 7.6). Most importantly here, Pcgf6 was efficiently deleted in *CD19-Cre/P6$^{fl/fl}$* B-cells (Figure 7.7), implying that the absence of alterations in the B-cell compartment of these mice was due neither to a low-recombination efficiency, nor to the counter-selection of recombined cells. Thus, at this level of resolution, loss of Pcgf6 did not cause detectable alterations in B-cell development, differentiation and homeostasis.

Altogether, we conclude that disease acceleration in *CD19-Cre/Eμ-myc/Pcgf6$^{fl/fl}$* mice did not stem from Pcgf6-dependent alterations in B-cell homeostasis *per se*, but most likely from select alterations in Myc-induced lymphomagenesis. In this regard, the prevalently monoclonal nature of the lymphomas suggests that Pcgf6 deletion could act at an early stage, most likely by expanding the population of pre-tumoral B-cells susceptible to undergo tumor progression. Such an effect, which we are currently investigating in our model, has been reported multiple times in the past, and is most frequently associated with a decrease in Myc-induced apoptosis (Eischen et al., 1999; Schmitt et al., 1999). As an alternative – but not exclusive – explanation, Pcgf6 may act trough non-cell autonomous mechanisms, such as immune-surveillance and tumor cell rejection, a possibility that will be considered below (see chapter 7.8).

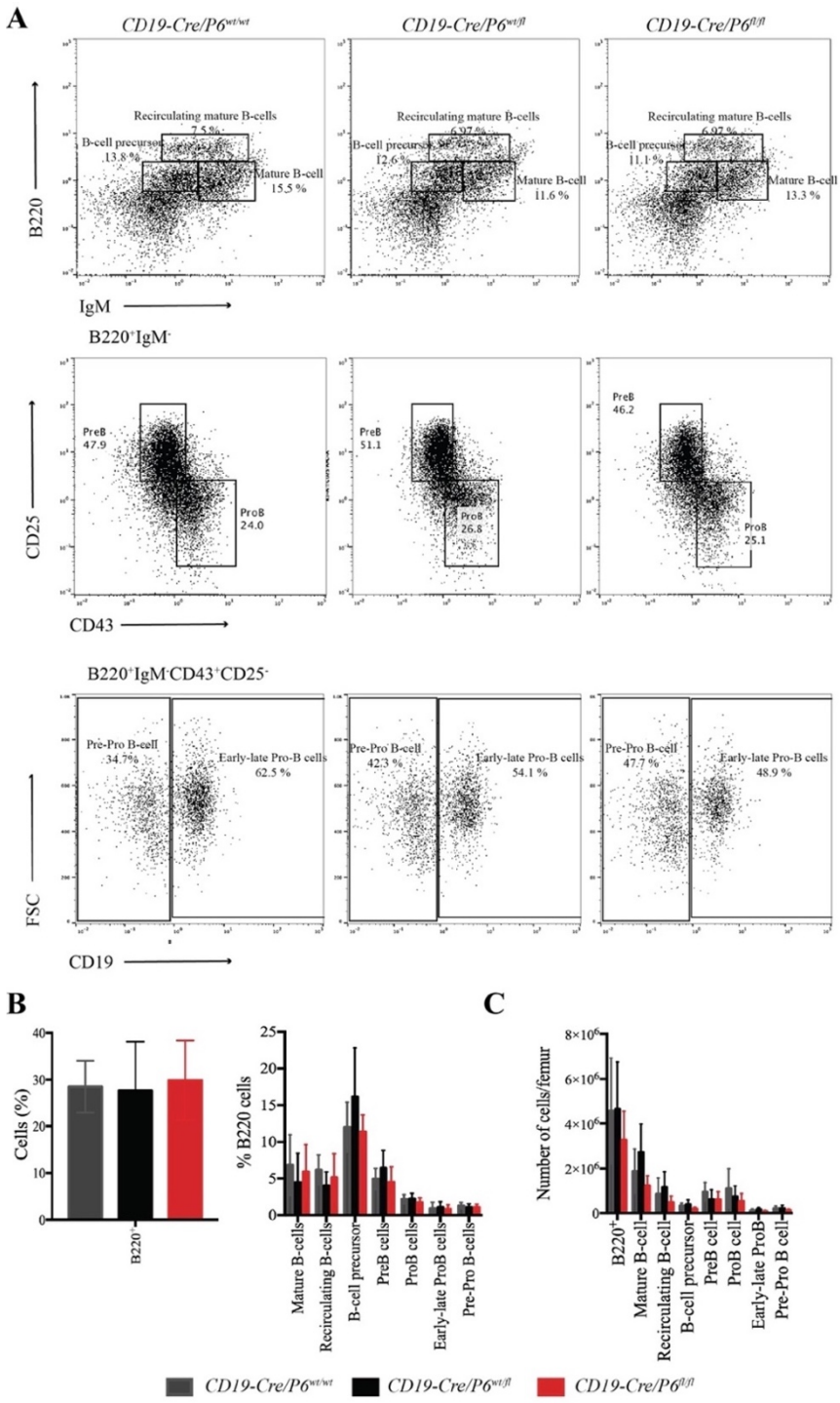

Figure 7.5 *Pcgf6* deletion does not alter BM-derived B-cell fractions.
A. Representative flow cytometric analysis of BM B-cells in 6-week-old *CD19-Cre/P6*$^{wt/wt}$, *CD19-Cre/P6*$^{wt/fl}$ and *CD19-Cre/P6*$^{fl/fl}$ mice. Number indicated the percentage of BM cells in each gate, relative to the total BM cells (top panel) or to the population indicated above the plot (bottom). **B.** Left- Percentage of B220^{+} population presented as % of total cells; right - percentage of mature B-cells (B220^{+}IgM^{+}), recirculating mature B-cells (B220^{hi}IgM^{int}) or B-cell precursors – Pre-B (B220^{+}IgM^{-}CD43^{-}CD25^{+}), Pro-B (B220^{+}IgM^{-}CD43^{+}CD25^{-}), Pre-Pro-B (B220^{+}IgM^{-}CD43^{+}CD25^{-}CD19^{-}) and early and late Pro-B-cells (B220^{+}IgM^{-}CD43^{+}CD25^{-}CD19^{+}) cells, represented as % of B220 cells and averaged from n=8 mice. Numbers represent the percentage of cells for each subset analyzed relative to total BM cells. **C.** Graph represent total number of cells of each fraction analyzed, isolated from one femur.

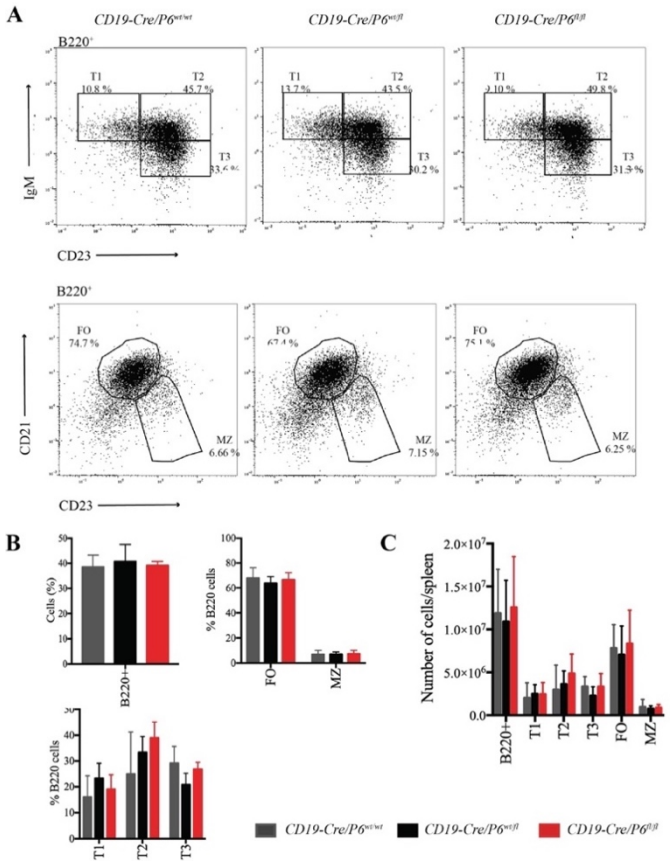

Figure 7.6 *Pcgf6* deletion does not alter splenic B-cell fractions
A. Representative flow cytometric analysis of splenic cell suspensions from 6-week-old wild type, *CD19-Cre/P6*$^{wt/fl}$ and *CD19-Cre/P6*$^{fl/fl}$ mice. The numbers indicate the percentage of cells in each gate, relative to splenic B220^{+} cells, with cell subsets defined as follows: T1 (B220^{+}IgM^{hi}CD23^{-}), T2 (B220^{+}IgM^{hi}CD23^{+}), T3 (B220^{+}IgM^{lo}CD23^{+}), FO (B220^{+}CD21^{int}CD23^{+}) and MZ (B220^{+}CD21^{high}CD23^{lo}). **B**. Left – percentage of B220^{+} population represented as % of total cells; right- percentage of the FO and MZ, relative to total splenocytes, represented as % of B220^{+} cells and averaged from n=8 mice; bottom - percentage of the T1,T2 and T3 relative to total splenocytes, represented as % of B220^{+} cells and averaged from n=8 mice. **C.** Graph represent total number of cells of each fraction analyzed, isolated from spleen.

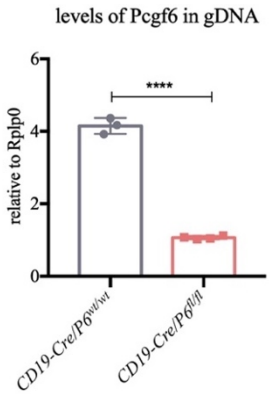

Figure 7.7 *Pcgf6* is recombined upon exposure to CD19-*Cre* recombinase.
Graph representing the quantification of qPCR of Pcgf6 performed on the gDNA of the sorted CD19^{+} B-cell population isolated from the spleen. Wild type Pcgf6 allele was measured, with normalization to the Rplp0 mRNA. **** $p<0.0001$.

7.3 Pcgf6 is not required for Myc binding to chromatin

The cooperation between Myc overexpression and Pcgf6 loss observed in Myc-driven lymphomagenesis is in concordance with our starting hypothesis that the PRC1.6 complex (containing Mga, Max and Pcgf6) and Myc/Max are competing for binding to common target genes, which in turn may be promoting lymphomagenesis. In order to verify this model, we performed chromatin immunoprecipitation coupled with high-throughput sequencing (ChIP-seq) for Myc, Max and Pcgf6 (note that Mga antibodies yielded no conclusive results so far). Besides these factors, we also profiled the PRC2 and/or PRC1-mediated histone marks, H3K27me3 and H2AK119Ub, as well as the active histone marks, H3K4me3, H3K4me1 and H3K27ac. We should thus be able to (i.) determine whether Pcgf6 associates either with PRC-repressed or, like Myc (Guccione et al., 2006; Kress et al., 2015; Sabò et al., 2014b), with active regulatory elements in lymphomas, and (ii.) address the possible effect of Pcgf6-kockout on Myc binding patterns in lymphomas.

To perform the ChIP-seq experiments, we isolated lymphoma cells from *CD19-Cre/Eμ-myc/P6*$^{wt/wt}$ (hereafter LyWT) and *CD19-Cre/Eμ-myc/P6*$^{fl/fl}$ (hereafter LyP6KO) and expanded these cells *in vitro*. Both lymphomas developed from naïve B-cells based on immune-staining with CD19 and IgM surface marker (Figure 7.8A). As expected, the LyP6KO cells lacked the Pcgf6 protein (Figure 7.8B). Myc and Max protein and mRNA levels were variable, which could be due to clonal variability (Figure 7.8B, C).

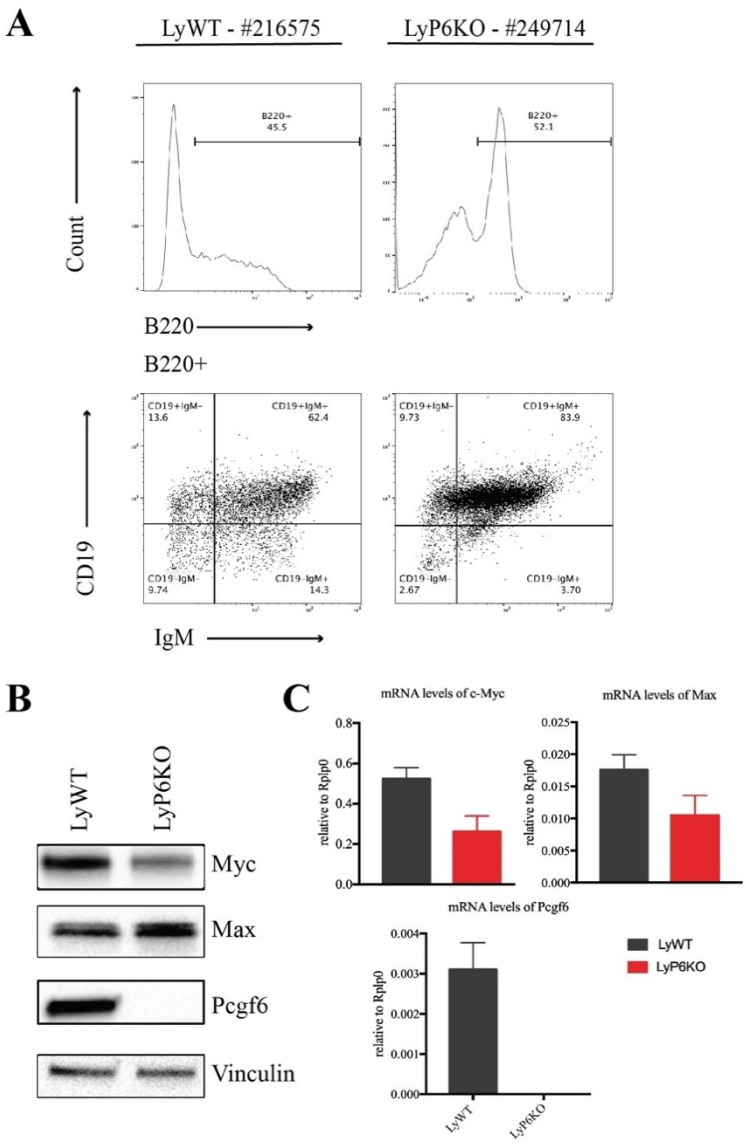

Figure 7.8 LyP6KO does not express Pcgf6 protein or mRNA levels, and is of the same origin as LyWT

A. FACS profiles of LyWT and LyP6KO. Upper panel represent $B220^{+}$ population, bottom $CD19^{+}IgM^{+}$. **B.** Western Blot of Myc, Max and Pcgf6 in LyWT and LyP6KO. **C.** Graph representing mRNA levels of c-Myc, Max and Pcgf6 normalized to Rplp0 in LyWT and LyP6KO. Primer used for detecting Pcgf6 mRNA expression are annealing on the LoxP sites of Pcgf6 allele.

To globally investigate the relationships between the genomic distributions of Myc, Max and Pcgf6 in the two lymphomas, we generated quantitative heatmaps representing their normalized ChIP-seq intensities, alongside the histone marks (all ranked according to Myc-binding intensity (Figure 7.9) As previously reported (Sabò et al., 2014b), Myc and Max

preferentially associated with active elements (marked by H3K4me3, H3K4me1 and H3K27ac) (Figure 7.9): H3K4me3 predominated over H3K4me1 at promoters and the opposite occurred at distal sites, identifying the latter as *bona fide* enhancers (Calo and Wysocka, 2013; Zhou et al., 2011). Surprisingly, Pcgf6 closely ranked alongside the same active elements, did not co-localize with the repressive marks H3K27me3 and H2AK119Ub, and showed preferential binding to promoters, as previously observed in mESCs (Scelfo et al., 2019) (Figure 7.9 and Figure 7.10D). We note here that the Pcgf6 signal was specific, as it was selectively lost in the LyP6KO sample (Figure 7.9 and Figure 7.10C).

We then examined the possible effects of Pcgf6 loss on Myc/Max binding profiles: remarkably, higher numbers of Myc- and Max-bound peaks were called in LyP6KO when compared to LyWT (Figure 7.10A, B and C). However, while increased binding of Myc was observed in LyP6KO, it was not specific for the previously Pcgf6-bound regions, neither at promoters, nor at distal sites (Figure 7.10F). In fact, while most (ca. 2/3) of the Myc/Max peaks called in the LyWT sample were located in promoter regions and virtually all were included in LyP6KO sample (Figure 7.10A, B), the new peaks called in LyP6KO were mainly distal (either intra- or extragenic locations) (Figure 7.10D). Surprisingly, Pcgf6-bound and Myc-bound peaks identified in LyWT showed major overlap, which implies that Myc and Pcgf6 are co-localizing, rather than competing for the same sites (Figure 7.10E).

Altogether, while Myc/Max and Pcgf6 show consistent binding to active promoters, our results do not point to a competition between Pcgf6 and Myc for the same genomic regions in B-cell lymphomas, contrasting the premises made with our starting hypothesis.

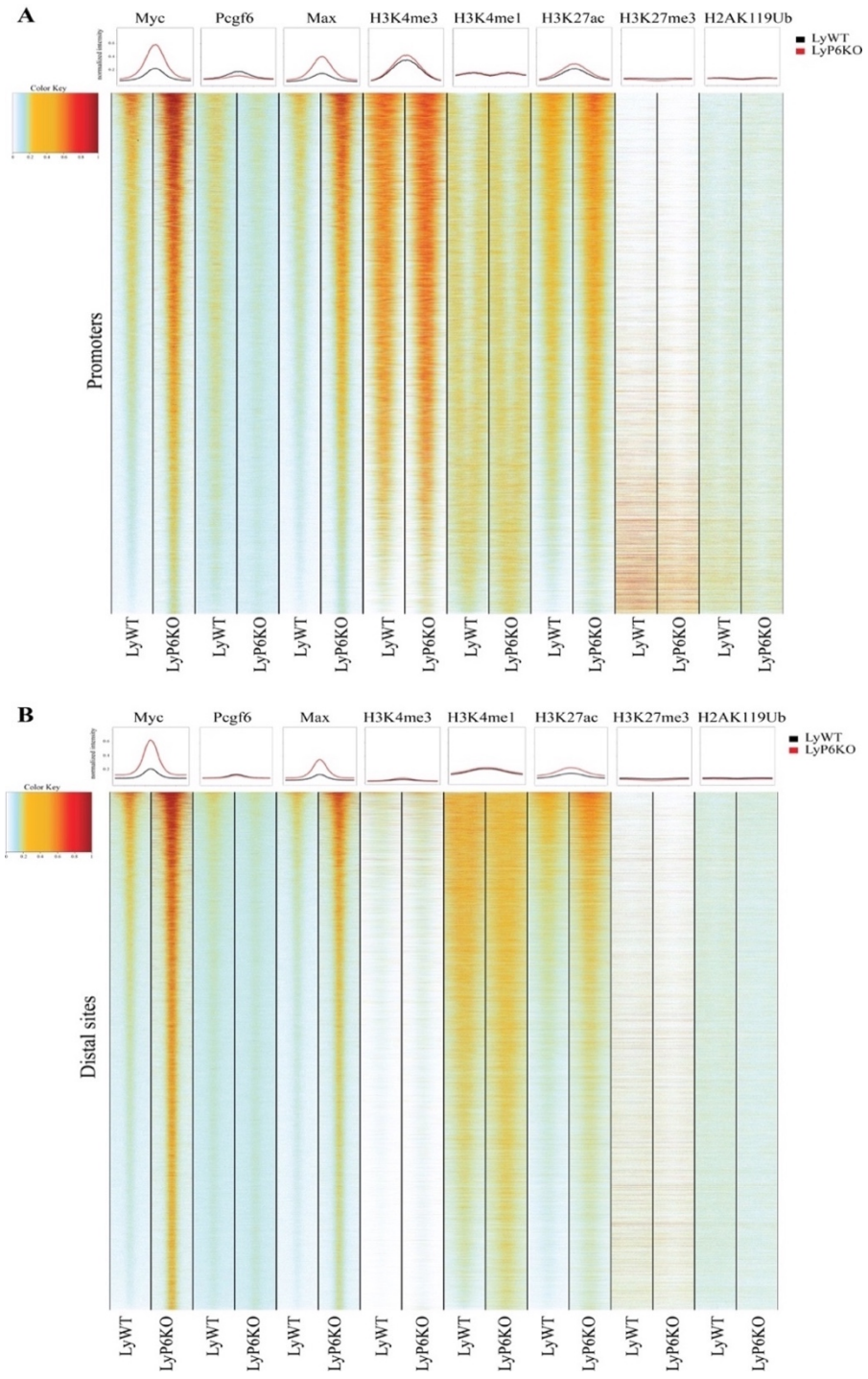

Figure 7.9 Peak density heatmap of Myc, Pcgf6, Max and histone marks in LyWT and LyP6KO.
A. Heatmap representing normalized ChIP-seq intensity for the indicated Myc, Pcgf6, Max proteins and histone marks over -2kb +1kb around TSS of the union of Myc, Pcgf6 and Max-bound promoters in stabilized lymphomas LyWT and LyP6KO. **B.** Heatmap representing normalized ChIP-seq intensity for the indicated Myc, Pcgf6, Max proteins and histone marks at the distal sites in stabilized lymphomas LyWT and LyP6KO. The panels A and B represents every annotated promoter in all the chromosomes that was called either as Myc-associated, Max-associated or Pcgf6-associated by ChIP-seq identified in at least one of the stabilized lymphomas. Above each IP is represented cumulative enrichment deposition centered at the peak summit for the indicated proteins in LyWT (black) and LyP6KO (red). ChIP enrichments are normalized to the input.

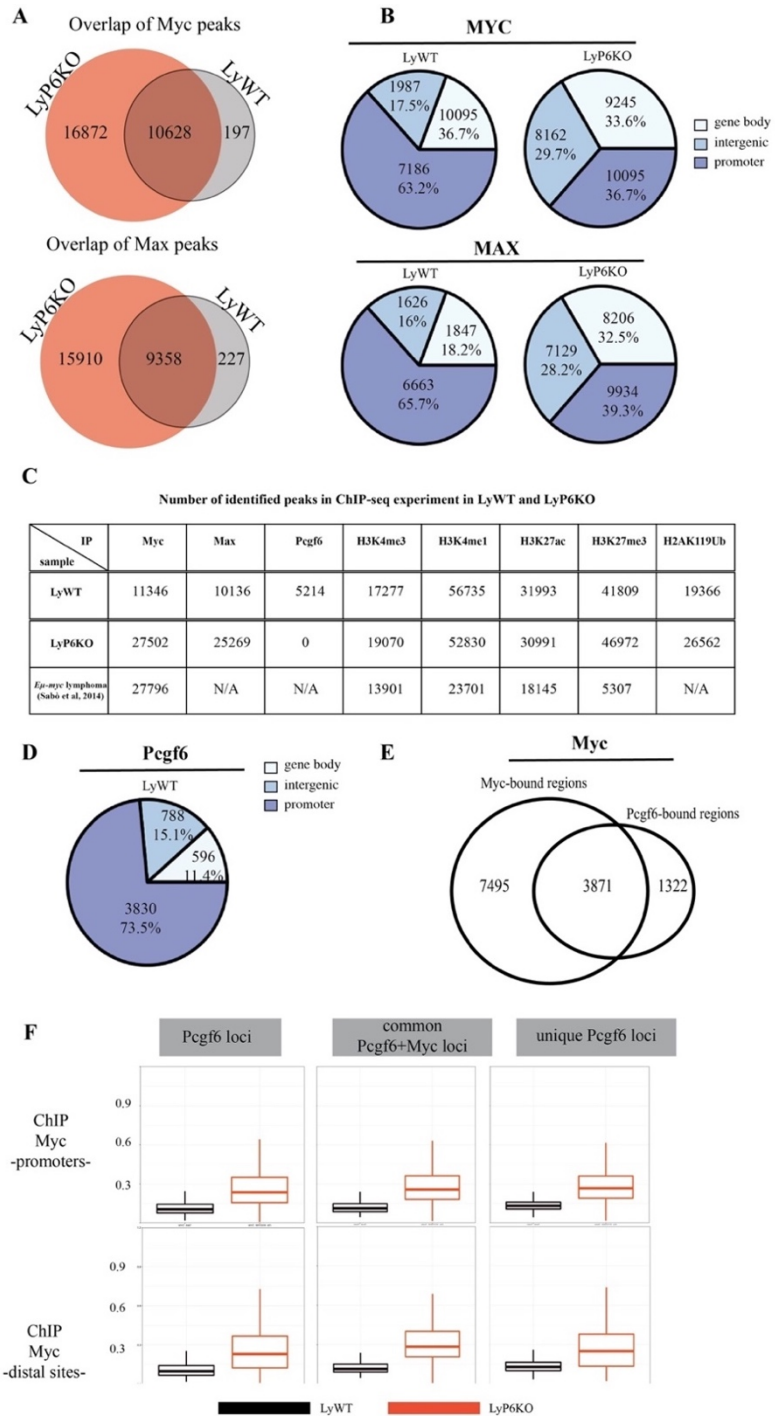

IP / sample	Myc	Max	Pcgf6	H3K4me3	H3K4me1	H3K27ac	H3K27me3	H2AK119Ub
LyWT	11346	10136	5214	17277	56735	31993	41809	19366
LyP6KO	27502	25269	0	19070	52830	30991	46972	26562
Eμ-myc lymphoma (Sabò et al, 2014)	27796	N/A	N/A	13901	23701	18145	5307	N/A

Figure 7.10 Vast majority of Myc and Max bound peaks are specific for LyP6KO.
A. Venn diagram representing the overlap of Myc-bound peaks (upper) and Max-bound peaks (bottom) in LyWT and LyP6KO. **B.** Pie charts showing genomic distribution of Myc and Max binding sites. The number of peaks is reported in subgroups on the basis of annotation: peaks on promoters, in intergenic region and gene body or intragenic regions. **C.** Table summarizing the number of peaks identified in each ChIP-seq experiment performed, including also previously published data in *Eμ-myc* lymphoma (Sabò et al., 2014b). **D.** Pie charts showing genomic distribution of Pcgf6 in LyWT. The number of peaks is reported in subgroups on the basis of annotation: peaks on promoters, in intergenic region and gene body or intragenic regions. **E.** Venn diagram representing overlap of Myc- and Pcgf6-bound regions in LyWT. **F.** Box plot presenting Myc enrichment score at the promoters (upper) or at the distal sites (bottom) in Pcgf6-bound loci, Pcgf6 and Myc overlapping loci and unique Pcgf6 loci.

Finally, a word of caution should be made here concerning the above ChIP-seq profiles. In particular, the numbers and distribution of Myc peaks called in LyP6KO are in line with previously published results for Myc in WT *Eμ-myc* lymphomas (Figure 7.10C) (Sabò et al., 2014b). Hence, the smaller numbers of peaks in our LyWT sample appear paradoxical, also considering the higher Myc level observed in WB analysis (Figure 7.8B). At the present time, this could have several contrasting explanations, including (i.) technical variability: for example, a less efficient Myc immunoprecipitation in our LyWT chromatin sample; (ii.) clonal variability: different tumor clones can show variable patterns (Sabò et al., 2014b), but this would be unrelated to the status of Pcgf6; (iii.) a true biological difference: Pcgf6 deletion may indeed cause the opening of more elements in the genome, though not simply related to its binding profiles in WT lymphomas. In order to address this issue, we undertook a different approach, which will be discussed in the following chapter.

7.4 Silencing of Pcgf6 in *Eμ-myc* lymphomas does not alter Myc binding

To verify which of the above scenarios may be relevant, we sought to knock down Pcgf6 in LyWT cells, thus confining our comparisons in the same lymphoma, with and without Pcgf6. In this way, we could avert the potential issue of tumor clonality and analyze the direct consequences of Pcgf6 loss on Myc/Max binding to chromatin. Toward this aim, we infected the cells with retroviruses expressing shRNAs targeting either Pcgf6 (shP6#1 and shP6#2), or *Renilla Luciferase* (shRen) as control, and assessed Pcgf6 expression after 72 hours of selection with puromycin (Figure 7.11A, B). Both Pcgf6 shRNAs yielded more than 80% knockdown of Pcgf6 at the mRNA level, reflected by a clear reduction of the Pcgf6 protein, compared either to parental cell line or to shRen sample (Figure 7.11A, B). Importantly, in these conditions Myc and Max mRNA and protein levels were comparable between the

samples. Furthermore, Pcgf6 knockdown had no significant impact on the proliferation rate of lymphoma over a period of 7 days, even though the knock down stayed constant throughout this period of time (Figure 7.11C).

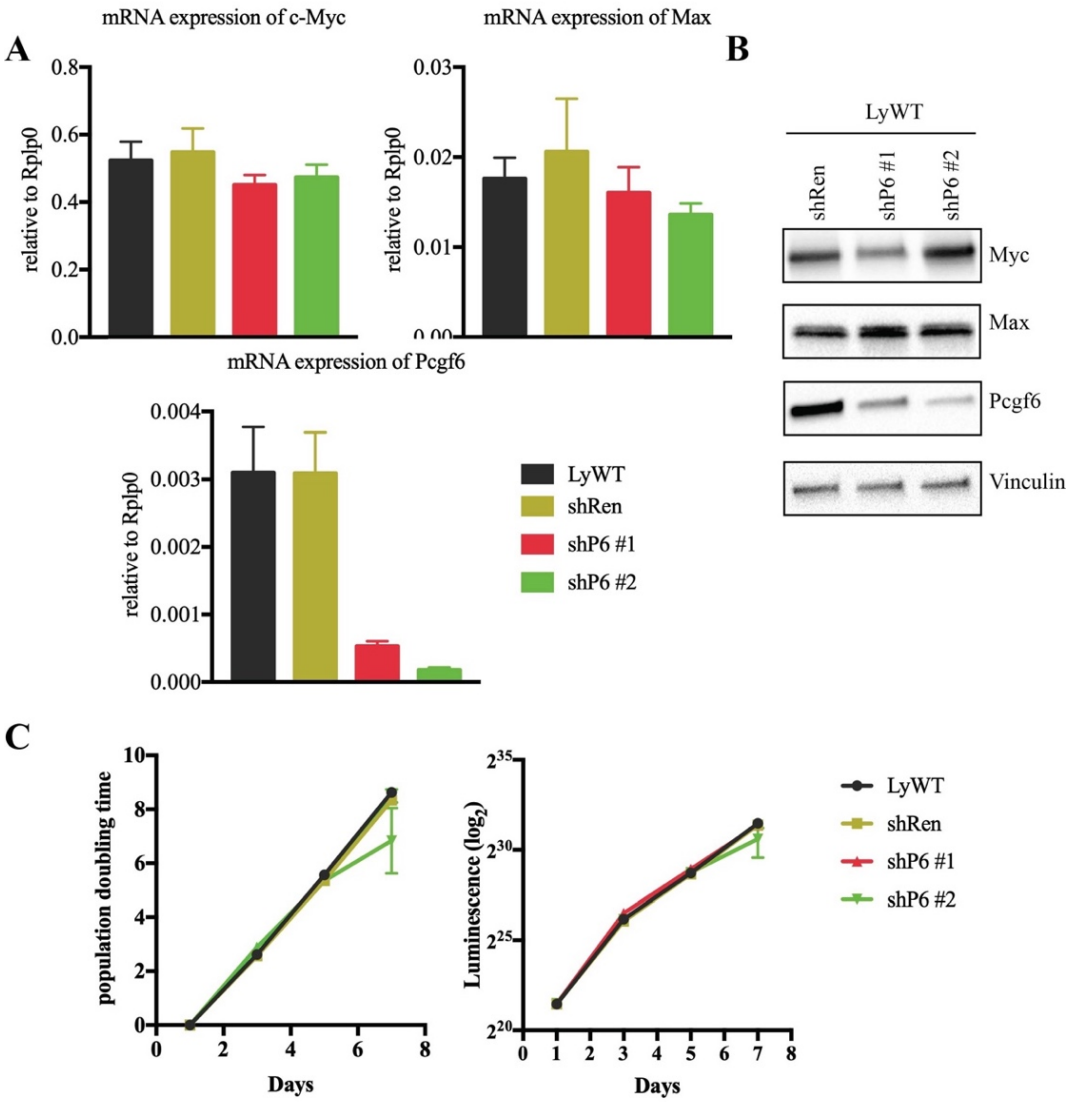

Figure 7.11 Pcgf6 knockdown in LyWT cells.
LyWT cells were infects with shRNAs targeting Pcgf6 (shP6#1,2) or Renilla Luciferase (shRen), as indicated. **A.** Pcgf6, Myc and Max mRNA levels, normalized to Rplp0. **B.** Western Blot analysis of Myc, Max and Pcgf6. **C.** Graph on the left represents the population doubling time calculated as followed: population doubling (PDs) = the log of the ratio of the final count (N) to the starting count (day 1 - Xo), divided by the log 2. PD = [log(N / Xo)] / log 2. On the right is represented the relative number of viable cells measured by Cell Titer Glo Luminescent Cell Viability assay.

We then performed ChIP-seq analysis for Myc, Max and histone marks (H3K4me3, H3K4me1, H3K27ac and H3K27me3) in the shRNA-infected cells. This experiment yielded high numbers of both Myc- and Max-bound peaks in all three conditions (Figure 7.12A), with almost 90% overlap between the samples (Figure 7.12B). Around 40% of either the Myc or Max peaks mapped at promoters, while the rest were equally distributed among intergenic regions and gene bodies (Figure 7.12C). These numbers and distributions were in fact similar to those of Myc and Max in LyP6KO (Figure 7.10), while different from LyWT. Indeed, the overlap of Myc peaks between the LyWT, LyP6KO and shRen samples confirmed that both LyP6KO and shRen (samples with more Myc-bound peaks identified) contained most of the Myc-bound peaks called in LyWT. Thus, suggesting that most likely the ChIP of Myc in LyWT was less efficient (Figure 7.12D). Moreover, the genomic distribution of Myc and Max-bound sites in these lymphomas, together with H3K4me3, H3K4me1, H3K27ac and H3K27me3 (Figure 7.13), further confirmed that Myc and Max were highly overlapping on the genome and that Pcgf6 silencing did not further alter the distribution of Myc. Again, Myc and Max-bound regions were decorated by histone marks of transcriptionally active chromatin (H3K4me3, H3K4me1 and H3K27ac), while low on H3K27me3, confirming that Myc and Max associated with active promoters and enhancers (Sabò et al., 2014b).

The above results support a scenario whereby the low number of Myc and Max peaks identified in LyWT, and therefore the supposed differences between LyWT and LyP6KO, were in fact derived from a technical artefact, and not due to the lack of Pcgf6 and its possible effect on the chromatin opening. Altogether, the available data suggest that Pcgf6 is not displacing Myc/Max from the chromatin, contradictory to our initial hypothesis. However, generation of ChIP-seq profiles with proper spike-in control are needed in order to exclude future variabilities in ChIP-seq efficiency.

A

Number of identified peaks in ChIP-seq experiment in LyWT upon knockdown of Pcgf6

IP / sample	Myc	Max	H3K4me3	H3K4me1	H3K27ac	H3K27me3
shRen	26180	17797	18378	51470	20050	41358
shP6 #1	24255	18468	18334	49271	21687	52743
shP6 #2	23267	17154	18880	51884	20119	39759

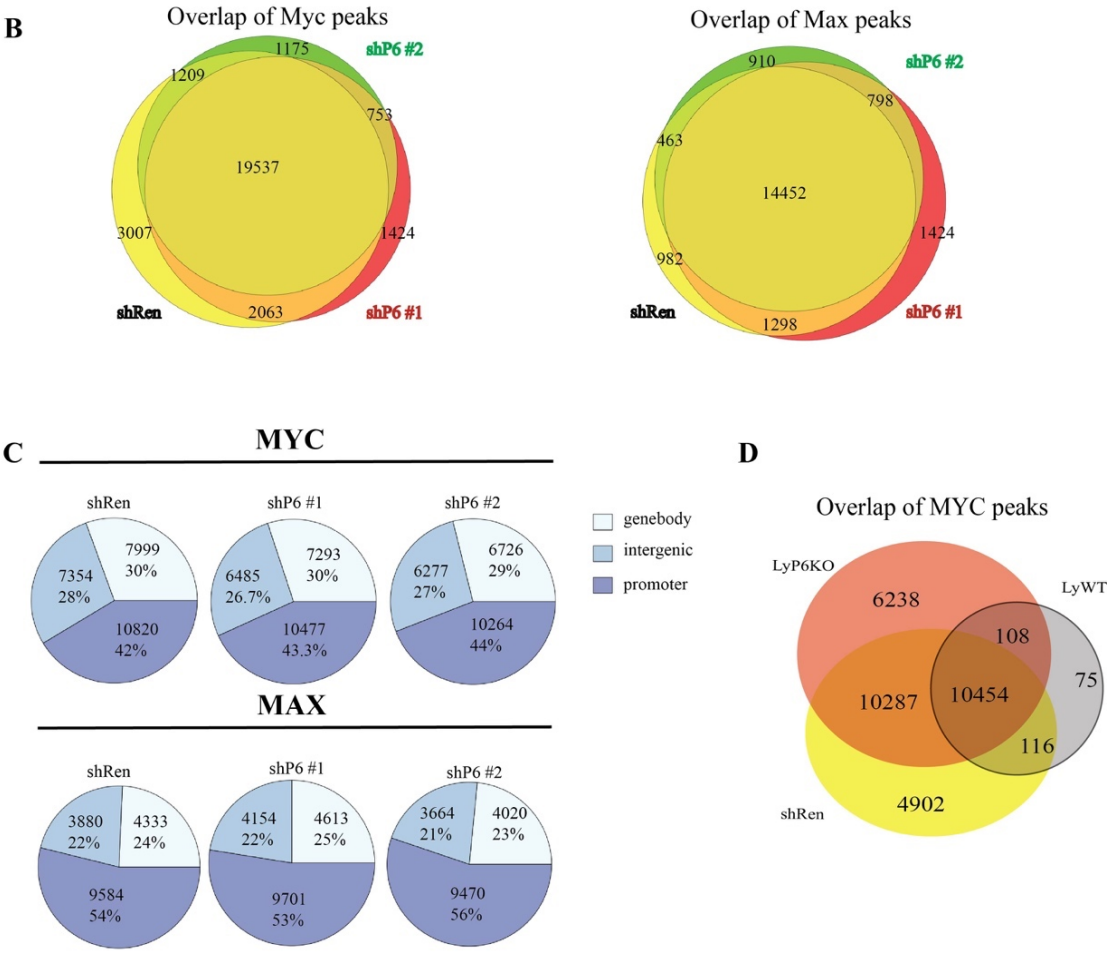

Figure 7.12 Distribution of Myc and Max binding sites does not change upon KD of Pcgf6.
A. Table summarizing the number of peaks identified in each ChIP-seq experiment performed. The first row presents different IP performed, while first column presents different lymphoma cell lines were ChIP experiments were performed. **B.** Venn diagram representing overlap of Myc-bound peaks (upper) or Max-bound peaks (bottom) in shP6 #1 (red), shP6 #2 (green) and shRen (yellow). **C.** Pie charts showing genomic distribution of Myc and Max binding sites. The number of peaks is reported in subgroups on the basis of annotation: peaks on promoters, in intergenic region and gene body or intragenic regions. **D.** Venn diagram representing overlap of Myc-bound peaks in LyWT (grey), LyP6KO (red) shRen (yellow).

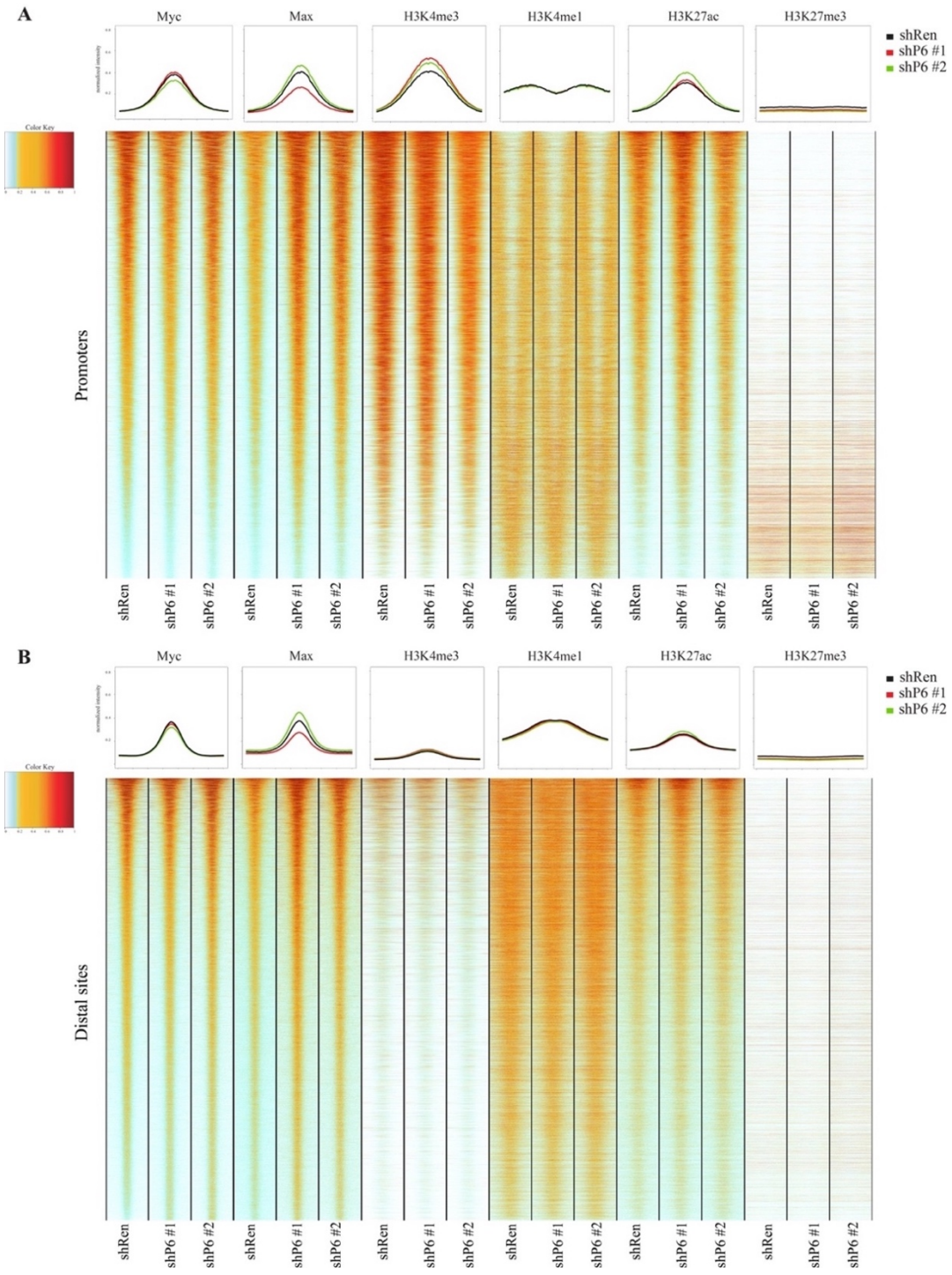

Figure 7.13 Peak density heatmap of Myc, Pcgf6, Max and histone marks in LyWT upon knockdown of Pcgf6

A. Heatmap representing normalized ChIP-seq intensity for the indicated Myc and Max proteins and histone marks over -2kb +1kb around TSS of the union of Myc and Max-bound promoters in shRen, shP6 #1 and #2. **B.** Heatmap representing normalized ChIP-seq intensity for the indicated Myc and Max proteins and histone marks at the distal sites in shRen, shP6 #1 and #2. The panels A and B represents every annotated promoter in all the chromosomes that was called either as Myc-associated or Max-associated by ChIP-seq identified in at least one of the three samples. Above each IP is represented cumulative enrichment deposition centered at the peak summit for the indicated proteins in shRen (black), shP6#1 (red) and shP6#2 (green). ChIP enrichments are normalized to the input.

7.5 Loss of Mga does not impair Myc-induced lymphomagenesis

The tumor suppressor activity of Pcgf6, demonstrated by the above data, suggested that the same might apply to Mga/Max dimers, in the context of the PRC1.6 complex. In order to address this question, we decided to target *Mga* in the *Eμ-myc* mouse model, taking advantage of the conditional Mga^{Inv} allele generated by the German Gene Trap Consortium (Washkowitz et al., 2015), in which intron 3 was targeted with an inverted cassette including a splice acceptor and the β-geo marker (encoding β-galactosidase and neomycin resistance) followed by a poly-adenylation site. Thus, in the absence of Cre recombinase, Mga^{Inv} produces a wild-type *Mga* transcript (Figure 7.14A, henceforth Mga^{wt}). Cre-mediated recombination will flip the cassette in the right orientation, leading to production of a truncated protein fused to the β-geo reported, thus allowing conditional complete elimination of *Mga* in the tissue of choice (Figure 7.14A, $Mga^{Re\text{-}inv}$; henceforth Mga^{null}). It is noteworthy here that $Mga^{Inv/Inv}$ mice were born below Mendelian frequency (only ~50% of expected frequency) suggesting that Mga^{Inv} is a hypomorphic allele (Washkowitz et al., 2015). Indeed, mRNA levels in mouse embryonic fibroblasts (MEFs) showed that $Mga^{Inv/Inv}$ cells expressed reduced levels of Mga compared to wild type control (Figure 7.14B). Most importantly here, those $Mga^{Inv/Inv}$ mice that were born developed with no apparent abnormalities, allowing us to address its effects in lymphomagenesis.

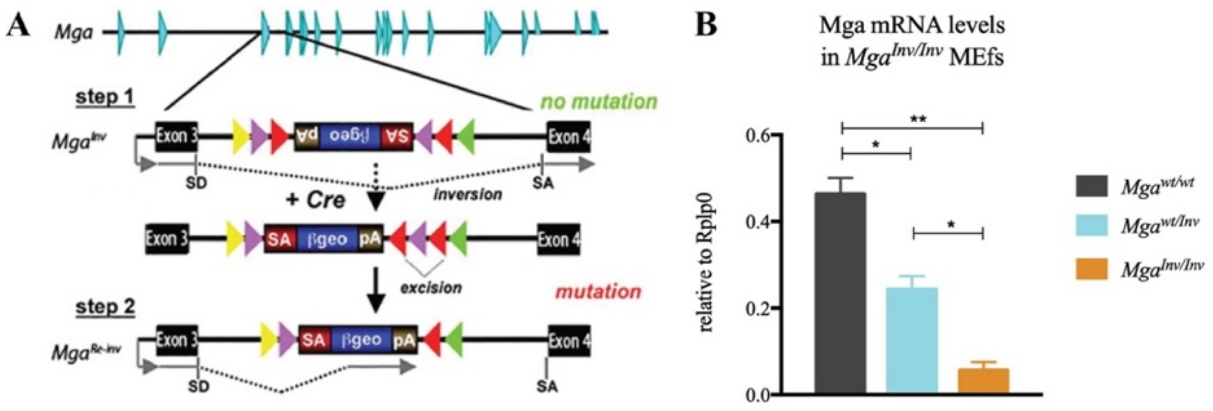

Figure 7.14 Conditional- mutated *Mga* allele is hypomorphic.
A. Schematical representation of Mga^{Inv} allele. Upon the exposure to Cre recombinase, there is a step of inversion and excision in order to have $Mga^{Re\text{-}Inv}$ allele produced (Washkowitz et al., 2015). B. Graph representing mRNA levels of Mga normalized to Rplp0 in MEFs isolated from $Mga^{Inv/Inv}$ mice. For each genotype were analyzed 2 different MEFs. * $p < 0.05$, ** $p < 0.005$, **** $p < 0.0001$.

Following a breeding strategy similar to the one used for *Pcgf6* (see above, chapter 7.1), we generated a cohort of *CD19-Cre/Eμ-myc/*$Mga^{f/f}$ mice in which *Mga* is conditionally deleted in B-cells in the presence or absence of *Eμ-myc* transgene, and monitored lymphoma development for a period of one year. Deletion of *Mga* had no effect on Myc-induced lymphomagenesis, with all *Eμ-myc* mice developing lymphomas with similar latencies (average onset: 120 days) and penetrance (Figure 7.15A), while animals without Myc overexpression did not show signs of illness during the time of the experiment. Where expected, lymphomas were properly recombined for *Mga*, as indicated by semiquantitative PCR on gDNA extracted from $CD19^+$ sorted primary cells from infiltrated lymph nodes (Figure 7.15B). Moreover, *Mga*-null lymphomas did not show differences in their cell-of-origin, with distributions of naïve mature ($B220^+IgM^+$) and immature ($B220^+IgM^-$) B-cell malignancies similar to those of the *Eμ-myc* control (Figure 7.15C). Thus, as opposed to what observed with Pcgf6, loss of Mga does not impact Myc-driven lymphomagenesis.

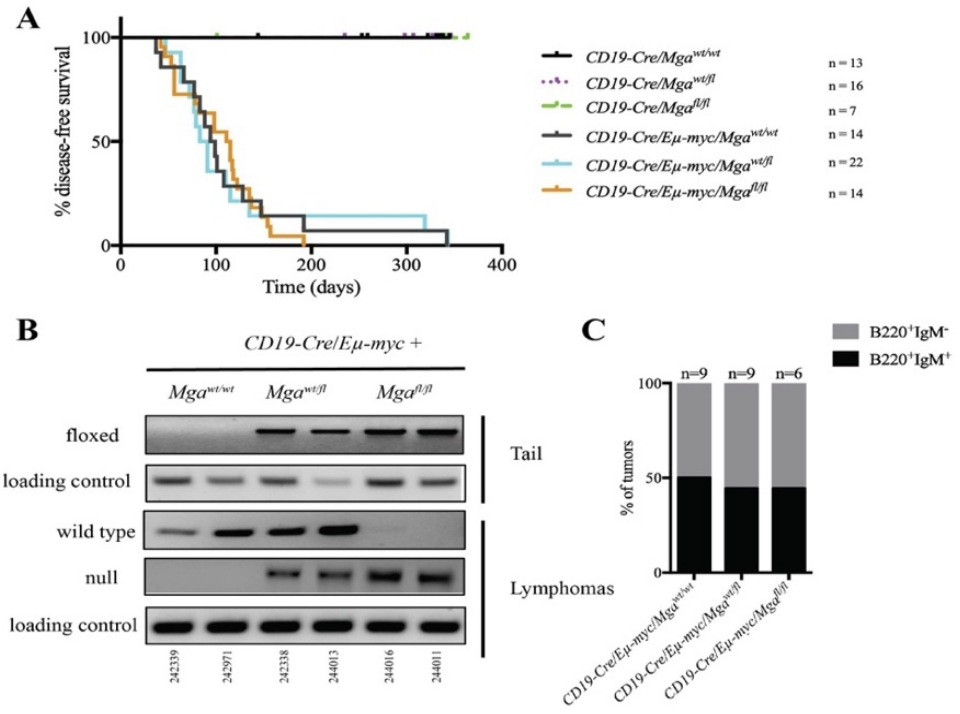

Figure 7.15 Loss of Mga does not accelerate Myc-induced lymphomagenesis.
A. Kaplan-Meier survival curve of *CD19-Cre/Eμ-myc/Mga$^{f/f}$* mice. Number is brackets represent the number of mice analyzed for each experimental group. Mice were followed for a period of one year. The median tumor onset for mice with the *Eμ-myc* transgene was around 120 days. **B.** Semi-quantitative PCR representing the recombination of *Mga* allele. The floxed allele was completely recombined only in *CD19-Cre/Eμ-myc/Mga$^{wt/fl}$* and *CD19-Cre/Eμ-myc/Mga$^{fl/fl}$* mice. Tails were used as a negative control, two mice/ genotyping group represented. **C.** Graph represent quantification of the FACS analysis according to the status of B220 and IgM. Y axis present percentage of tumors either immature (grey) or naïve B-cell origin (black). Numbers above each bar plot represent number of mice analyzed for each genotype.

7.6 Loss of Mga dissociates Pcgf6 but not Myc from chromatin

While having no apparent effect on tumor onset, Mga would be expected to be required for the association of the PRC1.6 complex – and thus of Pcgf6 – with chromatin, at least at a subset of its genomic targets. We thus performed ChIP-seq for Pcgf6 (alongside Myc, Max, and histone marks) in an *in vitro* stabilized *CD19-Cre/Eμ-myc/Mga$^{fl/fl}$* lymphoma (hereafter LyMgaKO). Remarkably, loss of Mga led to almost complete detachment of Pcgf6 from chromatin, with a low number of residual Pcgf6 peaks (Figure 7.16A). Even though Pcgf6 was expressed at a slightly lower level in the LyMgaKO sample, this difference appears unlikely to account for its virtual loss from chromatin (Figure 7.16A, B). Thus, in agreement with the

critical role of Mga for Pcgf6 recruitment (Scelfo et al., 2019; Stielow et al., 2018), its deletion in lymphomas led to a widespread loss of Pcgf6 on chromatin, at both promoters and distal sites (Figure 7.17).

Most noteworthy here, the requirement of Mga for recruiting Pcgf6 to chromatin is in sharp contrast with the finding that, unlike Pcgf6, Mga has no impact on tumor onset. Hence, in contrast with our initial hypothesis, these data point to a Mga- and PRC1.6-independent function of Pcgf6 in tumor suppression.

While loss of Mga had no impact in Myc-induced lymphomagenesis, the ChIP-seq data provided us with the opportunity to address its possible effects on Myc/Max binding to DNA. Genome wide analysis of recovered DNA yielded similar numbers of Myc- and Max-bound peaks in both LyWT and LyMgaKO that showed high overlap between the two samples (Figure 7.16D, E, F). The majority of the peaks were identified on the promoters, while the remaining peaks were equally distributed between intergenic regions and gene bodies (Figure 7.16E). With the caveat that the LyWT sample used in this experiment yielded less peaks than expected (see above), and that this problem that may apply also to the LyMgaKO sample, these results suggest that Mga deletion does not cause major changes in Myc and Max binding profiles. Quantitative heatmaps confirmed this observation (Figure 7.17), which is also corroborated by the fact that Mga deletion does not alters Myc and Max protein and mRNA levels (Figure 7.16B, C). Once again, Myc and Max-bound regions were enriched for the active histone marks (H3K4me3, H3K4me1, H3K27ac), while repressive marks (H3K27me3, H2AK119Ub) followed opposite trend, both on the promoters and distal sites (Figure 7.17A, B). Altogether, we will tentatively conclude here that Mga, while required for the association of Pcgf6 with chromatin, has limited impact on Myc/Max binding profiles. If supported by

definitive data, this conclusion would lend further support to the concept that Pcgf6 suppresses lymphomagenesis by an alternative mechanism

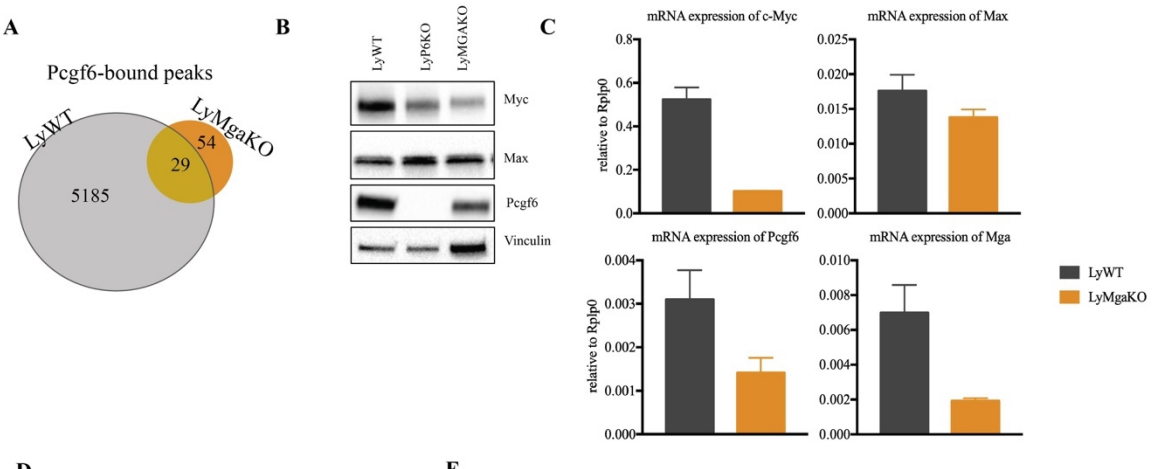

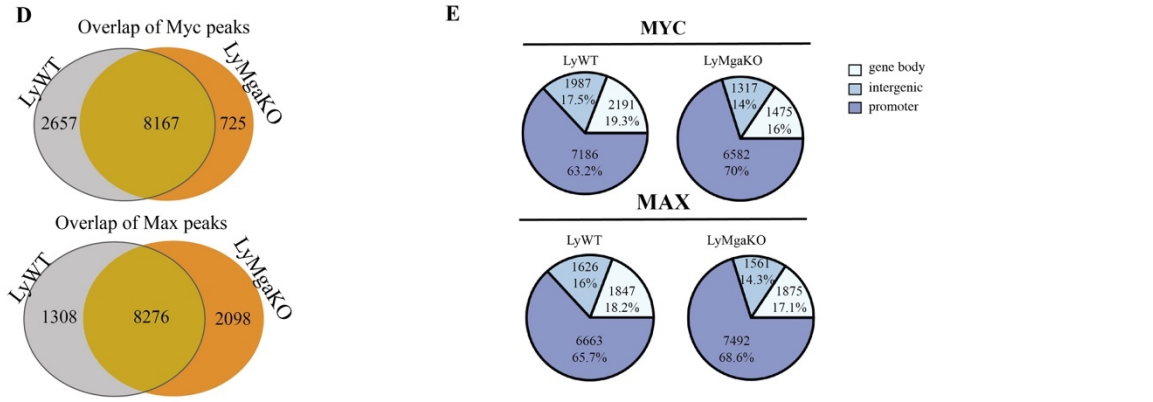

F

Number of identified peaks in ChIP-seq experiment in LyWT and LyMgaKO

IP / sample	Myc	Max	Pcgf6	H3K4me3	H3K4me1	H3K27ac	H3K27me3	H2AK119Ub
LyWT	11346	10136	5214	17277	56735	31993	41809	19366
LyMgaKO	9373	10928	83	17925	54998	29419	44284	30242

Figure 7.16 Pcgf6-bound peaks are lost in LyMgaKO, even though protein is still present
A. Venn diagram representing the overlap of Pcgf6-bound peaks in LyWT and LyMgaKO. LyWT was used in the previous ChIp-seq experiments in chapter 7.3 **B.** Western Blot of Myc, Max and Pcgf6 in LyWT, LyP6KO and LyMgaKO. **C.** Graph representing mRNA levels of Pcgf6, Myc, Max and Mga normalized to Rplp0 in LyWT and LyMgaKO. LyWT and LyP6KO samples both in Wetern Blot and mRNA levels are the samples also represented in chapter 7.3. **D.** Venn diagram shows overlap of Myc- (upper) and Max-bound peaks (bottom) in LyWT and LyMgaKO. **E.** Pie charts shows genomic distribution of Myc and Max-bound sites. The number of peaks is reported in subgroups on the basis of annotation: peaks on promoters, in intergenic region and gene body or intragenic regions. **F.** Table summarizing the number of peaks identified in ChIP-seq experiment performed in LyWT and LyMgaKO. Rows show specific IP, while columns different samples. LyWT sample was previously used in analysis explained in chapter 7.3.

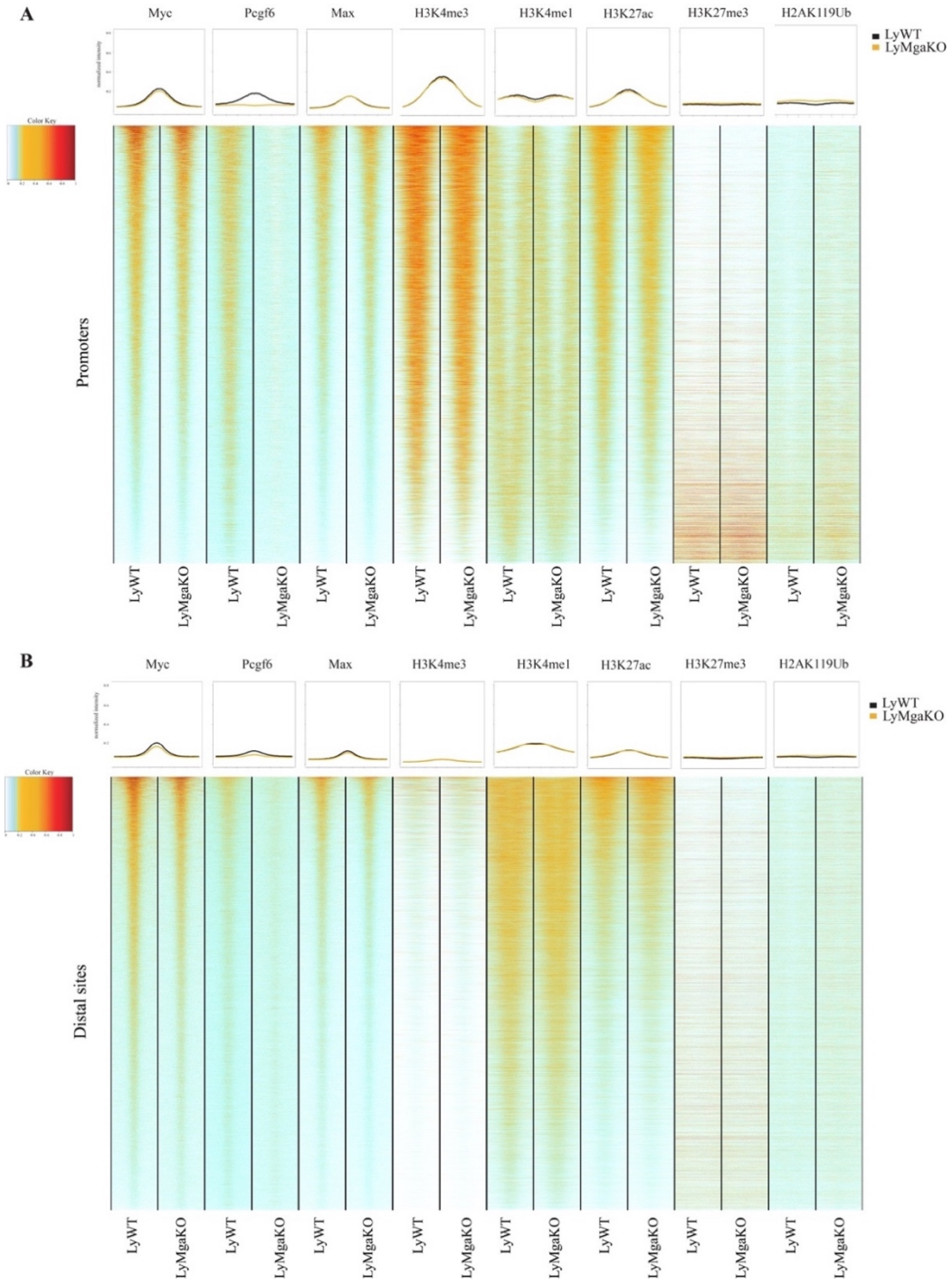

Figure 7.17 Peak density heatmap of Myc, Pcgf6, Max and histone marks in LyWT and LyMgaKO.

A. Heatmap representing normalized ChIP-seq intensity for the indicated Myc, Pcgf6, Max proteins and histone marks over -2kb +1kb around TSS of the union of Myc, Pcgf6 and Max-bound promoters in stabilized lymphomas LyWT and LyMgaKO. **B.** Heatmap representing normalized ChIP-seq intensity for the indicated Myc, Pcgf6, Max proteins and histone marks at the distal sites in stabilized lymphomas LyWT and LyMgaKO. The panels A and B represents every annotated promoter in all the chromosomes that was called either as Myc-associated, Max-associated or Pcgf6-associated by ChIP-seq identified in at least one of the stabilized lymphomas. Above each IP is represented cumulative enrichment deposition centered at the peak summit for the indicated proteins in LyWT (black) and LyMgaKO (orange). ChIP enrichments are normalized to the input. LyWT samples was previously used in analysis explained in detail in chapter 7.3.

7.7 Loss of Pcgf6 does not affect Myc-dependent transcription

The above results support an alternative working model in which Pcgf6 would promote Myc-induced lymphomagenesis by a Mga- and PRC1.6-independent mechanism, with no obvious alterations of Myc binding to chromatin. This notwithstanding, it remains possible that Pcgf6 may impact on Myc transcriptional activity by alternative mechanisms. In order to investigate this question and detect early changes that may promote tumor formation, we profiled gene expression by RNA-seq on pre-tumoral (preT) $CD19^{+}$ B-cells isolated from the spleens of 4-6 weeks old *Eμ-myc* mice, alongside control B-cells isolated from age-matched non-transgenic animals. Altogether, the genotypes analyzed included *CD19-Cre/P6*$^{wt/wt}$ (hereafter cont_WT), *CD19-Cre/P6*$^{fl/fl}$ (cont_P6KO), *CD19-Cre/Eμ-myc/P6*$^{wt/wt}$ (preT_WT) and *CD19-Cre/Eμ-myc/Pcgf6*$^{fl/fl}$ (preT_P6KO). As shown in Figure 7.18, monitoring of either Pcgf6 recombination (panel A) or protein expression (panel B) confirmed the efficient deletion of Pcgf6 in the cont_P6KO and preT_P6KO samples, and the increase in Myc levels in the *Eμ-myc* transgenic preT samples.

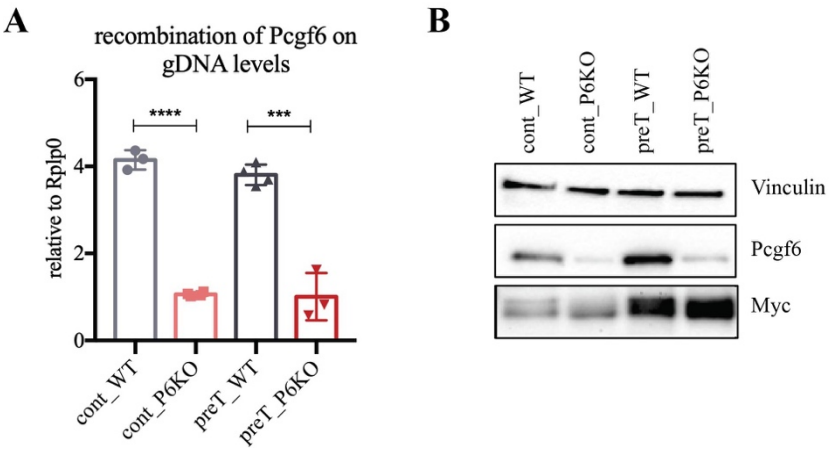

Figure 7.18 Pcgf6 is efficiently deleted at the pre-tumoral stage.
A. Graph representing the quantification of RT-PCR performed on the gDNA of $CD19^{+}$ B-cells isolated from the pre-tumoral samples. First two groups – cont_WT and cont_P6KO were already present in Figure 3.4. *** p value < 0.001, **** p value < 0.0001. **B.** Western blot of Pcgf6 and Myc in pre-tumoral stage of cont_WT, cont_P6KO, preT_WT and preT_P6KO samples. Vinculin was used as a loading control.

Clustering of the RNA-seq data showed a clear separation of the control and preT samples, while the WT and KO remained intermingled (Figure 7.19A, B): thus, non-transgenic and pre-tumoral *Eμ-myc* B-cells showed distinct mRNA profiles as expected (Sabò et al., 2014b), but this occurred without any major impact of Pcgf6. Analysis of differentially expressed genes (DEG) in experimental group relative to control WT B-cells confirmed that the major transcriptional changes are due to the presence of the *Eμ-myc* transgene, with no major effects of *Pcgf6* deletion (Figure 7.19B). Indeed, 5500 and 6300 DEGs were called in preT_WT and preT_P6KO, respectively (Figure 7.20A,B), with very similar profiles (Figure 7.21A). While DEG calling suggested that distinct groups of genes were selectively regulated in the preT_P6KO sample (141 up and 228 down, Figure 7.21B), gene ontology (GO) and GSEA analysis of these genes did not enrich for any specific signature, suggesting that these DEGs stemmed from experimental variability and did not reflect true biological difference between preT_WT and preT_P6KO. Indeed, the overall list DEGs in either sample enriched for almost identical functional categories with similar enrichment scores (Figure 7.21C): in line with previous data on *Eμ-myc* lymphoma (Sabò et al., 2014b), these categories included Myc targets, as well as E2F targets, G_2M checkpoint regulators, and other classes related to cell growth and proliferation (Figure 7.21D).

Finally, only 3 DEGs were called in the cont_P6KO sample (Figure 7.20C), and direct comparison between preT_P6KO and preT_WT yielded only 2 up-regulated genes (Figure 7.20D), once again confirming that Pcgf6 does not have any major effect on transcription and that the *Eμ-myc* transgene is leading the changes observed.

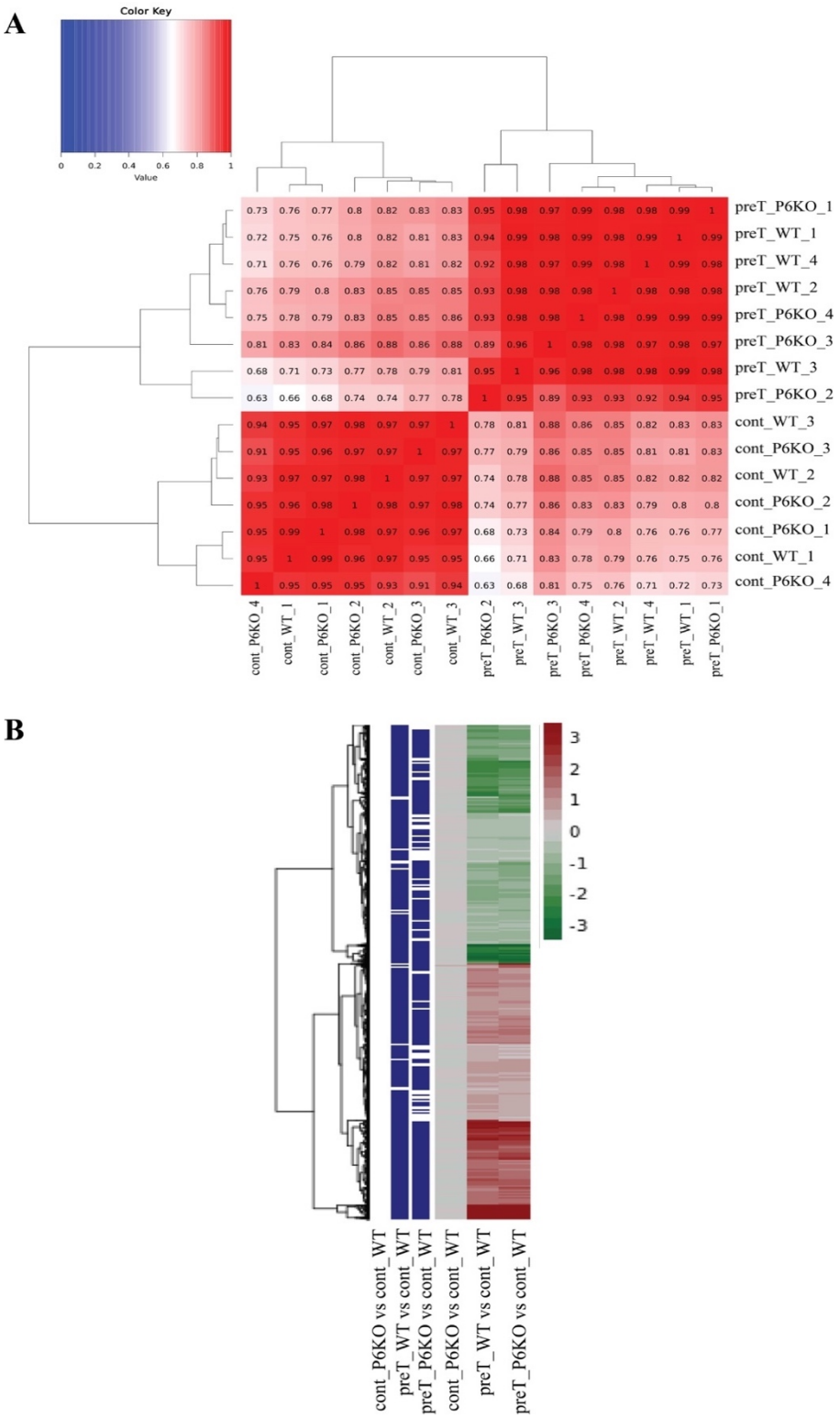

Figure 7.19 Pre-tumoral samples are highly correlated based on the presence/absence of *Eμ-myc* transgene.
A. Pearson correlation of reads per kilo base per million mapped reads (RPKM) of each replicate. **B.** Clustered heatmap representing the union of DEG in pre-tumoral samples. In the first part (left) DEGs are represented as expressed (blue) or not (white) with a p-value<0.05. In the second part (right) of the heatmap for each gene in each group is reported the Log2FC colored from green (-3) to red (3).

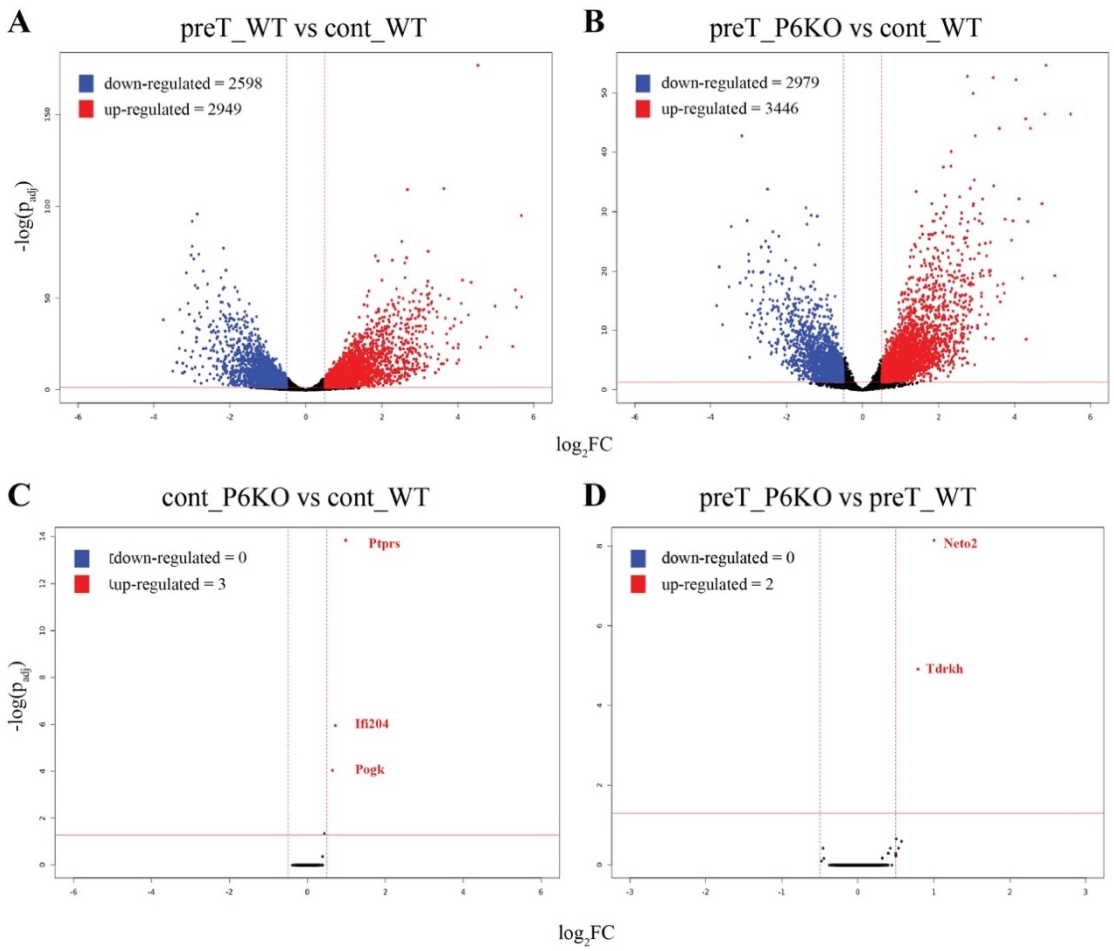

Figure 7.20 Pcgf6 does not affect transcriptional profiles in the pre-tumoral B-cells, on top of Myc.

Differential gene expression analysis shown as volcano plots, Differential gene expression analysis shown as volcano plots, comparing (**A.)** preT_WT (n = 4 animals) or (**B.**)preT_P6KO (n = 4 animals) (right panel) to cont_WT (n = 3 animals); or comparing (**C.**) cont_P6KO (n = 4 animals) to cont_WT (n = 3 animals) and (**D.**) preT_P6KO (n = 4 animals) to preT_WT (n = 4 animals). Lines represent the threshold mark of significance in this study: the horizontal line marks the statistical significance (P_{adj}<0.05) and the vertical line mark the fold change (FC) (|log_2FC>0.5|). The numbers of genes that pass this threshold are shown, with down-regulated genes in blue and up-regulated genes in red

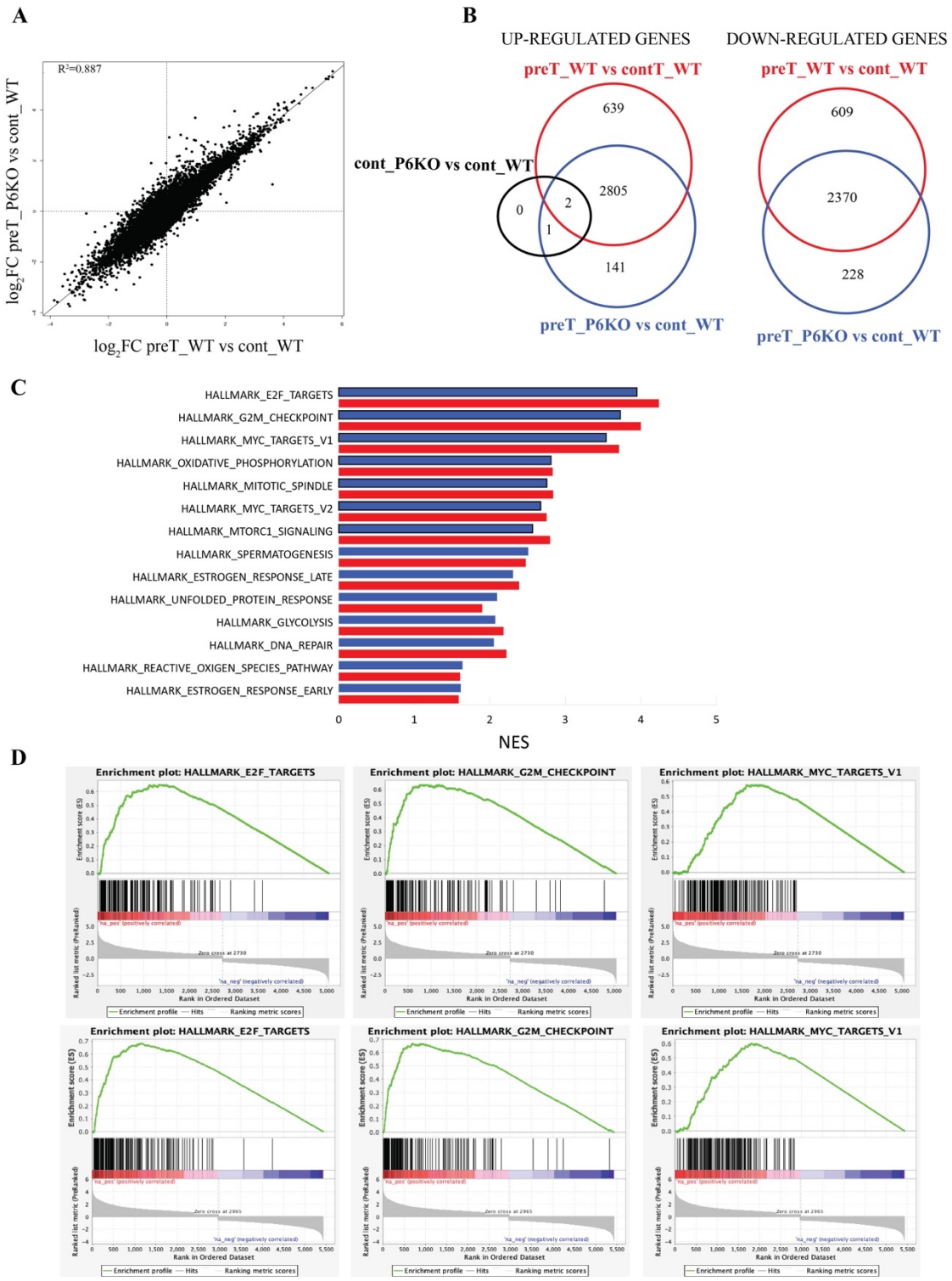

Figure 7.21 DEGs called in preT_P6KO and preT_Myc compared to cont_WT are enriching for the same categories and show high overlap.

A. Scatter plot of log_2FC in preT_WT vs cont_WT and log_2FC of preT_P6KO vs cont_WT. R^2=0.887 represents the correlation coefficient. **B.** Venn diagrams of overlap of DEG called in cont_P6KO, preT_WT and preT_P6KO. q cut-off value <0.05. **C.** Graph representing the normalized enrichment score (NES) of each category identified either in preT_P6KO (red) or in preT_WT (blue) compared to cont_WT. **D.** Representative GSEA normalized enrichment score (NES) graph of top three category: preT_WT (upper), PreT_P6KO compared to cont_WT (lower).

The same experimental flow used above for pre-tumoral samples was applied to advanced tumor (T) samples, through RNA-seq profiling of the bulk cell population in infiltrated lymph nodes (consisting mainly in lymphoma B-cells) (Sabò et al., 2014b). Hierarchical clustering of *CD19-Cre/Eμ-myc/P6*$^{wt/wt}$ and *CD19-Cre/Eμ-myc/P6*$^{fl/fl}$ (hereafter T_LyWT and T_LyP6KO, respectively) showed a high correlation index among all tumors (above 82% of similarity) and lack of clustering according to Pcgf6 status (Figure 7.22A). The high similarity of the transcriptional programs in T_LyWT and T_LyP6KO is also evident in the heatmap reported in Figure 7.22B, as well in the scatter plot of log_2FC between T_LyWT vs cont_WT and T_LyP6KO vs cont_WT (Figure 7.22C). In line with these observations, DEG calling between T_LyWT and T_LyP6KO identified limited numbers of genes, including 78 up-regulated and 65 down-regulated genes (Figure 7.22D). These sets of genes were too small to perform GSEA analysis, while interrogation of GO datasets highlighted the interferon gamma (IFN-γ) response among the genes down-regulated in T_LyP6KO samples: in particular, three genes in our dataset were part of this pathway, including Irf5 (interferon regulatory factor 5) which can regulated the induction of multiple pro-inflammatory cytokines (Krausgruber et al., 2011; Takaoka et al., 2005), HLA-DMA (major histocompatibility complex II, DM alpha) and SAMDL9 (sterile alpha motif domain containing 9 like).

To further interrogate possible biological differences between P6KO and WT lymphomas, we considered all expressed genes (RPKM >0) and ranked them by their ratio in the T_LyP6KO relative to the T_LyWT sample, yielding an enlarged list of 16350 genes, including 6477 up- and 9874 down-regulated mRNAs (log_2FC >0 and <0, respectively): in this setting, down-regulated genes enriched for regulators of immune surveillance, while up-regulated genes were identified as E2F and Myc targets (Figure 7.23).

Altogether, our RNA-seq analysis indicated that deletion of Pcgf6 does not alter Myc-dependent transcription and, more generally, does not significantly impact transcriptional programs in either pre-tumoral or control B-cells, the latter being consistent with the lack of effect of *Pcgf6* deletion on B-cell development and differentiation (Figure 7.5 and Figure 7.6). We surmise that Pcgf6 is likely to impact Myc-induced lymphomagenesis through alternative, transcription- and PRC1.6-independent mechanisms, the nature of which remains to be addressed.

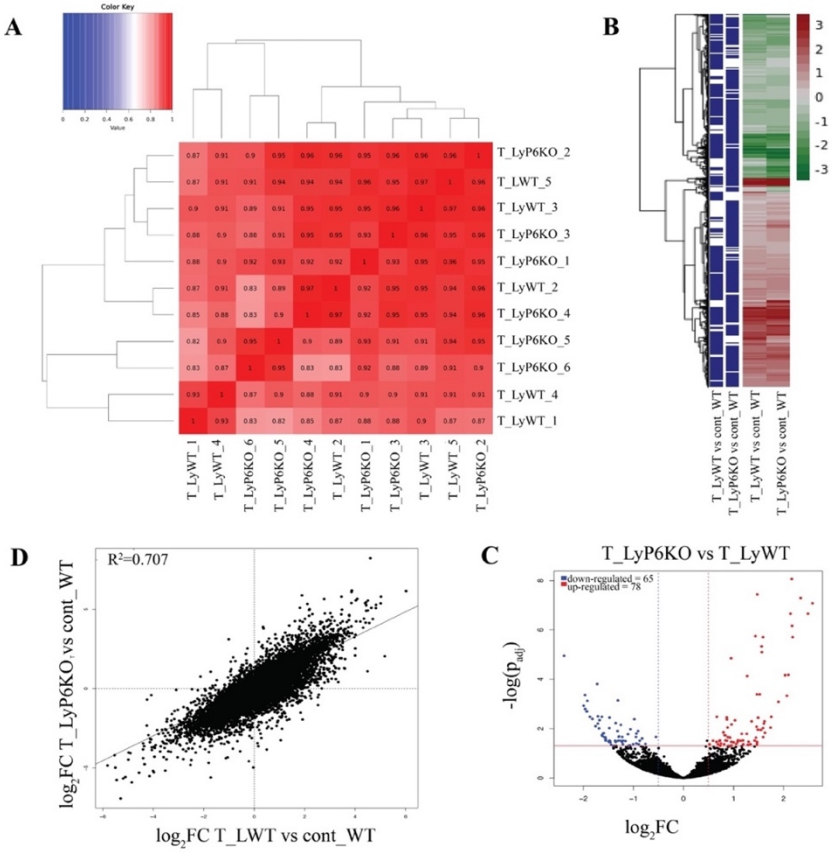

Figure 7.22 Tumor samples are highly correlated between each other.
A. Pearson correlation of reads per kilo base per million mapped reads (RPKM) of each replicate. **B.** Clustered heatmap representing the union of DEG in tumoral samples. In the first part (left) DEGs are represented as expressed (blue) or not (white) with a p-value<0.05. In the second part (right) of the heatmap for each gene in each group is reported the Log2FC colored from green (-3) to red (3). **C.** Scatter plot of log_2FC in T_LyWT vs cont_WT and log_2FC of T_LyP6KO vs cont_WT. R^2=0.7o7 represents the correlation coefficient. **C.** Differential gene expression analysis shown as volcano plots, comparing T_LyP6KO (n = 6 animals) to T_LyWT (n = 5 animals). Lines represent the threshold mark of significance in this study: the horizontal line marks the statistical significance (p_{adj}<0.05) and the vertical line mark the fold change (FC) (|log_2FC>0.5|). Down-regulated genes in blue and up-regulated genes in red.

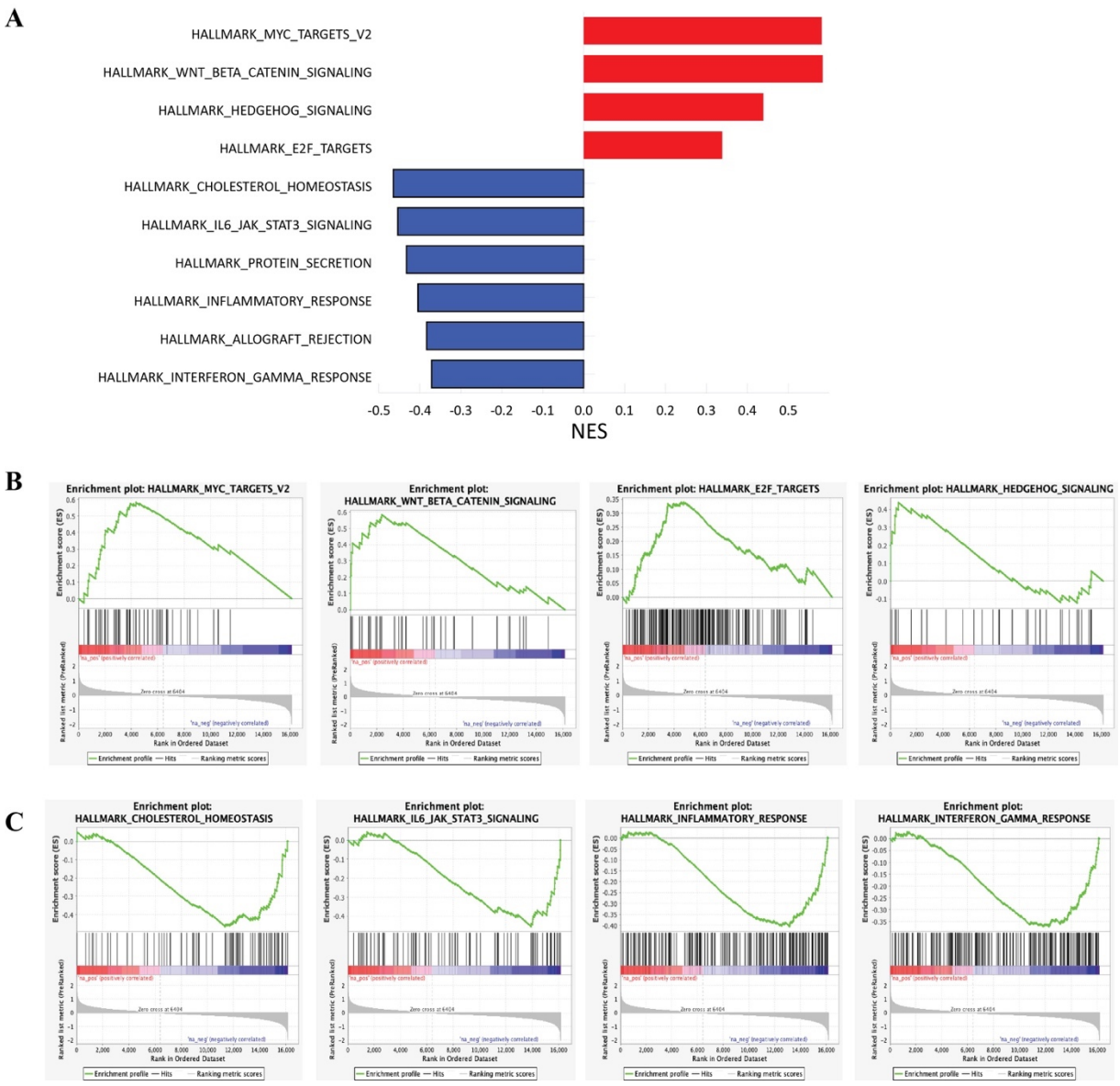

Figure 7.23 Genes expressed in T_LyP6KO when compared T_LyWT showed downregulation of inflammatory pathways and immune system response.
A. Graph representing the normalized enrichment score (NES) of each category identified T_LyP6KO when compared to T_LyWT and ranked by log_2FC. In red positively correlated gene sets, in blue negatively correlated gene sets. **B.** GSEA normalized enrichment score plots for top 4 positively correlated data sets. **C.** GSEA normalized enrichment score plots for top 4 negatively correlated data sets

To further compare gene expression profiles in WT and KO lymphomas, we focused on the genes deregulated in either of these tumor samples relative to WT B-cells, allowing identification of discrete sets of genes that were up- or down-regulated selectively in the KO versus WT tumors (Figure 7.24A). While GSEA analysis did not show any significant enriched category, GO analysis of up-regulated genes identified the same categories as before: G_2M checkpoint and Myc targets, while down-regulated genes identified specifically in T_LyP6KO (784 up, 703 down-regulated genes) enriched for genes belonging to the Inflammatory Response, TNFα and IFN-γ signaling (Figure 7.24B). Some of the identified Inflammatory Response genes are IL18, IL10RA, CD86 and CD274: strikingly these genes were expressed in both pre-tumoral and lymphoma samples, but were downregulated selectively in T_LyP6KO (Figure 7.24C). These genes are usually expressed in Antigen Presenting Cells (APC), such as B lymphocytes, dendritic cells and macrophages and have a role in activation of T-cell response, suggesting that their downregulation in either tumor-infiltrated cells or B-cells could impact T-cell activation.

Altogether, though the transcriptional changes in KO tumors barely differ from transcriptional profiles in WT tumors, our analyses pointed out the deregulation of genes involved in immune surveillance upon loss of Pcgf6 during Myc-induced lymphomagenesis. Since these differences were observed only in tumors, but not in sorted B-cells, they could reflect two alternative scenarios: i) these genes get down-regulated later during lymphomagenesis, and represent true transcriptional changes in tumor cells; ii) this apparent down-regulation does not reflect intrinsic changes in tumors cells but, perhaps more likely, the fact that these genes are expressed on infiltrating cells that may be altered or under-represented in Pcgf6 KO tumors, thus potentially impacting immune surveillance. In line with this concept recent work pointed out to a role of the canonical PRC1 and variant PRC1.1 complexes immune

surveillance in double-negative prostate cancer (Su et al., 2019). In order to address this issue, we undertook to analyze cellular infiltrates in Pcgf6 KO and WT lymphomas.

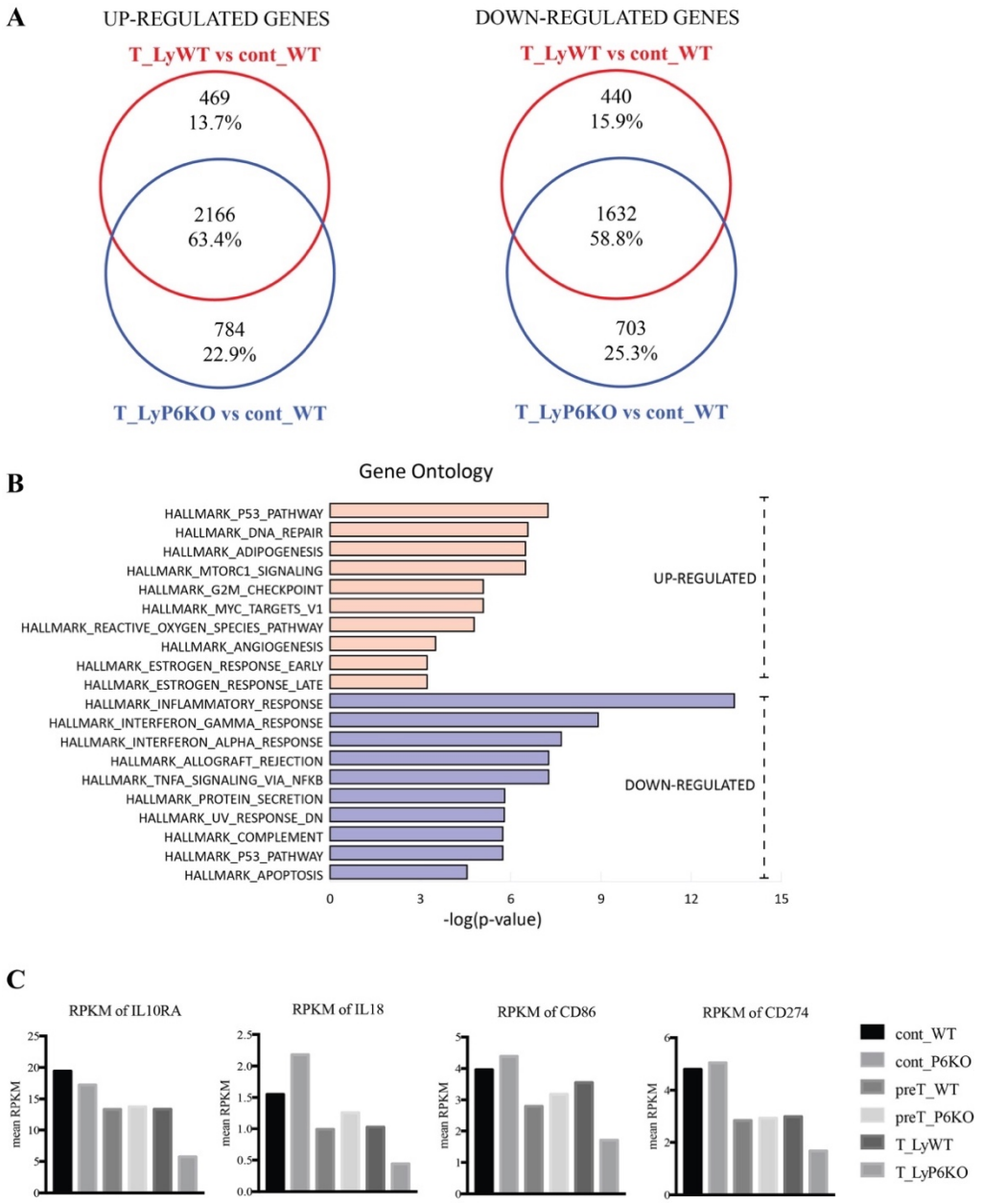

Figure 7.24 Gene Ontology analysis of DEGs specifically identified in T_LyP6KO experimental group.
A. Venn diagrams representing the overlap of DEG called in T_LyWT and T_LyP6KO compared to cont_WT. DEGs were defined by the q cut-off value <0.05; overlap of the up-regulated DEGs (upper), the overlap of the down-regulated genes from two comparisons (bottom). **B.** Graph representing GO classes identified in unique DEGs found in T_LyP6KO, either up-regulated or down-regulated genes. X-axis is representing the -log(p-value) and the numbers are depicting the number of genes overlapping with each class. **C.** Representative graph of mean RPKM value of genes identified in Inflammatory Response data set.

7.8 Analysis of cellular infiltrates in lymphomas

In order to address a possible role of Pcgf6 in controlling the recruitment of infiltrating cells and immune-surveillance, we initially transplanted primary *CD19-Cre/Eμ-myc/P6*$^{wt/wt}$ (T_WT) and *CD19-Cre/Eμ-myc/P6*$^{fl/fl}$ (T_P6KO) tumors in immunocompetent syngeneic mice, with each primary lymphoma transplanted in two recipient mice. While all (6/6) recipients of T_P6KO showed signs of illness and had to be sacrificed at day 19, 4/6 of the T_WT showed slightly slower progression, allowing survival until day 24 (Figure 7.25A). Additional experiments will be needed to address whether this represents a reproducible, Pcgf6-dependent difference in tumor progression.

Following sacrifice of the recipient animals, we recovered tumor cells from either infiltrated lymph nodes or spleen and analyzed the expression of select surface markers by flow cytometry. Single-cell suspensions were stained for CD45, a leukocyte surface marker expressed in all lymphocyte lineages, as well as for the B- and T-lymphocyte markers B220 and CD3, respectively (Figure 7.25B, C). We observed a high fraction of B-cells in infiltrated lymph nodes, as expected in *Eμ-myc* mouse lymphoma (Figure 7.25C)(Adams et al., 1985). Of note here, we were not able to distinguish whether B-cells in spleen originated from the donor or the recipient. This notwithstanding, a decrease in T-cell content was observed in P6KO tumors, in particular in the spleen (Figure 7.25C). Beside B- and T-cells, different myeloid linages were analyzed as well, such as NK cells, NKT cells, monocytes, macrophages and dendritic cells (DCs), but no significant changes were observed upon Pcgf6 deletion, even though there was high variation present in all the samples (Figure 7.25D). The above results suggest that there could be a reduction of infiltrating T-cells in tumors when Pcgf6 is deleted.

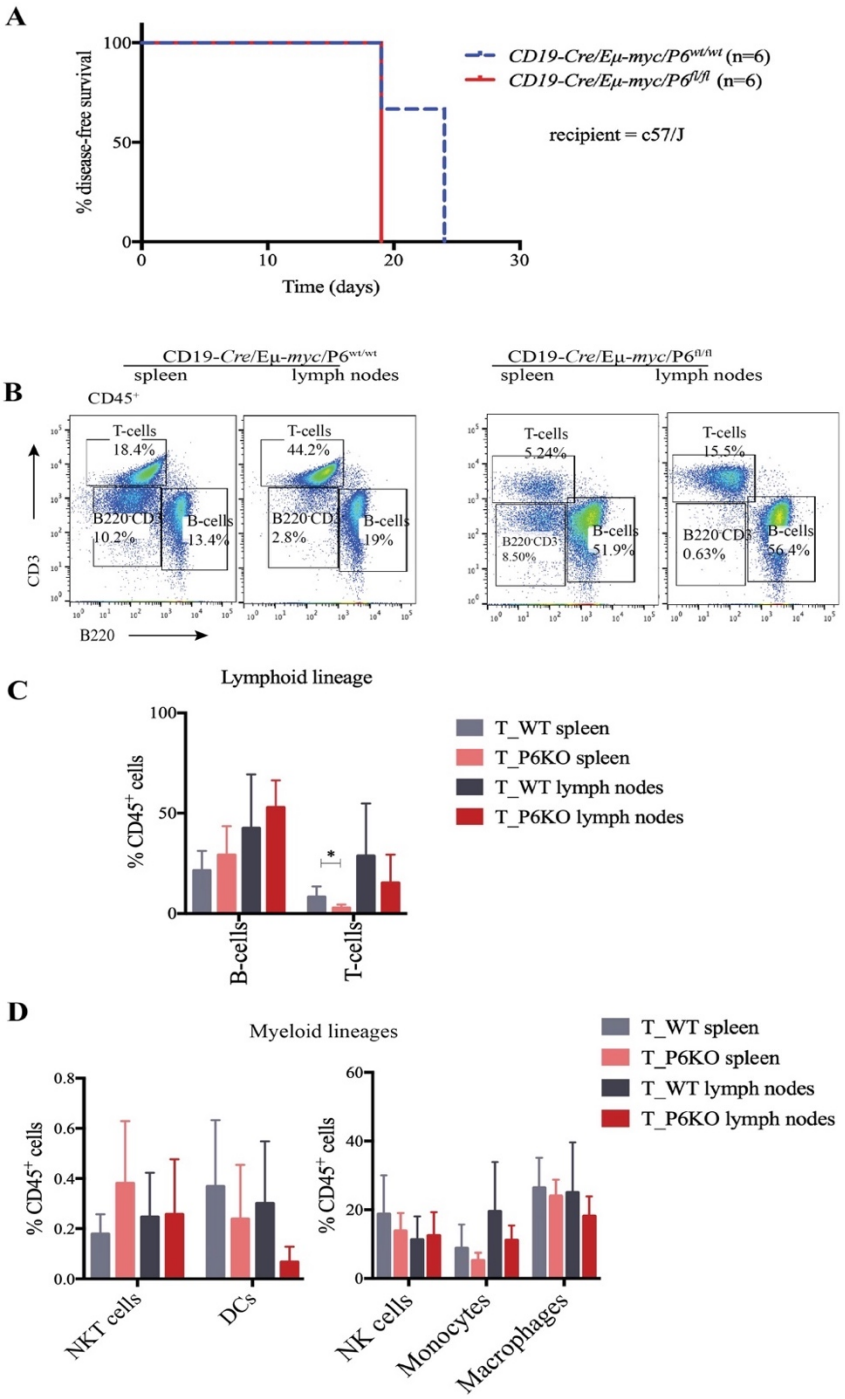

Figure 7.25 Analysis of myeloid and lymphoid lineages in tumors isolated from transplanted mice.

A. Kaplan-Meier survival curve of recipient c57/j mice transplanted with 3 different primary lymphomas for each genotype (2 mice per tumor). **B.** Representative FACS plot of each group. Number indicated in percentage in each gate are relative to the population indicated above the plot. **C.** Graph representing percentage of B-cells (CD45+B220+CD3-) and T-cells (CD45+B220-CD3+) are represented as percentage of CD45+ cells. D. Graph represents cumulative percentage of CD45+ population: NKT cells (CD45+B220-CD3+NK1.1+), DCs (CD45+B220-CD3-NK1.1+), NK cells (CD45+B220-CD3-MHCII+CD11c+), Monocytes (CD45+B220-CD3-Ly6G-CD11b+Ly6C+), Macrophages (CD45+B220-CD3-Ly6G-CD11b+F4/80+). * p value<0.05, ** p value < 0.005, **** p value < 0.0001. T_WT – transplanted CD19-Cre/Eμ-myc/P6wt/wt tumor; T_P6KO – transplanted CD19-Cre/Eμ-myc/P6fl/fl tumor.

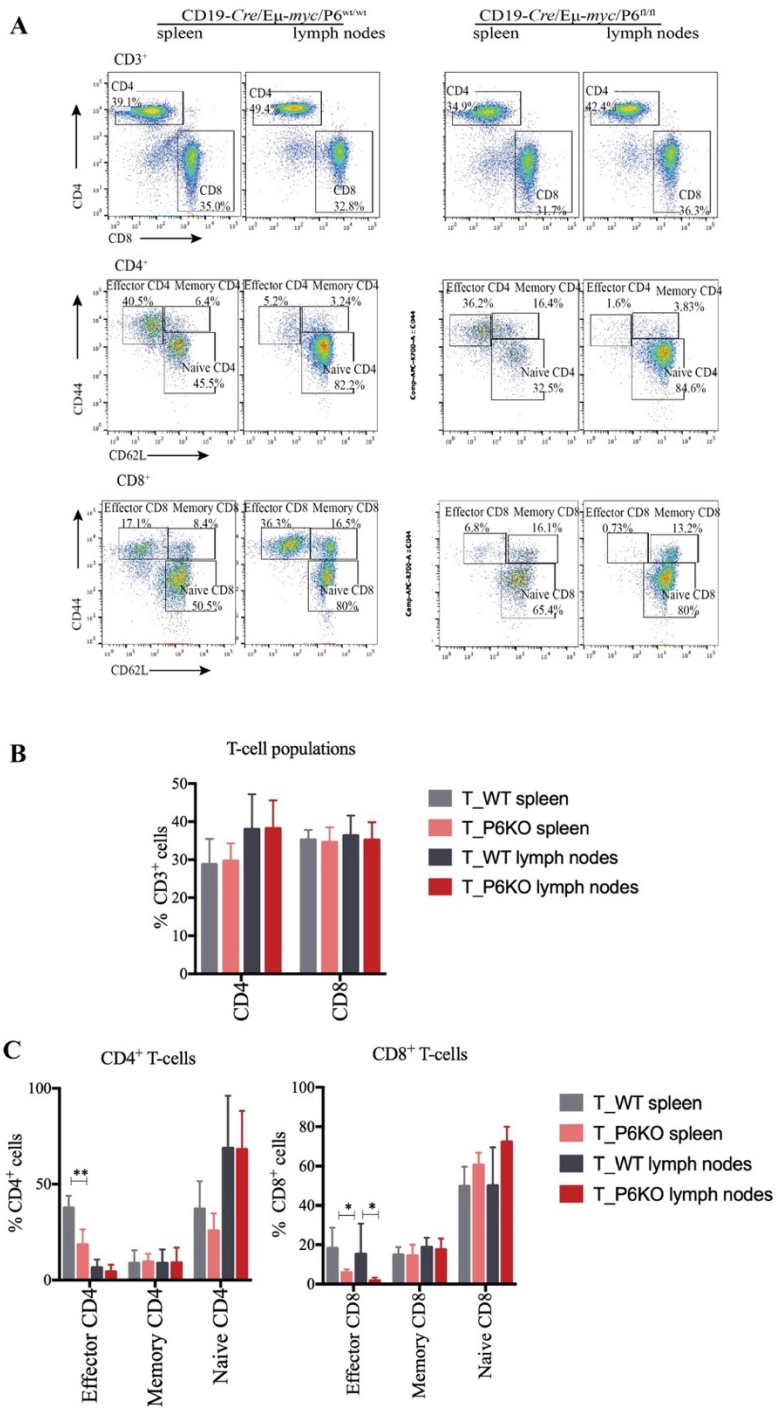

Figure 7.26 Analysis of T-cells of tumors isolated from transplanted mice.
A. Representative FACS plots of each group. Number indicated in percentage in each gate are relative to the population indicated above the plot. **B.** Graph representing $CD4^+$ and $CD8^+$ T-cell populations, represented as percentage of $CD3^+$ cells. **C**. left- $CD4^+$ T-cells: effector ($CD3^+CD4^+CD8^-CD44^+CD62L^-$), memory ($CD3^+CD4^+CD8^-CD44^+CD62L^+$) and naïve ($CD3^+CD4^+CD8^-CD44^-CD62L^+$), or right-$CD8^+$ T-cells: effector ($CD3^+$ $CD4^-CD8^+CD44^+CD62L^-$), memory ($CD3^+CD4^-CD8^+CD44^+CD62L^+$) and naïve ($CD3^+CD4^-CD8^+CD44^-CD62L^+$) are represented as percentage of $CD4^+$ and $CD8^+$T cells, respectively. * p value<0.05, ** p value < 0.005, **** p value < 0.0001. T_WT – transplanted *CD19-Cre/Eμ-myc/P6$^{wt/wt}$* tumor; T_P6KO – transplanted *CD19-Cre/Eμ-myc/P6$^{fl/fl}$* tumor.

Based on the above observation, we sought to dissect the distribution of specific T-cell subsets in lymphomas. Co-staining of CD4, CD8, CD44 and CD62L revealed no significant changes in the overall fraction of CD4+ T-cell population between WT and P6KO tumors (Figure 7.26A, B, C), even though a significant decrease in effector CD4+ T-cells was observed upon co-staining with CD44 and CD62L in spleens isolated from CD19-Cre/*Eμ-myc/P6*$^{fl/fl}$ transplanted mice (Figure 7.26A, C). This blockage in recruitment of the effector CD4$^+$ T cells is visible also in the lymph nodes, even though at much lower levels (Figure 7.26A, C). In line with this, we observed a decrease in naïve CD4$^+$ T cells in the spleen of mice transplanted with T_P6KO tumors (Figure 7.26A, C). In contrast, no major differences were observed in the percentage CD8$^+$ T-cell population between T_P6KO and T_WT (Figure 7.26A, B, C). However, further staining for CD44 and CD62L revealed a strong decrease in effector CD8$^+$ T-cells in transplanted P6KO tumors (Figure 7.26A, C). This loss of effector CD8$^+$ T-cells is balanced to some extend with a slight increase in naïve CD8$^+$ T-cells (Figure 7.26C). Finally, no differences were observed in memory or naïve CD8+ T-cells (Figure 7.26C). To summarize, we observed the decrease in T-cell population in our T_P6KO, specifically loss of effector CD4$^+$ and CD8$^+$ T-cells in tumor-infiltrated cells upon Pcgf6 deletion.

Altogether, the aforementioned preliminary results point to a non-cell autonomous role of Pcgf6 in supporting immune surveillance in B-cell lymphomas, possible by mediating the recruitment and/or activation of effector T-cells. In order to confirm these results, further analyses of primary lymphomas will be needed, followed by more detailed analysis of T-cells (by using markers of activation/exhaustion) that will help us understand if Pcgf6 is important for the recruitment or the activation of T-cells.

In conclusion, Pcgf6 act as Mga- and PRC1.6-independent tumor suppressor in B-cell lymphomas and may do so – at least in part – by supporting immune-surveillance in those tumors. Further research will be needed to directly address this mechanism of action.

8. DISCUSSION

The *MYC* oncogene is recurrently activated in a majority of human tumors (Dang, 2012; Kress et al., 2015). Its product, Myc, acts as a transcriptional regulator and exerts its function by dimerizing with the bHLH-LZ transcription factor Max. On the other hand, Max can dimerize with other bHLH-LZ factors with repressive activities, such as Mga, which may contribute to transcriptional repression of common target genes. Although Max was initially found to be essential for different cellular processes such as proliferation, apoptosis or cellular transformation, an exception was found in two neuroendocrine carcinomas, SCLC and PC, where Max is recurrently mutated (Comino-Mendez et al., 2011; Romero et al., 2014). This evidence suggested its possible tumor suppressive role in such setting. Moreover, in SCLC, this mutation was found to be mutually exclusive with Myc overexpression and Mga loss (see Figure 5.7), which suggested that SCLC development is associated with a selective pressure to either gain Myc/Max or lose Mga/Max activity. The fact that both Mga and Max are found to be part of repressive PRC1.6 complex, with Pcgf6 as its distinct subunit (see Figure 5.11 5.11 and Figure 5.12), led to the assumption that the repression of overlapping Myc-target genes may occur through this complex, endowing Pcgf6 and Mga with tumor suppressor activity. We further postulated that this might represent a general function of the Mga/Max/Pcgf6 complex and might therefore be relevant to other tumors than PC or SCLC. We thus investigated if Pcgf6 and Mga may fulfill these predictions in B-cell lymphomas – taken as a paradigmatic example of Myc-driven malignancy.

By taking advantage of the *Eμ-myc* mouse model, we were able to characterize lymphomagenesis upon deletion of either *Pcgf6* or *Mga* in B-cells (see chapter 7.1 and 7.5). Indeed, B-cell specific deletion of *Pcgf6*, either partial or complete, led to a significant acceleration of lymphomagenesis, demonstrating a tumor suppressive function of Pcgf6 in

Myc-induced lymphomas. The accelerated lymphomagenesis in *CD19-Cre/Eμ-myc/P6*$^{fl/fl}$ mice could be due to different acquired mutations respect to *CD19-Cre/Eμ-myc/P6*$^{wt/wt}$ tumors which needs further investigation.

We then assumed that the same outcome would occur upon *Mga* deletion, which would further confirm that the mechanism of tumor suppression goes through PRC1.6 complex (Scelfo et al., 2019; Stielow et al., 2018). To our surprise, hetero- or homozygous deletion of *Mga* in B-cells had no impact on lymphomagenesis (see chapter 7.5). However, the overall survival and penetrance of *CD19-Cre/Eμ-myc/P6*$^{wt/wt}$ and *CD19-Cre/Eμ-myc/Mga*$^{wt/wt}$ mice were different (see Figure 7.2 A and Figure 7.15 A). These differences are probably due to a different background of Mga$^{f/f}$ and Pcgf6$^{f/f}$ mice. Overall, these results strongly suggest that Pcgf6, unlike Mga, do have a role in tumor suppression in B-cell lymphomas, and exerts this function independently from its involvement in the PRC1.6 complex.

The fact that tumors developed in our *CD19-Cre/Eμ-myc/P6*$^{f/f}$ mouse model are prevalently monoclonal implied that Pcgf6 could promote the expansion of the pre-tumoral B-cell pool susceptible of tumor development, a characteristic feature of in the *Eμ-myc* model (Langdon et al., 1986). While we still have to complete the analysis of the pre-tumoral B-cells in our *CD19-Cre/Eμ-myc/P6*$^{f/f}$ mice, we have addressed normal B-cell development upon the deletion of *Pcgf6* in non-transgenic mice (see chapter 7.2) and upon detailed dissection of different stages of B-lymphoid differentiation, both in bone marrow and spleen, we did not observe any changes in B-cell differentiation and homeostasis in mice with Pcgf6 depletion and WT control. These observations suggested that Pcgf6 loss does not lead to tumorigenesis by affecting normal B-cell development and homeostasis, unlike other Polycomb Group Finger Proteins, such as Pcgf2 or Pcgf4 (Akasaka et al., 1997; Cales et al., 2008) (see chapter 5.2.2).

In order to further address the mechanisms underlying the tumor suppressor activity of Pcgf6 in Myc-induced lymphomagenesis, we analyzed the genomic distribution of Myc, Max and Pcgf6 in *CD19-Cre/Eμ-myc/P6*$^{fl/fl}$ tumors. We performed ChIP-seq experiments in stabilized lymphoma cell lines, derived from primary B-cell lymphomas either WT (LyWT) or KO (LyP6KO) for Pcgf6 (see chapter 7.3). We observed that in LyWT, Myc and Pcg6f co-localize in many binding sites, mostly positioned at active promoters. More in general, Pcgf6 was co-mapping with marks of active chromatin (H3K4me3, H3K4me1 and HK3K27ac active histone marks), and not with repressive PRC1- and PRC2-related histone marks (H3K27me3 and H2AK119Ub). These results suggest that the canonical PRC1 and PRC2 complexes are not involved in Pcgf6 distribution on chromatin and suggest Pcgf6 preferential binding to active promoters, which could be most likely driven by the same E-boxes that are bound by Myc.

Strangely, the LyP6KO tumor lacking Pcgf6 exhibited an increase in overall Myc-binding, associated with a similar increase in Max binding, both at the promoters and distal sites. However, the Myc-binding profile obtained in LyP6KO was similar to that seen in control *Eμ-myc* lymphomas analyzed in previous studies (Sabò et al., 2014b), while the peaks obtained in our LyWT were three times less. This discrepancy could be explained by either a technical artefact, differences in tumor clonality, or alternatively, a true consequence of Pcgf6 deletion in B-cells which renders chromatin more susceptible for Myc binding. The latter appears unlikely, however, as a ChIP-seq experiments performed in stabilized LyWT showed that (i.) Myc peaks were more abundant in that sample, and (ii.) the knockdown of Pcgf6 caused no increase in Myc-binding (see chapter 7.4). Altogether, the data provide no evidence for a role of Pcgf6 in controlling the association of Myc with chromatin and suggest that the lower number of Myc peaks in our first LyWT sample should be taken with circumspection. Addressing the above questions in a definitive manner will entail higher numbers of stabilized

lymphomas of each group, as well as the generation of ChIP-seq profiles of Myc, Max and histone marks with a spike-in control for normalization across samples.

Although Mga deletion did not result in acceleration of lymphomagenesis in *CD19-Cre/Eμ-myc/Mga*$^{f/f}$ mouse model, it completely erased Pcgf6 from chromatin (see chapter 7.6) as already reported in mESCs (Scelfo et al., 2019; Stielow et al., 2018), confirming the importance of Mga for recruitment of the PRC1.6 complex onto chromatin. However, Pcgf6 loss did not appear to affect the association of Myc and Max with chromatin: thus, while the PRC1.6 complex (as assessed by Pcgf6) and Myc bind to a common set of sites, PRC1.6 may not effectively limit Myc's association with chromatin.

Altogether, the above results support an alternative model where Pcgf6 would promote Myc-induced lymphomagenesis by Mga- and PRC1.6-independent mechanism, without evident change on the Myc-chromatin binding. However, these results did not exclude the possibility that Pcgf6 loss may alter specific transcriptional programs that would result in accelerated lymphomagenesis. In order to investigate such possibility, we performed RNA-seq analyses on non-transgenic B-cells that lack Pcgf6 and wild type control (see chapter 7.7). We observed that these B-cells are very similar, if not identical, to their wild type counterpart, which is in concordance with previously obtained results that Pcgf6 is not involved in B-cell development and homeostasis. Furthermore, using *Eμ-myc* mouse model, we were able to dissect the transcriptional changes of B-cells which appear upon Pcgf6 deletion in young transgenic mice at the preneoplastic stage, as well as of control B-cells from non-transgenic, aged-matched mice (see chapter 7.7). We observed the expected differences in gene expression in the presence or absence of *Eμ-myc* transgene (Sabò et al., 2014b), but no Pcgf6-dependent changes in expression profiles. Thus, the characteristic Myc-dependent alterations in

transcriptional programs in polyclonal pre-tumoral B-cells occurred independently from the Pcgf6 status.

Similarly, when comparing already established lymphomas, absence of Pcgf6 lead to the deregulation of only few genes. Interestingly, Downregulation was observed in genes involved in IFN-γ response, inflammatory response and JAK/STAT pathway - all of which are involved in innate immune response. Notably, these mild transcriptional differences were observed when analyzing the whole tumor samples, but not in the purified B-cells used for the analysis of pre-tumoral samples: in this setting, the calling of a DEGs may derive from two phenomena, i) true transcriptional changes in tumor cells of the different genotypes or – perhaps more likely - ii) the expression of these genes in infiltrating non-tumor cells that may be either altered or underrepresented in Pcgf6 KO tumors, potentially impacting on immune surveillance or other non-cell autonomous effects in the tumor micro-environment.

To further characterize these mild differences, we attempted to detect subtle changes in lymphomas by analyzing differences in transcriptional programs comparing tumor samples either wild-type or knock-out for Pcgf6 to wild type B-cells. Again, we observed the downregulation of the same group of genes involved in Inflammatory Response, TNFα and IFN-γ signaling, which strongly suggested that these events are the true differences between our tumor samples. Upon closer look at these datasets, we were able to identify genes such as ILR10, IL18, CD274 and CD86 that were specifically downregulated in Pcgf6 KO samples, while expressed in WT tumors and pre-tumoral samples. This observation strongly implied that these changes occur in a Pcgf6-dependent manner, yet it remains unclear whether they occur in tumor or infiltrating cells. It is known that *IL10RA*, encoding the Interleukin 10 receptor alpha subunit, is primarily expressed in hematopoietic cells such as B-cells, T-cells and natural killer (NK) cells, mediates the immunosuppressive signal of IL10 and inhibits the

synthesis of proinflammatory cytokines (Yoon et al., 2006). IL18 is involved in augmenting NK cell activity in the spleen and stimulates IFN-γ production in T-cells (Kato et al., 2003), while expressed mainly the myeloid lineage. CD86 is present on antigen-presenting cells (APC), providing costimulatory signals necessary for T-cell activation and survival (Chen and Flies, 2013). CD274, also known as programmed death-ligand 1 (PD-L1), is a transmembrane protein expressed on tumor cells and it is a ligand of immune-checkpoint receptor programmed death-1 (PD-1) expressed on T-cells. This PD-1/PD-L1 interaction lead to a negative regulation of T-cell proliferation, migration and activation, leading tumor cells to evade the anti-tumor immune response (Butte et al., 2007). It is known that Myc can regulated anti-tumor response in different cancers, by binding directly to promoter of PD-L1 and regulating its expression (Casey et al., 2016). All of these gene products, or their interactors, are usually expressed on APCs, such as B lymphocytes, dendritic cells and macrophages and have a role in the activation of T-cell response, suggesting that their expression in infiltrating cells could lead to non-cell autonomous effect in promoting immune surveillance, all this being mediated by a yet-to-be characterized cross-talk with Pcgf6 in tumor cells.

Based on these premises, we set out to characterize the populations of infiltrated cells in Pcgf6 WT and KO tumors. Specifically, we performed immune-profiling of different myeloid and lymphoid lineages in transplanted primary tumors (see chapter 7.8): our preliminary data showed that the percentage of different myeloid populations (i.e. NK cells, macrophages, monocytes, NKT cells, DCs), both in spleen and lymph nodes, were similar between Pcgf6 KO and WT tumors, thus suggesting that myeloid lineages are not involved in promoting the Pcgf6-dependent phenotype. On the contrary, when lymphoid lineages were analyzed, we observed a significant reduction in the T-cell compartment, both in spleen and lymph nodes, in Pcgf6 KO tumors relative to the WT. This decrease was observed in both effector $CD4^+$ and

$CD8^+$ T-cells: while effector $CD4^+$ T cells were decreased exclusively in the spleen of transplanted mice, the decrease of $CD8^+$ T effectors was observed also in the lymph nodes. It is known that the primary immune response is triggered by APC-mediated antigen exposure that primes naïve $CD8^+$ T-cells in secondary lymph nodes, leading to their excessive proliferation and differentiation into effector $CD8^+$ T-cells. Such T-cells are then able to eliminate foreign cells (Kaech and Ahmed, 2001). Upon the clearance of these cells, a majority of effector $CD8^+$ T-cells undergo apoptosis, while a small number form a memory $CD8^+$ T-cell pool, which is further important for the adaptive immune response. It is generally accepted that B-cells can present antigen and prime naïve $CD4^+$ T-cells (Kambayashi and Laufer, 2014). However, B-cell dependent activation of $CD8^+$ T-cells still remains unclear. Our preliminary data suggest that in the absence of Pcgf6, B-cells fail to educate naïve T-cells into effectors, and thus halt the promotion of immune surveillance. This could imply an important role of Pcgf6 in B-cell dependent T-cell recruitment or activation, which would ultimately lead to tumor suppression. However, it remains unclear whether the Pcgf6-dependent immunological mechanism of tumor suppression could occur through direct interaction between B-cells and $CD8^+$ T-cells, or via $CD4^+$ T-cells activation. Further analyses will be necessary to thoroughly address this question.

It is important to note that, independently from its presence in the PRC1.6 complex, Pcgf6 has been found to interact also with the histone demethylase Jarid1c, thereby contributing to the removal of H3K4me3 and reduction of transcriptional activity at genes involved in DC activation (Boukhaled et al., 2016). In apparent contrast with this model, however, H3K4me3 and H3K4me1 ChIP-seq profiles in our stabilized lymphomas (LyWT and LyP6KO) were not altered upon Pcgf6 loss (either deletion or silencing). Thus, it remains to be addressed the possible involvement of Jarid1c – or other Pcgf6 interactors – in lymphomagenesis.

Altogether, we unraveled a novel role of Pcgf6 as a tumor suppressor in Myc-induced lymphomagenesis. The absence of major transcriptional alterations upon Pcgf6 loss would be in favor a non-transcriptional, PRC1.6-independent mechanism of action. Even if possible cell-autonomous effects of Pcgf6 in pre-tumoral *Eμ-myc* B-cells that could also explain this function - in particular possible Pcgf6 functions on Myc-induced B-cell apoptosis and proliferation - still need to be addressed, our data indicate that Pcgf6 may act by promoting non-cell autonomous effects through either recruitment or activation of T-cells. We surmise that Pcgf6 tumor suppressive function could be not restricted to lymphomas, but extended to different tumor types. In this regard it's noteworthy that Pcgf6 has been found recurrently downregulated in metastatic prostate cancers (Grasso et al., 2012). We speculate that the characterization of this novel Pcgf6 tumor suppressive function may unveil a novel level of regulation of Myc-dependent tumorigenesis and may lead to the development of more efficient targeted therapies for broad spectrum of tumors.

9. REFERENCE

Adams, J.M., Harris, A.W., Pinkert, C.A., Corcoran, L.M., Alexander, W.S., Cory, S., Palmiter, R.D., and Brinster, R.L. (1985). The c-myc oncogene driven by immunoglobulin enhancers induces lymphoid malignancy in transgenic mice. Nature *318*, 533-538.

Akasaka, T., Takahashi, N., Suzuki, M., Koseki, H., Bodmer, R., and Koga, H. (2002). MBLR, a new RING finger protein resembling mammalian Polycomb gene products, is regulated by cell cycle-dependent phosphorylation. Genes Cells *7*, 835-850.

Akasaka, T., Tsuji, K., Kawahira, H., Kanno, M., Harigaya, K., Hu, L., Ebihara, Y., Nakahata, T., Tetsu, O., Taniguchi, M.*, et al.* (1997). The role of mel-18, a mammalian Polycomb group gene, during IL-7-dependent proliferation of lymphocyte precursors. Immunity *7*, 135-146.

Alevizopoulos, K., Vlach, J., Hennecke, S., and Amati, B. (1997). Cyclin E and c-Myc promote cell proliferation in the presence of p16INK4a and of hypophosphorylated retinoblastoma family proteins. EMBO J *16*, 5322-5333.

Alexander, W.S., Schrader, J.W., and Adams, J.M. (1987). Expression of the c-myc oncogene under control of an immunoglobulin enhancer in E mu-myc transgenic mice. Mol Cell Biol *7*, 1436-1444.

Alkema, M.J., Jacobs, H., van Lohuizen, M., and Berns, A. (1997). Pertubation of B and T cell development and predisposition to lymphomagenesis in Emu Bmi1 transgenic mice require the Bmi1 RING finger. Oncogene *15*, 899-910.

Amati, B., Brooks, M.W., Levy, N., Littlewood, T.D., Evan, G.I., and Land, H. (1993a). Oncogenic activity of the c-Myc protein requires dimerization with Max. Cell *72*, 233-245.

Amati, B., Dalton, S., Brooks, M.W., Littlewood, T.D., Evan, G.I., and Land, H. (1992). Transcriptional activation by the human c-Myc oncoprotein in yeast requires interaction with Max. Nature *359*, 423-426.

Amati, B., Littlewood, T.D., Evan, G.I., and Land, H. (1993b). The c-Myc protein induces cell cycle progression and apoptosis through dimerization with Max. EMBO J *12*, 5083-5087.

Arabi, A., Wu, S., Ridderstrale, K., Bierhoff, H., Shiue, C., Fatyol, K., Fahlen, S., Hydbring, P., Soderberg, O., Grummt, I., *et al.* (2005). c-Myc associates with ribosomal DNA and activates RNA polymerase I transcription. Nat Cell Biol *7*, 303-310.

Arnold, H.K., and Sears, R.C. (2006). Protein phosphatase 2A regulatory subunit b56 alpha associates with c-Myc and negatively regulates c-Myc accumulation. Molecular and Cellular Biology *26*, 2832-2844.

Ayer, D.E. (1999). Histone deacetylases: transcriptional repression with SINers and NuRDs. Trends Cell Biol *9*, 193-198.

Ayer, D.E., Kretzner, L., and Eisenman, R.N. (1993). Mad: a heterodimeric partner for Max that antagonizes Myc transcriptional activity. Cell *72*, 211-222.

Ayer, D.E., Lawrence, Q.A., and Eisenman, R.N. (1995). Mad-Max transcriptional repression is mediated by ternary complex formation with mammalian homologs of yeast repressor Sin3. Cell *80*, 767-776.

Basso, K., and Dalla-Favera, R. (2015). Germinal centres and B cell lymphomagenesis. Nat Rev Immunol *15*, 172-184.

Beguelin, W., Teater, M., Gearhart, M.D., Calvo Fernandez, M.T., Goldstein, R.L., Cardenas, M.G., Hatzi, K., Rosen, M., Shen, H., Corcoran, C.M., *et al.* (2016). EZH2 and BCL6 Cooperate to Assemble CBX8-BCOR Complex to Repress Bivalent Promoters, Mediate Germinal Center Formation and Lymphomagenesis. Cancer Cell *30*, 197-213.

Beier, R., Burgin, A., Kiermaier, A., Fero, M., Karsunky, H., Saffrich, R., Moroy, T., Ansorge, W., Roberts, J., and Eilers, M. (2000). Induction of cyclin E-cdk2 kinase activity, E2F-dependent transcription and cell growth by Myc are genetically separable events. EMBO J *19*, 5813-5823.

Bentley, D.L., and Groudine, M. (1986). A block to elongation is largely responsible for decreased transcription of c-myc in differentiated HL60 cells. Nature *321*, 702-706.

Beroukhim, R., Mermel, C.H., Porter, D., Wei, G., Raychaudhuri, S., Donovan, J., Barretina, J., Boehm, J.S., Dobson, J., Urashima, M., *et al.* (2010). The landscape of somatic copy-number alteration across human cancers. Nature *463*, 899-905.

Bhatia, K., Huppi, K., Spangler, G., Siwarski, D., Iyer, R., and Magrath, I. (1993). Point mutations in the c-Myc transactivation domain are common in Burkitt's lymphoma and mouse plasmacytomas. Nat Genet *5*, 56-61.

Bianchi, V., Ceol, A., Ogier, A.G., de Pretis, S., Galeota, E., Kishore, K., Bora, P., Croci, O., Campaner, S., Amati, B., *et al.* (2016). Integrated Systems for NGS Data Management and Analysis: Open Issues and Available Solutions. Front Genet *7*, 75.

Bisso, A., Sabo, A., and Amati, B. (2019). MYC in Germinal Center-derived lymphomas: Mechanisms and therapeutic opportunities. Immunol Rev *288*, 178-197.

Bissonnette, R.P., Echeverri, F., Mahboubi, A., and Green, D.R. (1992). Apoptotic cell death induced by c-myc is inhibited by bcl-2. Nature *359*, 552-554.

Blackledge, N.P., Farcas, A.M., Kondo, T., King, H.W., McGouran, J.F., Hanssen, L.L., Ito, S., Cooper, S., Kondo, K., Koseki, Y.*, et al.* (2014). Variant PRC1 complex-dependent H2A ubiquitylation drives PRC2 recruitment and polycomb domain formation. Cell *157*, 1445-1459.

Blackledge, N.P., Rose, N.R., and Klose, R.J. (2015). Targeting Polycomb systems to regulate gene expression: modifications to a complex story. Nat Rev Mol Cell Biol *16*, 643-649.

Blackwell, T.K., and Weintraub, H. (1990). Differences and similarities in DNA-binding preferences of MyoD and E2A protein complexes revealed by binding site selection. Science *250*, 1104-1110.

Blackwood, E.M., and Eisenman, R.N. (1991). Max: a helix-loop-helix zipper protein that forms a sequence-specific DNA-binding complex with Myc. Science *251*, 1211-1217.

Bouchard, C., Marquardt, J., Bras, A., Medema, R.H., and Eilers, M. (2004). Myc-induced proliferation and transformation require Akt-mediated phosphorylation of FoxO proteins. EMBO J *23*, 2830-2840.

Boukhaled, G.M., Cordeiro, B., Deblois, G., Dimitrov, V., Bailey, S.D., Holowka, T., Domi, A., Guak, H., Chiu, H.H., Everts, B.*, et al.* (2016). The Transcriptional Repressor Polycomb Group Factor 6, PCGF6, Negatively Regulates Dendritic Cell Activation and Promotes Quiescence. Cell Rep *16*, 1829-1837.

Bracken, A.P., and Helin, K. (2009). Polycomb group proteins: navigators of lineage pathways led astray in cancer. Nat Rev Cancer *9*, 773-784.

Bromberg, J.F., Wrzeszczynska, M.H., Devgan, G., Zhao, Y., Pestell, R.G., Albanese, C., and Darnell, J.E., Jr. (1999). Stat3 as an oncogene. Cell *98*, 295-303.

Butte, M.J., Keir, M.E., Phamduy, T.B., Sharpe, A.H., and Freeman, G.J. (2007). Programmed death-1 ligand 1 interacts specifically with the B7-1 costimulatory molecule to inhibit T cell responses. Immunity *27*, 111-122.

Caganova, M., Carrisi, C., Varano, G., Mainoldi, F., Zanardi, F., Germain, P.L., George, L., Alberghini, F., Ferrarini, L., Talukder, A.K.*, et al.* (2013). Germinal center dysregulation by histone methyltransferase EZH2 promotes lymphomagenesis. J Clin Invest *123*, 5009-5022.

Calado, D.P., Sasaki, Y., Godinho, S.A., Pellerin, A., Kochert, K., Sleckman, B.P., de Alboran, I.M., Janz, M., Rodig, S., and Rajewsky, K. (2012). The cell-cycle regulator c-Myc is essential for the formation and maintenance of germinal centers. Nat Immunol *13*, 1092-1100.

Cales, C., Roman-Trufero, M., Pavon, L., Serrano, I., Melgar, T., Endoh, M., Perez, C., Koseki, H., and Vidal, M. (2008). Inactivation of the polycomb group protein Ring1B unveils an antiproliferative role in hematopoietic cell expansion and cooperation with tumorigenesis associated with Ink4a deletion. Mol Cell Biol *28*, 1018-1028.

Calo, E., and Wysocka, J. (2013). Modification of enhancer chromatin: what, how, and why? Mol Cell *49*, 825-837.

Campaner, S., Doni, M., Hydbring, P., Verrecchia, A., Bianchi, L., Sardella, D., Schleker, T., Perna, D., Tronnersjo, S., Murga, M.*, et al.* (2010). Cdk2 suppresses cellular senescence induced by the c-myc oncogene. Nat Cell Biol *12*, 54-59; sup pp 51-14.

Cao, R., Tsukada, Y., and Zhang, Y. (2005). Role of Bmi-1 and Ring1A in H2A ubiquitylation and Hox gene silencing. Mol Cell *20*, 845-854.

Cao, R., Wang, L., Wang, H., Xia, L., Erdjument-Bromage, H., Tempst, P., Jones, R.S., and Zhang, Y. (2002). Role of histone H3 lysine 27 methylation in Polycomb-group silencing. Science *298*, 1039-1043.

Carsetti, R., Kohler, G., and Lamers, M.C. (1995). Transitional B cells are the target of negative selection in the B cell compartment. J Exp Med *181*, 2129-2140.

Carugo, A., Genovese, G., Seth, S., Nezi, L., Rose, J.L., Bossi, D., Cicalese, A., Shah, P.K., Viale, A., Pettazzoni, P.F.*, et al.* (2016). In Vivo Functional Platform Targeting Patient-Derived Xenografts Identifies WDR5-Myc Association as a Critical Determinant of Pancreatic Cancer. Cell Rep *16*, 133-147.

Casey, S.C., Tong, L., Li, Y., Do, R., Walz, S., Fitzgerald, K.N., Gouw, A.M., Baylot, V., Gutgemann, I., Eilers, M.*, et al.* (2016). MYC regulates the antitumor immune response through CD47 and PD-L1. Science *352*, 227-231.

Cedar, H., and Bergman, Y. (2008). Choreography of Ig allelic exclusion. Curr Opin Immunol *20*, 308-317.

Chappell, S.A., LeQuesne, J.P., Paulin, F.E., deSchoolmeester, M.L., Stoneley, M., Soutar, R.L., Ralston, S.H., Helfrich, M.H., and Willis, A.E. (2000). A mutation in the c-myc-IRES leads to enhanced internal ribosome entry in multiple myeloma: a novel mechanism of oncogene de-regulation. Oncogene *19*, 4437-4440.

Charron, J., Malynn, B.A., Fisher, P., Stewart, V., Jeannotte, L., Goff, S.P., Robertson, E.J., and Alt, F.W. (1992). Embryonic lethality in mice homozygous for a targeted disruption of the N-myc gene. Genes Dev *6*, 2248-2257.

Chen, L., and Flies, D.B. (2013). Molecular mechanisms of T cell co-stimulation and co-inhibition. Nat Rev Immunol *13*, 227-242.

Cheng, S.W., Davies, K.P., Yung, E., Beltran, R.J., Yu, J., and Kalpana, G.V. (1999). c-MYC interacts with INI1/hSNF5 and requires the SWI/SNF complex for transactivation function. Nat Genet *22*, 102-105.

Chigrinova, E., Rinaldi, A., Kwee, I., Rossi, D., Rancoita, P.M., Strefford, J.C., Oscier, D., Stamatopoulos, K., Papadaki, T., Berger, F.*, et al.* (2013). Two main genetic pathways lead to the transformation of chronic lymphocytic leukemia to Richter syndrome. Blood *122*, 2673-2682.

Chipuk, J.E., Kuwana, T., Bouchier-Hayes, L., Droin, N.M., Newmeyer, D., Schuler, M., and Green, D.R. (2004). Direct activation of Bax by p53 mediates mitochondrial membrane permeabilization and apoptosis. Science *303*, 1010-1014.

Chou, C., Pinto, A.K., Curtis, J.D., Persaud, S.P., Cella, M., Lin, C.C., Edelson, B.T., Allen, P.M., Colonna, M., Pearce, E.L.*, et al.* (2014). c-Myc-induced transcription factor AP4 is required for host protection mediated by CD8+ T cells. Nat Immunol *15*, 884-893.

Ciriello, G., Miller, M.L., Aksoy, B.A., Senbabaoglu, Y., Schultz, N., and Sander, C. (2013). Emerging landscape of oncogenic signatures across human cancers. Nat Genet *45*, 1127-1133.

Clegg, N.J., Couto, S.S., Wongvipat, J., Hieronymus, H., Carver, B.S., Taylor, B.S., Ellwood-Yen, K., Gerald, W.L., Sander, C., and Sawyers, C.L. (2011). MYC cooperates with AKT in prostate tumorigenesis and alters sensitivity to mTOR inhibitors. PLoS One *6*, e17449.

Comino-Mendez, I., Gracia-Aznarez, F.J., Schiavi, F., Landa, I., Leandro-Garcia, L.J., Leton, R., Honrado, E., Ramos-Medina, R., Caronia, D., Pita, G.*, et al.* (2011). Exome sequencing identifies MAX mutations as a cause of hereditary pheochromocytoma. Nat Genet *43*, 663-667.

Conacci-Sorrell, M., McFerrin, L., and Eisenman, R.N. (2014). An overview of MYC and its interactome. Cold Spring Harb Perspect Med *4*, a014357.

Connelly, K.E., and Dykhuizen, E.C. (2017). Compositional and functional diversity of canonical PRC1 complexes in mammals. Biochim Biophys Acta Gene Regul Mech *1860*, 233-245.

Cory, S. (1986). Activation of cellular oncogenes in hemopoietic cells by chromosome translocation. Adv Cancer Res *47*, 189-234.

Cowling, V.H., Chandriani, S., Whitfield, M.L., and Cole, M.D. (2006). A conserved Myc protein domain, MBIV, regulates DNA binding, apoptosis, transformation, and G2 arrest. Mol Cell Biol *26*, 4226-4239.

Crouch, D.H., Fisher, F., Clark, W., Jayaraman, P.S., Goding, C.R., and Gillespie, D.A. (1993). Gene-regulatory properties of Myc helix-loop-helix/leucine zipper mutants: Max-dependent DNA binding and transcriptional activation in yeast correlates with transforming capacity. Oncogene *8*, 1849-1855.

Csibi, A., Lee, G., Yoon, S.O., Tong, H., Ilter, D., Elia, I., Fendt, S.M., Roberts, T.M., and Blenis, J. (2014). The mTORC1/S6K1 pathway regulates glutamine metabolism through the eIF4B-dependent control of c-Myc translation. Curr Biol *24*, 2274-2280.

Culjkovic, B., Topisirovic, I., Skrabanek, L., Ruiz-Gutierrez, M., and Borden, K.L. (2006). eIF4E is a central node of an RNA regulon that governs cellular proliferation. J Cell Biol *175*, 415-426.

Dal Porto, J.M., Haberman, A.M., Kelsoe, G., and Shlomchik, M.J. (2002). Very low affinity B cells form germinal centers, become memory B cells, and participate in secondary immune responses when higher affinity competition is reduced. J Exp Med *195*, 1215-1221.

Dang, C.V. (2012). MYC on the path to cancer. Cell *149*, 22-35.

Dang, C.V. (2013). MYC, metabolism, cell growth, and tumorigenesis. Cold Spring Harb Perspect Med *3*.

Dang, C.V., Barrett, J., Villa-Garcia, M., Resar, L.M., Kato, G.J., and Fearon, E.R. (1991). Intracellular leucine zipper interactions suggest c-Myc hetero-oligomerization. Mol Cell Biol *11*, 954-962.

Dang, C.V., and Lee, W.M. (1988). Identification of the human c-myc protein nuclear translocation signal. Mol Cell Biol *8*, 4048-4054.

Dani, C., Blanchard, J.M., Piechaczyk, M., El Sabouty, S., Marty, L., and Jeanteur, P. (1984). Extreme instability of myc mRNA in normal and transformed human cells. Proc Natl Acad Sci U S A *81*, 7046-7050.

Darzynkiewicz, Z., Traganos, F., and Melamed, M.R. (1980). New cell cycle compartments identified by multiparameter flow cytometry. Cytometry *1*, 98-108.

Davis, A.C., Wims, M., Spotts, G.D., Hann, S.R., and Bradley, A. (1993). A null c-myc mutation causes lethality before 10.5 days of gestation in homozygotes and reduced fertility in heterozygous female mice. Genes Dev *7*, 671-682.

de Alboran, I.M., Baena, E., and Martinez, A.C. (2004). c-Myc-deficient B lymphocytes are resistant to spontaneous and induced cell death. Cell Death Differ *11*, 61-68.

de Alboran, I.M., O'Hagan, R.C., Gartner, F., Malynn, B., Davidson, L., Rickert, R., Rajewsky, K., DePinho, R.A., and Alt, F.W. (2001). Analysis of C-MYC function in normal cells via conditional gene-targeted mutation. Immunity *14*, 45-55.

De Paoli, L., Cerri, M., Monti, S., Rasi, S., Spina, V., Bruscaggin, A., Greco, M., Ciardullo, C., Fama, R., Cresta, S.*, et al.* (2013). MGA, a suppressor of MYC, is recurrently inactivated in high risk chronic lymphocytic leukemia. Leuk Lymphoma *54*, 1087-1090.

de Pretis, S., Kress, T.R., Morelli, M.J., Sabò, A., Locarno, C., Verrecchia, A., Doni, M., Campaner, S., Amati, B., and Pelizzola, M. (2017). Integrative analysis of RNA polymerase II and transcriptional dynamics upon MYC activation. Genome Res *27*, 1658-1664.

De Silva, N.S., and Klein, U. (2015). Dynamics of B cells in germinal centres. Nat Rev Immunol *15*, 137-148.

Dejure, F.R., and Eilers, M. (2017). MYC and tumor metabolism: chicken and egg. EMBO J *36*, 3409-3420.

DeoCampo, N.D., Wilson, M.R., and Trosko, J.E. (2000). Cooperation of bcl-2 and myc in the neoplastic transformation of normal rat liver epithelial cells is related to the down-regulation of gap junction-mediated intercellular communication. Carcinogenesis *21*, 1501-1506.

Deshaies, R.J. (1999). SCF and Cullin/Ring H2-based ubiquitin ligases. Annu Rev Cell Dev Biol *15*, 435-467.

Di Carlo, V., Mocavini, I., and Di Croce, L. (2019). Polycomb complexes in normal and malignant hematopoiesis. J Cell Biol *218*, 55-69.

Di Croce, L., and Helin, K. (2013). Transcriptional regulation by Polycomb group proteins. Nat Struct Mol Biol *20*, 1147-1155.

Diolaiti, D., McFerrin, L., Carroll, P.A., and Eisenman, R.N. (2015). Functional interactions among members of the MAX and MLX transcriptional network during oncogenesis. Biochim Biophys Acta *1849*, 484-500.

Dominguez-Sola, D., and Gautier, J. (2014). MYC and the control of DNA replication. Cold Spring Harb Perspect Med *4*.

Dominguez-Sola, D., Victora, G.D., Ying, C.Y., Phan, R.T., Saito, M., Nussenzweig, M.C., and Dalla-Favera, R. (2012). The proto-oncogene MYC is required for selection in the germinal center and cyclic reentry. Nat Immunol *13*, 1083-1091.

Dominguez-Sola, D., Ying, C.Y., Grandori, C., Ruggiero, L., Chen, B., Li, M., Galloway, D.A., Gu, W., Gautier, J., and Dalla-Favera, R. (2007). Non-transcriptional control of DNA replication by c-Myc. Nature *448*, 445-451.

Eberhardy, S.R., and Farnham, P.J. (2002). Myc recruits P-TEFb to mediate the final step in the transcriptional activation of the cad promoter. J Biol Chem *277*, 40156-40162.

Edelmann, J., Holzmann, K., Miller, F., Winkler, D., Buhler, A., Zenz, T., Bullinger, L., Kuhn, M.W., Gerhardinger, A., Bloehdorn, J.*, et al.* (2012). High-resolution genomic profiling of chronic lymphocytic leukemia reveals new recurrent genomic alterations. Blood *120*, 4783-4794.

Eick, D., and Bornkamm, G.W. (1986). Transcriptional arrest within the first exon is a fast control mechanism in c-myc gene expression. Nucleic Acids Res *14*, 8331-8346.

Eilers, M., and Eisenman, R.N. (2008). Myc's broad reach. Genes Dev *22*, 2755-2766.

Eischen, C.M., Weber, J.D., Roussel, M.F., Sherr, C.J., and Cleveland, J.L. (1999). Disruption of the ARF-Mdm2-p53 tumor suppressor pathway in Myc-induced lymphomagenesis. Genes Dev *13*, 2658-2669.

Eischen, C.M., Woo, D., Roussel, M.F., and Cleveland, J.L. (2001). Apoptosis triggered by Myc-induced suppression of Bcl-X(L) or Bcl-2 is bypassed during lymphomagenesis. Mol Cell Biol *21*, 5063-5070.

Eissenberg, J.C., and Elgin, S.C. (2000). The HP1 protein family: getting a grip on chromatin. Curr Opin Genet Dev *10*, 204-210.

Elderkin, S., Maertens, G.N., Endoh, M., Mallery, D.L., Morrice, N., Koseki, H., Peters, G., Brockdorff, N., and Hiom, K. (2007). A phosphorylated form of Mel-18 targets the Ring1B histone H2A ubiquitin ligase to chromatin. Mol Cell *28*, 107-120.

Endoh, M., Endo, T.A., Shinga, J., Hayashi, K., Farcas, A., Ma, K.W., Ito, S., Sharif, J., Endoh, T., Onaga, N.*, et al.* (2017). PCGF6-PRC1 suppresses premature differentiation of mouse embryonic stem cells by regulating germ cell-related genes. Elife *6*.

Era, T., Ogawa, M., Nishikawa, S., Okamoto, M., Honjo, T., Akagi, K., Miyazaki, J., and Yamamura, K. (1991). Differentiation of growth signal requirement of B lymphocyte precursor is directed by expression of immunoglobulin. EMBO J *10*, 337-342.

Evan, G.I., Wyllie, A.H., Gilbert, C.S., Littlewood, T.D., Land, H., Brooks, M., Waters, C.M., Penn, L.Z., and Hancock, D.C. (1992). Induction of apoptosis in fibroblasts by c-myc protein. Cell *69*, 119-128.

Ezhkova, E., Lien, W.H., Stokes, N., Pasolli, H.A., Silva, J.M., and Fuchs, E. (2011). EZH1 and EZH2 cogovern histone H3K27 trimethylation and are essential for hair follicle homeostasis and wound repair. Genes Dev *25*, 485-498.

Faiola, F., Liu, X., Lo, S., Pan, S., Zhang, K., Lymar, E., Farina, A., and Martinez, E. (2005). Dual regulation of c-Myc by p300 via acetylation-dependent control of Myc protein turnover and coactivation of Myc-induced transcription. Mol Cell Biol *25*, 10220-10234.

Farrell, A.S., and Sears, R.C. (2014). MYC degradation. Cold Spring Harb Perspect Med *4*.

Faust, C., Schumacher, A., Holdener, B., and Magnuson, T. (1995). The eed mutation disrupts anterior mesoderm production in mice. Development *121*, 273-285.

Fellmann, C., Hoffmann, T., Sridhar, V., Hopfgartner, B., Muhar, M., Roth, M., Lai, D.Y., Barbosa, I.A., Kwon, J.S., Guan, Y.*, et al.* (2013). An optimized microRNA backbone for effective single-copy RNAi. Cell Rep *5*, 1704-1713.

Felsher, D.W., and Bishop, J.M. (1999). Reversible tumorigenesis by MYC in hematopoietic lineages. Mol Cell *4*, 199-207.

Felsher, D.W., Zetterberg, A., Zhu, J., Tlsty, T., and Bishop, J.M. (2000). Overexpression of MYC causes p53-dependent G2 arrest of normal fibroblasts. Proc Natl Acad Sci U S A *97*, 10544-10548.

Fernandez, P.C., Frank, S.R., Wang, L., Schroeder, M., Liu, S., Greene, J., Cocito, A., and Amati, B. (2003). Genomic targets of the human c-Myc protein. Genes Dev *17*, 1115-1129.

Finkin, S., Hartweger, H., Oliveira, T.Y., Kara, E.E., and Nussenzweig, M.C. (2019). Protein Amounts of the MYC Transcription Factor Determine Germinal Center B Cell Division Capacity. Immunity *51*, 324-336 e325.

Fischle, W., Wang, Y., Jacobs, S.A., Kim, Y., Allis, C.D., and Khorasanizadeh, S. (2003). Molecular basis for the discrimination of repressive methyl-lysine marks in histone H3 by Polycomb and HP1 chromodomains. Genes Dev *17*, 1870-1881.

Foley, K.P., McArthur, G.A., Queva, C., Hurlin, P.J., Soriano, P., and Eisenman, R.N. (1998). Targeted disruption of the MYC antagonist MAD1 inhibits cell cycle exit during granulocyte differentiation. EMBO J *17*, 774-785.

Frank, S.R., Parisi, T., Taubert, S., Fernandez, P., Fuchs, M., Chan, H.M., Livingston, D.M., and Amati, B. (2003). MYC recruits the TIP60 histone acetyltransferase complex to chromatin. EMBO Rep *4*, 575-580.

Fursova, N.A., Blackledge, N.P., Nakayama, M., Ito, S., Koseki, Y., Farcas, A.M., King, H.W., Koseki, H., and Klose, R.J. (2019). Synergy between Variant PRC1 Complexes Defines Polycomb-Mediated Gene Repression. Mol Cell *74*, 1020-1036 e1028.

Gabay, M., Li, Y., and Felsher, D.W. (2014). MYC activation is a hallmark of cancer initiation and maintenance. Cold Spring Harb Perspect Med *4*.

Gao, Z., Zhang, J., Bonasio, R., Strino, F., Sawai, A., Parisi, F., Kluger, Y., and Reinberg, D. (2012). PCGF homologs, CBX proteins, and RYBP define functionally distinct PRC1 family complexes. Mol Cell *45*, 344-356.

Gartel, A.L., Ye, X., Goufman, E., Shianov, P., Hay, N., Najmabadi, F., and Tyner, A.L. (2001). Myc represses the p21(WAF1/CIP1) promoter and interacts with Sp1/Sp3. Proc Natl Acad Sci U S A *98*, 4510-4515.

Gentleman, R.C., Carey, V.J., Bates, D.M., Bolstad, B., Dettling, M., Dudoit, S., Ellis, B., Gautier, L., Ge, Y., Gentry, J.*, et al.* (2004). Bioconductor: open software development for computational biology and bioinformatics. Genome Biol *5*, R80.

Gonzalez-Prieto, R., Cuijpers, S.A., Kumar, R., Hendriks, I.A., and Vertegaal, A.C. (2015). c-Myc is targeted to the proteasome for degradation in a SUMOylation-dependent manner, regulated by PIAS1, SENP7 and RNF4. Cell Cycle *14*, 1859-1872.

Gorrini, C., Squatrito, M., Luise, C., Syed, N., Perna, D., Wark, L., Martinato, F., Sardella, D., Verrecchia, A., Bennett, S.*, et al.* (2007). Tip60 is a haplo-insufficient tumour suppressor required for an oncogene-induced DNA damage response. Nature *448*, 1063-1067.

Grande, B.M., Gerhard, D.S., Jiang, A., Griner, N.B., Abramson, J.S., Alexander, T.B., Allen, H., Ayers, L.W., Bethony, J.M., Bhatia, K.*, et al.* (2019). Genome-wide discovery of somatic coding and noncoding mutations in pediatric endemic and sporadic Burkitt lymphoma. Blood *133*, 1313-1324.

Grandori, C., Wu, K.J., Fernandez, P., Ngouenet, C., Grim, J., Clurman, B.E., Moser, M.J., Oshima, J., Russell, D.W., Swisshelm, K.*, et al.* (2003). Werner syndrome protein limits MYC-induced cellular senescence. Genes Dev *17*, 1569-1574.

Grasso, C.S., Wu, Y.M., Robinson, D.R., Cao, X., Dhanasekaran, S.M., Khan, A.P., Quist, M.J., Jing, X., Lonigro, R.J., Brenner, J.C.*, et al.* (2012). The mutational landscape of lethal castration-resistant prostate cancer. Nature *487*, 239-243.

Guccione, E., Martinato, F., Finocchiaro, G., Luzi, L., Tizzoni, L., Dall' Olio, V., Zardo, G., Nervi, C., Bernard, L., and Amati, B. (2006). Myc-binding-site recognition in the human genome is determined by chromatin context. Nat Cell Biol *8*, 764-770.

Guo, Y., Nady, N., Qi, C., Allali-Hassani, A., Zhu, H., Pan, P., Adams-Cioaba, M.A., Amaya, M.F., Dong, A., Vedadi, M.*, et al.* (2009). Methylation-state-specific recognition of histones by the MBT repeat protein L3MBTL2. Nucleic Acids Res *37*, 2204-2210.

Hardy, R.R., Carmack, C.E., Shinton, S.A., Kemp, J.D., and Hayakawa, K. (1991). Resolution and characterization of pro-B and pre-pro-B cell stages in normal mouse bone marrow. J Exp Med *173*, 1213-1225.

Hardy, R.R., and Hayakawa, K. (1991). A developmental switch in B lymphopoiesis. Proc Natl Acad Sci U S A *88*, 11550-11554.

Hassig, C.A., Fleischer, T.C., Billin, A.N., Schreiber, S.L., and Ayer, D.E. (1997). Histone deacetylase activity is required for full transcriptional repression by mSin3A. Cell *89*, 341-347.

Hatton, K.S., Mahon, K., Chin, L., Chiu, F.C., Lee, H.W., Peng, D., Morgenbesser, S.D., Horner, J., and DePinho, R.A. (1996). Expression and activity of L-Myc in normal mouse development. Mol Cell Biol *16*, 1794-1804.

Hatzi, K., and Melnick, A. (2014). Breaking bad in the germinal center: how deregulation of BCL6 contributes to lymphomagenesis. Trends Mol Med *20*, 343-352.

Hauri, S., Comoglio, F., Seimiya, M., Gerstung, M., Glatter, T., Hansen, K., Aebersold, R., Paro, R., Gstaiger, M., and Beisel, C. (2016). A High-Density Map for Navigating the Human Polycomb Complexome. Cell Rep *17*, 583-595.

He, T.C., Sparks, A.B., Rago, C., Hermeking, H., Zawel, L., da Costa, L.T., Morin, P.J., Vogelstein, B., and Kinzler, K.W. (1998). Identification of c-MYC as a target of the APC pathway. Science *281*, 1509-1512.

Heinzel, S., Binh Giang, T., Kan, A., Marchingo, J.M., Lye, B.K., Corcoran, L.M., and Hodgkin, P.D. (2017). A Myc-dependent division timer complements a cell-death timer to regulate T cell and B cell responses. Nat Immunol *18*, 96-103.

Hemann, M.T., Bric, A., Teruya-Feldstein, J., Herbst, A., Nilsson, J.A., Cordon-Cardo, C., Cleveland, J.L., Tansey, W.P., and Lowe, S.W. (2005). Evasion of the p53 tumour surveillance network by tumour-derived MYC mutants. Nature *436*, 807-811.

Herbst, A., Hemann, M.T., Tworkowski, K.A., Salghetti, S.E., Lowe, S.W., and Tansey, W.P. (2005). A conserved element in Myc that negatively regulates its proapoptotic activity. EMBO Rep *6*, 177-183.

Herold, S., Wanzel, M., Beuger, V., Frohme, C., Beul, D., Hillukkala, T., Syvaoja, J., Saluz, H.P., Haenel, F., and Eilers, M. (2002). Negative regulation of the mammalian UV response by Myc through association with Miz-1. Mol Cell *10*, 509-521.

Hu, G., Kim, J., Xu, Q., Leng, Y., Orkin, S.H., and Elledge, S.J. (2009). A genome-wide RNAi screen identifies a new transcriptional module required for self-renewal. Genes Dev *23*, 837-848.

Huang, Y., Zhao, W., Wang, C., Zhu, Y., Liu, M., Tong, H., Xia, Y., Jiang, Q., and Qin, J. (2018). Combinatorial Control of Recruitment of a Variant PRC1.6 Complex in Embryonic Stem Cells. Cell Rep *22*, 3032-3043.

Huh, Y.O., Lin, K.I., Vega, F., Schlette, E., Yin, C.C., Keating, M.J., Luthra, R., Medeiros, L.J., and Abruzzo, L.V. (2008). MYC translocation in chronic lymphocytic leukaemia is associated with increased prolymphocytes and a poor prognosis. Br J Haematol *142*, 36-44.

Hurlin, P.J., and Huang, J. (2006). The MAX-interacting transcription factor network. Semin Cancer Biol *16*, 265-274.

Hurlin, P.J., Queva, C., and Eisenman, R.N. (1997). Mnt: a novel Max-interacting protein and Myc antagonist. Curr Top Microbiol Immunol *224*, 115-121.

Hurlin, P.J., Queva, C., Koskinen, P.J., Steingrimsson, E., Ayer, D.E., Copeland, N.G., Jenkins, N.A., and Eisenman, R.N. (1995). Mad3 and Mad4: novel Max-interacting transcriptional repressors that suppress c-myc dependent transformation and are expressed during neural and epidermal differentiation. EMBO J *14*, 5646-5659.

Hurlin, P.J., Steingrimsson, E., Copeland, N.G., Jenkins, N.A., and Eisenman, R.N. (1999). Mga, a dual-specificity transcription factor that interacts with Max and contains a T-domain DNA-binding motif. EMBO J *18*, 7019-7028.

Hurlin, P.J., Zhou, Z.Q., Toyo-oka, K., Ota, S., Walker, W.L., Hirotsune, S., and Wynshaw-Boris, A. (2003). Deletion of Mnt leads to disrupted cell cycle control and tumorigenesis. EMBO J *22*, 4584-4596.

Inoue, T., Morita, M., Hijikata, A., Fukuda-Yuzawa, Y., Adachi, S., Isono, K., Ikawa, T., Kawamoto, H., Koseki, H., Natsume, T.*, et al.* (2015). CNOT3 contributes to early B cell development by controlling Igh rearrangement and p53 mRNA stability. J Exp Med *212*, 1465-1479.

Iritani, B.M., and Eisenman, R.N. (1999). c-Myc enhances protein synthesis and cell size during B lymphocyte development. Proc Natl Acad Sci U S A *96*, 13180-13185.

Jacobs, J.J., Scheijen, B., Voncken, J.W., Kieboom, K., Berns, A., and van Lohuizen, M. (1999). Bmi-1 collaborates with c-Myc in tumorigenesis by inhibiting c-Myc-induced apoptosis via INK4a/ARF. Genes Dev *13*, 2678-2690.

Jain, M., Arvanitis, C., Chu, K., Dewey, W., Leonhardt, E., Trinh, M., Sundberg, C.D., Bishop, J.M., and Felsher, D.W. (2002). Sustained loss of a neoplastic phenotype by brief inactivation of MYC. Science *297*, 102-104.

Johansson, K., Persson, H., Lewis, A.M., Pettersson, U., Tibbetts, C., and Philipson, L. (1978). Viral DNA sequences and gene products in hamster cells transformed by adenovirus type 2. J Virol *27*, 628-639.

Kaech, S.M., and Ahmed, R. (2001). Memory CD8+ T cell differentiation: initial antigen encounter triggers a developmental program in naive cells. Nat Immunol *2*, 415-422.

Kalkat, M., Resetca, D., Lourenco, C., Chan, P.K., Wei, Y., Shiah, Y.J., Vitkin, N., Tong, Y., Sunnerhagen, M., Done, S.J.*, et al.* (2018). MYC Protein Interactome Profiling Reveals Functionally Distinct Regions that Cooperate to Drive Tumorigenesis. Mol Cell *72*, 836-848 e837.

Kambayashi, T., and Laufer, T.M. (2014). Atypical MHC class II-expressing antigen-presenting cells: can anything replace a dendritic cell? Nat Rev Immunol *14*, 719-730.

Kato, G.J., Barrett, J., Villa-Garcia, M., and Dang, C.V. (1990). An amino-terminal c-myc domain required for neoplastic transformation activates transcription. Mol Cell Biol *10*, 5914-5920.

Kato, Z., Jee, J., Shikano, H., Mishima, M., Ohki, I., Ohnishi, H., Li, A., Hashimoto, K., Matsukuma, E., Omoya, K.*, et al.* (2003). The structure and binding mode of interleukin-18. Nat Struct Biol *10*, 966-971.

Kelly, K., Cochran, B.H., Stiles, C.D., and Leder, P. (1983). Cell-specific regulation of the c-myc gene by lymphocyte mitogens and platelet-derived growth factor. Cell *35*, 603-610.

Ketel, C.S., Andersen, E.F., Vargas, M.L., Suh, J., Strome, S., and Simon, J.A. (2005). Subunit contributions to histone methyltransferase activities of fly and worm polycomb group complexes. Mol Cell Biol *25*, 6857-6868.

Kieffer-Kwon, K.R., Nimura, K., Rao, S.S.P., Xu, J., Jung, S., Pekowska, A., Dose, M., Stevens, E., Mathe, E., Dong, P.*, et al.* (2017). Myc Regulates Chromatin Decompaction and Nuclear Architecture during B Cell Activation. Mol Cell *67*, 566-578 e510.

Kim, D., Pertea, G., Trapnell, C., Pimentel, H., Kelley, R., and Salzberg, S.L. (2013). TopHat2: accurate alignment of transcriptomes in the presence of insertions, deletions and gene fusions. Genome Biol *14*, R36.

Kim, H., Kang, K., and Kim, J. (2009a). AEBP2 as a potential targeting protein for Polycomb Repression Complex PRC2. Nucleic Acids Res *37*, 2940-2950.

Kim, H.H., Kuwano, Y., Srikantan, S., Lee, E.K., Martindale, J.L., and Gorospe, M. (2009b). HuR recruits let-7/RISC to repress c-Myc expression. Genes Dev *23*, 1743-1748.

Kim, J.W., Gao, P., Liu, Y.C., Semenza, G.L., and Dang, C.V. (2007). Hypoxia-inducible factor 1 and dysregulated c-Myc cooperatively induce vascular endothelial growth factor and metabolic switches hexokinase 2 and pyruvate dehydrogenase kinase 1. Mol Cell Biol *27*, 7381-7393.

Kim, S.Y., Herbst, A., Tworkowski, K.A., Salghetti, S.E., and Tansey, W.P. (2003). Skp2 regulates Myc protein stability and activity. Mol Cell *11*, 1177-1188.

Kishore, K., de Pretis, S., Lister, R., Morelli, M.J., Bianchi, V., Amati, B., Ecker, J.R., and Pelizzola, M. (2015). methylPipe and compEpiTools: a suite of R packages for the integrative analysis of epigenomics data. BMC Bioinformatics *16*, 313.

Kiuchi, N., Nakajima, K., Ichiba, M., Fukada, T., Narimatsu, M., Mizuno, K., Hibi, M., and Hirano, T. (1999). STAT3 is required for the gp130-mediated full activation of the c-myc gene. J Exp Med *189*, 63-73.

Konuma, T., Oguro, H., and Iwama, A. (2010). Role of the polycomb group proteins in hematopoietic stem cells. Dev Growth Differ *52*, 505-516.

Kovalchuk, A.L., Qi, C.F., Torrey, T.A., Taddesse-Heath, L., Feigenbaum, L., Park, S.S., Gerbitz, A., Klobeck, G., Hoertnagel, K., Polack, A.*, et al.* (2000). Burkitt lymphoma in the mouse. J Exp Med *192*, 1183-1190.

Kozak, M. (1989). The scanning model for translation: an update. J Cell Biol *108*, 229-241.

Krausgruber, T., Blazek, K., Smallie, T., Alzabin, S., Lockstone, H., Sahgal, N., Hussell, T., Feldmann, M., and Udalova, I.A. (2011). IRF5 promotes inflammatory macrophage polarization and TH1-TH17 responses. Nat Immunol *12*, 231-238.

Kress, T.R., Pellanda, P., Pellegrinet, L., Bianchi, V., Nicoli, P., Doni, M., Recordati, C., Bianchi, S., Rotta, L., Capra, T.*, et al.* (2016). Identification of MYC-Dependent Transcriptional Programs in Oncogene-Addicted Liver Tumors. Cancer Res *76*, 3463-3472.

Kress, T.R., Sabò, A., and Amati, B. (2015). MYC: connecting selective transcriptional control to global RNA production. Nat Rev Cancer *15*, 593-607.

Kretzner, L., Blackwood, E.M., and Eisenman, R.N. (1992). Myc and Max proteins possess distinct transcriptional activities. Nature *359*, 426-429.

Krop, I., de Fougerolles, A.R., Hardy, R.R., Allison, M., Schlissel, M.S., and Fearon, D.T. (1996). Self-renewal of B-1 lymphocytes is dependent on CD19. Eur J Immunol *26*, 238-242.

Krystal, G., Birrer, M., Way, J., Nau, M., Sausville, E., Thompson, C., Minna, J., and Battey, J. (1988). Multiple mechanisms for transcriptional regulation of the myc gene family in small-cell lung cancer. Mol Cell Biol *8*, 3373-3381.

Kuppers, R., and Dalla-Favera, R. (2001). Mechanisms of chromosomal translocations in B cell lymphomas. Oncogene *20*, 5580-5594.

Kwan, K.Y., Shen, J., and Corey, D.P. (2015). C-MYC transcriptionally amplifies SOX2 target genes to regulate self-renewal in multipotent otic progenitor cells. Stem Cell Reports *4*, 47-60.

Laherty, C.D., Yang, W.M., Sun, J.M., Davie, J.R., Seto, E., and Eisenman, R.N. (1997). Histone deacetylases associated with the mSin3 corepressor mediate mad transcriptional repression. Cell *89*, 349-356.

Langdon, W.Y., Harris, A.W., Cory, S., and Adams, J.M. (1986). The c-myc oncogene perturbs B lymphocyte development in E-mu-myc transgenic mice. Cell *47*, 11-18.

Lee, M.G., Norman, J., Shilatifard, A., and Shiekhattar, R. (2007). Physical and functional association of a trimethyl H3K4 demethylase and Ring6a/MBLR, a polycomb-like protein. Cell *128*, 877-887.

Lee, S.C., Phipson, B., Hyland, C.D., Leong, H.S., Allan, R.S., Lun, A., Hilton, D.J., Nutt, S.L., Blewitt, M.E., Smyth, G.K.*, et al.* (2013). Polycomb repressive complex 2 (PRC2) suppresses Emu-myc lymphoma. Blood *122*, 2654-2663.

Lee, S.H., Singh, I., Tisdale, S., Abdel-Wahab, O., Leslie, C.S., and Mayr, C. (2018). Widespread intronic polyadenylation inactivates tumour suppressor genes in leukaemia. Nature *561*, 127-131.

Lefebure, M., Tothill, R.W., Kruse, E., Hawkins, E.D., Shortt, J., Matthews, G.M., Gregory, G.P., Martin, B.P., Kelly, M.J., Todorovski, I.*, et al.* (2017). Genomic characterisation of Emu-Myc mouse lymphomas identifies Bcor as a Myc co-operative tumour-suppressor gene. Nat Commun *8*, 14581.

Leone, G., Sears, R., Huang, E., Rempel, R., Nuckolls, F., Park, C.H., Giangrande, P., Wu, L., Saavedra, H.I., Field, S.J.*, et al.* (2001). Myc requires distinct E2F activities to induce S phase and apoptosis. Mol Cell *8*, 105-113.

Lessard, J., and Sauvageau, G. (2003). Bmi-1 determines the proliferative capacity of normal and leukaemic stem cells. Nature *423*, 255-260.

Levine, S.S., Weiss, A., Erdjument-Bromage, H., Shao, Z., Tempst, P., and Kingston, R.E. (2002). The core of the polycomb repressive complex is compositionally and functionally conserved in flies and humans. Mol Cell Biol *22*, 6070-6078.

Li, F., Wang, Y., Zeller, K.I., Potter, J.J., Wonsey, D.R., O'Donnell, K.A., Kim, J.W., Yustein, J.T., Lee, L.A., and Dang, C.V. (2005). Myc stimulates nuclearly encoded mitochondrial genes and mitochondrial biogenesis. Mol Cell Biol *25*, 6225-6234.

Li, G., Margueron, R., Ku, M., Chambon, P., Bernstein, B.E., and Reinberg, D. (2010). Jarid2 and PRC2, partners in regulating gene expression. Genes Dev *24*, 368-380.

Liao, B., Hu, Y., and Brewer, G. (2007). Competitive binding of AUF1 and TIAR to MYC mRNA controls its translation. Nat Struct Mol Biol *14*, 511-518.

Liao, Y., Smyth, G.K., and Shi, W. (2014). featureCounts: an efficient general purpose program for assigning sequence reads to genomic features. Bioinformatics *30*, 923-930.

Lin, C.Y., Loven, J., Rahl, P.B., Paranal, R.M., Burge, C.B., Bradner, J.E., Lee, T.I., and Young, R.A. (2012). Transcriptional amplification in tumor cells with elevated c-Myc. Cell *151*, 56-67.

Lin, H., and Grosschedl, R. (1995). Failure of B-cell differentiation in mice lacking the transcription factor EBF. Nature *376*, 263-267.

Lorenzin, F., Benary, U., Baluapuri, A., Walz, S., Jung, L.A., von Eyss, B., Kisker, C., Wolf, J., Eilers, M., and Wolf, E. (2016). Different promoter affinities account for specificity in MYC-dependent gene regulation. Elife *5*.

Love, M.I., Huber, W., and Anders, S. (2014). Moderated estimation of fold change and dispersion for RNA-seq data with DESeq2. Genome Biol *15*, 550.

Luscher, B., and Larsson, L.G. (1999). The basic region/helix-loop-helix/leucine zipper domain of Myc proto-oncoproteins: function and regulation. Oncogene *18*, 2955-2966.

Luscher, B., and Vervoorts, J. (2012). Regulation of gene transcription by the oncoprotein MYC. Gene *494*, 145-160.

Maclean, K.H., Keller, U.B., Rodriguez-Galindo, C., Nilsson, J.A., and Cleveland, J.L. (2003). c-Myc augments gamma irradiation-induced apoptosis by suppressing Bcl-X-L. Molecular and Cellular Biology *23*, 7256-7270.

Maggi, L.B., Jr., Kuchenruether, M., Dadey, D.Y., Schwope, R.M., Grisendi, S., Townsend, R.R., Pandolfi, P.P., and Weber, J.D. (2008). Nucleophosmin serves as a rate-limiting nuclear export chaperone for the Mammalian ribosome. Mol Cell Biol *28*, 7050-7065.

Malynn, B.A., de Alboran, I.M., O'Hagan, R.C., Bronson, R., Davidson, L., DePinho, R.A., and Alt, F.W. (2000). N-myc can functionally replace c-myc in murine development, cellular growth, and differentiation. Genes Dev *14*, 1390-1399.

Mao, D.Y., Watson, J.D., Yan, P.S., Barsyte-Lovejoy, D., Khosravi, F., Wong, W.W., Farnham, P.J., Huang, T.H., and Penn, L.Z. (2003). Analysis of Myc bound loci identified by CpG island arrays shows that Max is essential for Myc-dependent repression. Curr Biol *13*, 882-886.

Margueron, R., Li, G., Sarma, K., Blais, A., Zavadil, J., Woodcock, C.L., Dynlacht, B.D., and Reinberg, D. (2008). Ezh1 and Ezh2 maintain repressive chromatin through different mechanisms. Mol Cell *32*, 503-518.

Margueron, R., and Reinberg, D. (2011). The Polycomb complex PRC2 and its mark in life. Nature *469*, 343-349.

Mathsyaraja, H., Freie, B., Cheng, P.-F., Babaeva, E., Janssens, D., Henikoff, S., and Eisenman, R.N. (2019). *Max* deletion destabilizes MYC protein and abrogates Eμ-*Myc* lymphomagenesis. BioRxiv.

Matsuoka, Y., Fukamachi, K., Uehara, N., Tsuda, H., and Tsubura, A. (2008). Induction of a novel histone deacetylase 1/c-Myc/Mnt/Max complex formation is implicated in parity-induced refractoriness to mammary carcinogenesis. Cancer Sci *99*, 309-315.

Matthias, P., and Rolink, A.G. (2005). Transcriptional networks in developing and mature B cells. Nat Rev Immunol *5*, 497-508.

Mazan-Mamczarz, K., Lal, A., Martindale, J.L., Kawai, T., and Gorospe, M. (2006). Translational repression by RNA-binding protein TIAR. Mol Cell Biol *26*, 2716-2727.

McMahon, S.B., Wood, M.A., and Cole, M.D. (2000). The essential cofactor TRRAP recruits the histone acetyltransferase hGCN5 to c-Myc. Mol Cell Biol *20*, 556-562.

Meroni, G., Reymond, A., Alcalay, M., Borsani, G., Tanigami, A., Tonlorenzi, R., Lo Nigro, C., Messali, S., Zollo, M., Ledbetter, D.H.*, et al.* (1997). Rox, a novel bHLHZip protein expressed in quiescent cells that heterodimerizes with Max, binds a non-canonical E box and acts as a transcriptional repressor. EMBO J *16*, 2892-2906.

Meyer, N., and Penn, L.Z. (2008). Reflecting on 25 years with MYC. Nat Rev Cancer *8*, 976-990.

Min, J., Zhang, Y., and Xu, R.M. (2003). Structural basis for specific binding of Polycomb chromodomain to histone H3 methylated at Lys 27. Genes Dev *17*, 1823-1828.

Mitchell, K.O., Ricci, M.S., Miyashita, T., Dicker, D.T., Jin, Z., Reed, J.C., and El-Deiry, W.S. (2000). Bax is a transcriptional target and mediator of c-myc-induced apoptosis. Cancer Res *60*, 6318-6325.

Muhar, M., Ebert, A., Neumann, T., Umkehrer, C., Jude, J., Wieshofer, C., Rescheneder, P., Lipp, J.J., Herzog, V.A., Reichholf, B.*, et al.* (2018). SLAM-seq defines direct gene-regulatory functions of the BRD4-MYC axis. Science *360*, 800-805.

Murn, J., Mlinaric-Rascan, I., Vaigot, P., Alibert, O., Frouin, V., and Gidrol, X. (2009). A Myc-regulated transcriptional network controls B-cell fate in response to BCR triggering. BMC Genomics *10*, 323.

Nie, Z., Hu, G., Wei, G., Cui, K., Yamane, A., Resch, W., Wang, R., Green, D.R., Tessarollo, L., Casellas, R.*, et al.* (2012). c-Myc is a universal amplifier of expressed genes in lymphocytes and embryonic stem cells. Cell *151*, 68-79.

O'Carroll, D., Erhardt, S., Pagani, M., Barton, S.C., Surani, M.A., and Jenuwein, T. (2001). The polycomb-group gene Ezh2 is required for early mouse development. Mol Cell Biol *21*, 4330-4336.

Oda, E., Ohki, R., Murasawa, H., Nemoto, J., Shibue, T., Yamashita, T., Tokino, T., Taniguchi, T., and Tanaka, N. (2000). Nora, a BH3-only member of the Bcl-2 family and candidate mediator of p53-induced apoptosis. Science *288*, 1053-1058.

Ogawa, H., Ishiguro, K., Gaubatz, S., Livingston, D.M., and Nakatani, Y. (2002). A complex with chromatin modifiers that occupies E2F- and Myc-responsive genes in G0 cells. Science *296*, 1132-1136.

Osawa, M., Hanada, K., Hamada, H., and Nakauchi, H. (1996). Long-term lymphohematopoietic reconstitution by a single CD34-low/negative hematopoietic stem cell. Science *273*, 242-245.

Oster, S.K., Ho, C.S., Soucie, E.L., and Penn, L.Z. (2002). The myc oncogene: MarvelouslY Complex. Adv Cancer Res *84*, 81-154.

Pal, S., Yun, R., Datta, A., Lacomis, L., Erdjument-Bromage, H., Kumar, J., Tempst, P., and Sif, S. (2003). mSin3A/histone deacetylase 2- and PRMT5-containing Brg1 complex is involved in transcriptional repression of the Myc target gene cad. Mol Cell Biol *23*, 7475-7487.

Palomero, T., Lim, W.K., Odom, D.T., Sulis, M.L., Real, P.J., Margolin, A., Barnes, K.C., O'Neil, J., Neuberg, D., Weng, A.P.*, et al.* (2006). NOTCH1 directly regulates c-MYC and activates a feed-forward-loop transcriptional network promoting leukemic cell growth. Proc Natl Acad Sci U S A *103*, 18261-18266.

Park, J., Wood, M.A., and Cole, M.D. (2002). BAF53 forms distinct nuclear complexes and functions as a critical c-Myc-interacting nuclear cofactor for oncogenic transformation. Mol Cell Biol *22*, 1307-1316.

Park, S., Chung, S., Kim, K.M., Jung, K.C., Park, C., Hahm, E.R., and Yang, C.H. (2004). Determination of binding constant of transcription factor myc-max/max-max and E-box DNA: the effect of inhibitors on the binding. Biochim Biophys Acta *1670*, 217-228.

Pasini, D., Bracken, A.P., Jensen, M.R., Lazzerini Denchi, E., and Helin, K. (2004). Suz12 is essential for mouse development and for EZH2 histone methyltransferase activity. EMBO J *23*, 4061-4071.

Pasini, D., Cloos, P.A., Walfridsson, J., Olsson, L., Bukowski, J.P., Johansen, J.V., Bak, M., Tommerup, N., Rappsilber, J., and Helin, K. (2010). JARID2 regulates binding of the Polycomb repressive complex 2 to target genes in ES cells. Nature *464*, 306-310.

Pasqualucci, L., and Dalla-Favera, R. (2018). Genetics of diffuse large B-cell lymphoma. Blood *131*, 2307-2319.

Pasqualucci, L., Khiabanian, H., Fangazio, M., Vasishtha, M., Messina, M., Holmes, A.B., Ouillette, P., Trifonov, V., Rossi, D., Tabbo, F.*, et al.* (2014). Genetics of follicular lymphoma transformation. Cell Rep *6*, 130-140.

Paulin, F.E., Chappell, S.A., and Willis, A.E. (1998). A single nucleotide change in the c-myc internal ribosome entry segment leads to enhanced binding of a group of protein factors. Nucleic Acids Res *26*, 3097-3103.

Pelossof, R., Fairchild, L., Huang, C.H., Widmer, C., Sreedharan, V.T., Sinha, N., Lai, D.Y., Guan, Y., Premsrirut, P.K., Tschaharganeh, D.F.*, et al.* (2017). Prediction of potent shRNAs with a sequential classification algorithm. Nat Biotechnol *35*, 350-353.

Perez-Olivares, M., Trento, A., Rodriguez-Acebes, S., Gonzalez-Acosta, D., Fernandez-Antoran, D., Roman-Garcia, S., Martinez, D., Lopez-Briones, T., Torroja, C., Carrasco, Y.R.*, et al.* (2018). Functional interplay between c-Myc and Max in B lymphocyte differentiation. EMBO Rep *19*.

Perez-Roger, I., Kim, S.H., Griffiths, B., Sewing, A., and Land, H. (1999). Cyclins D1 and D2 mediate myc-induced proliferation via sequestration of p27(Kip1) and p21(Cip1). EMBO J *18*, 5310-5320.

Perna, D., Faga, G., Verrecchia, A., Gorski, M.M., Barozzi, I., Narang, V., Khng, J., Lim, K.C., Sung, W.K., Sanges, R.*, et al.* (2012). Genome-wide mapping of Myc binding and gene regulation in serum-stimulated fibroblasts. Oncogene *31*, 1695-1709.

Pillai, S., Cariappa, A., and Moran, S.T. (2004). Positive selection and lineage commitment during peripheral B-lymphocyte development. Immunol Rev *197*, 206-218.

Poortinga, G., Hannan, K.M., Snelling, H., Walkley, C.R., Jenkins, A., Sharkey, K., Wall, M., Brandenburger, Y., Palatsides, M., Pearson, R.B.*, et al.* (2004). MAD1 and c-MYC regulate UBF and rDNA transcription during granulocyte differentiation. EMBO J *23*, 3325-3335.

Popov, N., Schulein, C., Jaenicke, L.A., and Eilers, M. (2010). Ubiquitylation of the amino terminus of Myc by SCF(beta-TrCP) antagonizes SCF(Fbw7)-mediated turnover. Nat Cell Biol *12*, 973-981.

Popov, N., Wahlstrom, T., Hurlin, P.J., and Henriksson, M. (2005). Mnt transcriptional repressor is functionally regulated during cell cycle progression. Oncogene *24*, 8326-8337.

Prendergast, G.C., Lawe, D., and Ziff, E.B. (1991). Association of Myn, the murine homolog of max, with c-Myc stimulates methylation-sensitive DNA binding and ras cotransformation. Cell *65*, 395-407.

Pulverer, B.J., Fisher, C., Vousden, K., Littlewood, T., Evan, G., and Woodgett, J.R. (1994). Site-specific modulation of c-Myc cotransformation by residues phosphorylated in vivo. Oncogene *9*, 59-70.

Qin, J., Whyte, W.A., Anderssen, E., Apostolou, E., Chen, H.H., Akbarian, S., Bronson, R.T., Hochedlinger, K., Ramaswamy, S., Young, R.A.*, et al.* (2012). The polycomb group protein L3mbtl2 assembles an atypical PRC1-family complex that is essential in pluripotent stem cells and early development. Cell Stem Cell *11*, 319-332.

Queva, C., McArthur, G.A., Iritani, B.M., and Eisenman, R.N. (2001). Targeted deletion of the S-phase-specific Myc antagonist Mad3 sensitizes neuronal and lymphoid cells to radiation-induced apoptosis. Mol Cell Biol *21*, 703-712.

Rabellino, A., Melegari, M., Tompkins, V.S., Chen, W., Van Ness, B.G., Teruya-Feldstein, J., Conacci-Sorrell, M., Janz, S., and Scaglioni, P.P. (2016). PIAS1 Promotes Lymphomagenesis through MYC Upregulation. Cell Rep *15*, 2266-2278.

Rahl, P.B., Lin, C.Y., Seila, A.C., Flynn, R.A., McCuine, S., Burge, C.B., Sharp, P.A., and Young, R.A. (2010). c-Myc regulates transcriptional pause release. Cell *141*, 432-445.

Rahl, P.B., and Young, R.A. (2014). MYC and transcription elongation. Cold Spring Harb Perspect Med *4*, a020990.

Rajewsky, K. (1996). Clonal selection and learning in the antibody system. Nature *381*, 751-758.

Reddy, C.D., Dasgupta, P., Saikumar, P., Dudek, H., Rauscher, F.J., 3rd, and Reddy, E.P. (1992). Mutational analysis of Max: role of basic, helix-loop-helix/leucine zipper domains in DNA binding, dimerization and regulation of Myc-mediated transcriptional activation. Oncogene *7*, 2085-2092.

Rickert, R.C., Roes, J., and Rajewsky, K. (1997). B lymphocyte-specific, Cre-mediated mutagenesis in mice. Nucleic Acids Res *25*, 1317-1318.

Romero, O.A., Torres-Diz, M., Pros, E., Savola, S., Gomez, A., Moran, S., Saez, C., Iwakawa, R., Villanueva, A., Montuenga, L.M.*, et al.* (2014). MAX inactivation in small cell lung cancer disrupts MYC-SWI/SNF programs and is synthetic lethal with BRG1. Cancer Discov *4*, 292-303.

Roussel, M., Saule, S., Lagrou, C., Rommens, C., Beug, H., Graf, T., and Stehelin, D. (1979). Three new types of viral oncogene of cellular origin specific for haematopoietic cell transformation. Nature *281*, 452-455.

Sabò, A., and Amati, B. (2014). Genome recognition by MYC. Cold Spring Harb Perspect Med *4*.

Sabo, A., Doni, M., and Amati, B. (2014). SUMOylation of Myc-family proteins. PLoS One *9*, e91072.

Sabò, A., Doni, M., and Amati, B. (2014a). SUMOylation of Myc-family proteins. PLoS One *9*, e91072.

Sabò, A., Kress, T.R., Pelizzola, M., de Pretis, S., Gorski, M.M., Tesi, A., Morelli, M.J., Bora, P., Doni, M., Verrecchia, A.*, et al.* (2014b). Selective transcriptional regulation by Myc in cellular growth control and lymphomagenesis. Nature *511*, 488-492.

Sanchez-Pulido, L., Devos, D., Sung, Z.R., and Calonje, M. (2008). RAWUL: a new ubiquitin-like domain in PRC1 ring finger proteins that unveils putative plant and worm PRC1 orthologs. BMC Genomics *9*, 308.

Sander, S., Calado, D.P., Srinivasan, L., Kochert, K., Zhang, B., Rosolowski, M., Rodig, S.J., Holzmann, K., Stilgenbauer, S., Siebert, R.*, et al.* (2012). Synergy between PI3K signaling and MYC in Burkitt lymphomagenesis. Cancer Cell *22*, 167-179.

Sansom, O.J., Meniel, V.S., Muncan, V., Phesse, T.J., Wilkins, J.A., Reed, K.R., Vass, J.K., Athineos, D., Clevers, H., and Clarke, A.R. (2007). Myc deletion rescues Apc deficiency in the small intestine. Nature *446*, 676-679.

Sarma, K., Margueron, R., Ivanov, A., Pirrotta, V., and Reinberg, D. (2008). Ezh2 requires PHF1 to efficiently catalyze H3 lysine 27 trimethylation in vivo. Mol Cell Biol *28*, 2718-2731.

Sauvageau, M., and Sauvageau, G. (2010). Polycomb group proteins: multi-faceted regulators of somatic stem cells and cancer. Cell Stem Cell *7*, 299-313.

Scelfo, A., Fernandez-Perez, D., Tamburri, S., Zanotti, M., Lavarone, E., Soldi, M., Bonaldi, T., Ferrari, K.J., and Pasini, D. (2019). Functional Landscape of PCGF Proteins Reveals Both RING1A/B-Dependent-and RING1A/B-Independent-Specific Activities. Mol Cell.

Scelfo, A., Piunti, A., and Pasini, D. (2015). The controversial role of the Polycomb group proteins in transcription and cancer: how much do we not understand Polycomb proteins? FEBS J *282*, 1703-1722.

Schlosser, I., Holzel, M., Murnseer, M., Burtscher, H., Weidle, U.H., and Eick, D. (2003). A role for c-Myc in the regulation of ribosomal RNA processing. Nucleic Acids Res *31*, 6148-6156.

Schmitt, C.A., McCurrach, M.E., de Stanchina, E., Wallace-Brodeur, R.R., and Lowe, S.W. (1999). INK4a/ARF mutations accelerate lymphomagenesis and promote chemoresistance by disabling p53. Genes Dev *13*, 2670-2677.

Schoeftner, S., Sengupta, A.K., Kubicek, S., Mechtler, K., Spahn, L., Koseki, H., Jenuwein, T., and Wutz, A. (2006). Recruitment of PRC1 function at the initiation of X inactivation independent of PRC2 and silencing. EMBO J *25*, 3110-3122.

Schreiber-Agus, N., Chin, L., Chen, K., Torres, R., Rao, G., Guida, P., Skoultchi, A.I., and DePinho, R.A. (1995). An amino-terminal domain of Mxi1 mediates anti-Myc oncogenic activity and interacts with a homolog of the yeast transcriptional repressor SIN3. Cell *80*, 777-786.

Schreiber-Agus, N., Meng, Y., Hoang, T., Hou, H., Jr., Chen, K., Greenberg, R., Cordon-Cardo, C., Lee, H.W., and DePinho, R.A. (1998). Role of Mxi1 in ageing organ systems and the regulation of normal and neoplastic growth. Nature *393*, 483-487.

Sears, R., Nuckolls, F., Haura, E., Taya, Y., Tamai, K., and Nevins, J.R. (2000). Multiple Ras-dependent phosphorylation pathways regulate Myc protein stability. Genes Dev *14*, 2501-2514.

Secombe, J., and Eisenman, R.N. (2007). The function and regulation of the JARID1 family of histone H3 lysine 4 demethylases: the Myc connection. Cell Cycle *6*, 1324-1328.

Seoane, J., Pouponnot, C., Staller, P., Schader, M., Eilers, M., and Massague, J. (2001). TGFbeta influences Myc, Miz-1 and Smad to control the CDK inhibitor p15INK4b. Nat Cell Biol *3*, 400-408.

Shachaf, C.M., Kopelman, A.M., Arvanitis, C., Karlsson, A., Beer, S., Mandl, S., Bachmann, M.H., Borowsky, A.D., Ruebner, B., Cardiff, R.D*., et al.* (2004). MYC inactivation uncovers pluripotent differentiation and tumour dormancy in hepatocellular cancer. Nature *431*, 1112-1117.

Shao, Z., Raible, F., Mollaaghababa, R., Guyon, J.R., Wu, C.T., Bender, W., and Kingston, R.E. (1999). Stabilization of chromatin structure by PRC1, a Polycomb complex. Cell *98*, 37-46.

Sharma, V.M., Calvo, J.A., Draheim, K.M., Cunningham, L.A., Hermance, N., Beverly, L., Krishnamoorthy, V., Bhasin, M., Capobianco, A.J., and Kelliher, M.A. (2006). Notch1 contributes to mouse T-cell leukemia by directly inducing the expression of c-myc. Mol Cell Biol *26*, 8022-8031.

Shen, X., Liu, Y., Hsu, Y.J., Fujiwara, Y., Kim, J., Mao, X., Yuan, G.C., and Orkin, S.H. (2008). EZH1 mediates methylation on histone H3 lysine 27 and complements EZH2 in maintaining stem cell identity and executing pluripotency. Mol Cell *32*, 491-502.

Shiue, C.N., Berkson, R.G., and Wright, A.P. (2009). c-Myc induces changes in higher order rDNA structure on stimulation of quiescent cells. Oncogene *28*, 1833-1842.

Shou, Y., Martelli, M.L., Gabrea, A., Qi, Y., Brents, L.A., Roschke, A., Dewald, G., Kirsch, I.R., Bergsagel, P.L., and Kuehl, W.M. (2000). Diverse karyotypic abnormalities of the c-myc locus associated with c-myc dysregulation and tumor progression in multiple myeloma. Proc Natl Acad Sci U S A *97*, 228-233.

Simon, J.A., and Kingston, R.E. (2009). Mechanisms of polycomb gene silencing: knowns and unknowns. Nat Rev Mol Cell Biol *10*, 697-708.

Smith, M.J., Charron-Prochownik, D.C., and Prochownik, E.V. (1990). The leucine zipper of c-Myc is required for full inhibition of erythroleukemia differentiation. Mol Cell Biol *10*, 5333-5339.

Song, H., and Cerny, J. (2003). Functional heterogeneity of marginal zone B cells revealed by their ability to generate both early antibody-forming cells and germinal centers with hypermutation and memory in response to a T-dependent antigen. J Exp Med *198*, 1923-1935.

Soucek, L., Whitfield, J.R., Sodir, N.M., Masso-Valles, D., Serrano, E., Karnezis, A.N., Swigart, L.B., and Evan, G.I. (2013). Inhibition of Myc family proteins eradicates KRas-driven lung cancer in mice. Genes Dev *27*, 504-513.

Staller, P., Peukert, K., Kiermaier, A., Seoane, J., Lukas, J., Karsunky, H., Moroy, T., Bartek, J., Massague, J., Hanel, F*., et al.* (2001). Repression of p15INK4b expression by Myc through association with Miz-1. Nat Cell Biol *3*, 392-399.

Stanton, B.R., Perkins, A.S., Tessarollo, L., Sassoon, D.A., and Parada, L.F. (1992). Loss of N-myc function results in embryonic lethality and failure of the epithelial component of the embryo to develop. Genes Dev *6*, 2235-2247.

Stielow, B., Finkernagel, F., Stiewe, T., Nist, A., and Suske, G. (2018). MGA, L3MBTL2 and E2F6 determine genomic binding of the non-canonical Polycomb repressive complex PRC1.6. PLoS Genet *14*, e1007193.

Stoneley, M., Paulin, F.E., Le Quesne, J.P., Chappell, S.A., and Willis, A.E. (1998). C-Myc 5' untranslated region contains an internal ribosome entry segment. Oncogene *16*, 423-428.

Su, I.H., Basavaraj, A., Krutchinsky, A.N., Hobert, O., Ullrich, A., Chait, B.T., and Tarakhovsky, A. (2003). Ezh2 controls B cell development through histone H3 methylation and Igh rearrangement. Nat Immunol *4*, 124-131.

Su, I.H., Dobenecker, M.W., Dickinson, E., Oser, M., Basavaraj, A., Marqueron, R., Viale, A., Reinberg, D., Wulfing, C., and Tarakhovsky, A. (2005). Polycomb group protein ezh2 controls actin polymerization and cell signaling. Cell *121*, 425-436.

Su, W., Han, H.H., Wang, Y., Zhang, B., Zhou, B., Cheng, Y., Rumandla, A., Gurrapu, S., Chakraborty, G., Su, J.*, et al.* (2019). The Polycomb Repressor Complex 1 Drives Double-Negative Prostate Cancer Metastasis by Coordinating Stemness and Immune Suppression. Cancer Cell *36*, 139-155 e110.

Su, Y., Pelz, C., Huang, T., Torkenczy, K., Wang, X., Cherry, A., Daniel, C.J., Liang, J., Nan, X., Dai, M.S.*, et al.* (2018). Post-translational modification localizes MYC to the nuclear pore basket to regulate a subset of target genes involved in cellular responses to environmental signals. Genes Dev *32*, 1398-1419.

Subramanian, A., Tamayo, P., Mootha, V.K., Mukherjee, S., Ebert, B.L., Gillette, M.A., Paulovich, A., Pomeroy, S.L., Golub, T.R., Lander, E.S.*, et al.* (2005). Gene set enrichment analysis: a knowledge-based approach for interpreting genome-wide expression profiles. Proc Natl Acad Sci U S A *102*, 15545-15550.

Sun, J., Wang, J., He, L., Lin, Y., and Wu, J. (2015). Knockdown of polycomb-group RING finger 6 modulates mouse male germ cell differentiation in vitro. Cell Physiol Biochem *35*, 339-352.

Sun, Y., Tseng, W.C., Fan, X., Ball, R., and Dougan, S.T. (2014). Extraembryonic signals under the control of MGA, Max, and Smad4 are required for dorsoventral patterning. Dev Cell *28*, 322-334.

Suzuki, A., Hirasaki, M., Hishida, T., Wu, J., Okamura, D., Ueda, A., Nishimoto, M., Nakachi, Y., Mizuno, Y., Okazaki, Y.*, et al.* (2016). Loss of MAX results in meiotic entry in mouse embryonic and germline stem cells. Nat Commun *7*, 11056.

Takaoka, A., Yanai, H., Kondo, S., Duncan, G., Negishi, H., Mizutani, T., Kano, S., Honda, K., Ohba, Y., Mak, T.W.*, et al.* (2005). Integral role of IRF-5 in the gene induction programme activated by Toll-like receptors. Nature *434*, 243-249.

Takayama, M., Taira, T., Iguchi-Ariga, S.M., and Ariga, H. (2000a). CDC6 interacts with c-Myc to inhibit E-box-dependent transcription by abrogating c-Myc/Max complex. FEBS Lett *477*, 43-48.

Takayama, M.A., Taira, T., Tamai, K., Iguchi-Ariga, S.M., and Ariga, H. (2000b). ORC1 interacts with c-Myc to inhibit E-box-dependent transcription by abrogating c-Myc-SNF5/INI1 interaction. Genes Cells *5*, 481-490.

Tansey, W.P. (2014). Mammalian MYC proteins in cancer. Hindawi Publishing Corporation New Journal of Science *2014*, 27.

Tesi, A., de Pretis, S., Furlan, M., Filipuzzi, M., Morelli, M.J., Andronache, A., Doni, M., Verrecchia, A., Pelizzola, M., Amati, B.*, et al.* (2019). An early Myc-dependent transcriptional program orchestrates cell growth during B-cell activation. EMBO Rep, e47987.

Thomas, L.R., Foshage, A.M., Weissmiller, A.M., and Tansey, W.P. (2015a). The MYC-WDR5 Nexus and Cancer. Cancer Res *75*, 4012-4015.

Thomas, L.R., and Tansey, W.P. (2011). Proteolytic control of the oncoprotein transcription factor Myc. Adv Cancer Res *110*, 77-106.

Thomas, L.R., Wang, Q., Grieb, B.C., Phan, J., Foshage, A.M., Sun, Q., Olejniczak, E.T., Clark, T., Dey, S., Lorey, S.*, et al.* (2015b). Interaction with WDR5 promotes target gene recognition and tumorigenesis by MYC. Mol Cell *58*, 440-452.

Toyo-oka, K., Hirotsune, S., Gambello, M.J., Zhou, Z.Q., Olson, L., Rosenfeld, M.G., Eisenman, R., Hurlin, P., and Wynshaw-Boris, A. (2004). Loss of the Max-interacting protein Mnt in mice results in decreased viability, defective embryonic growth and craniofacial defects: relevance to Miller-Dieker syndrome. Hum Mol Genet *13*, 1057-1067.

Trimarchi, J.M., Fairchild, B., Verona, R., Moberg, K., Andon, N., and Lees, J.A. (1998). E2F-6, a member of the E2F family that can behave as a transcriptional repressor. Proc Natl Acad Sci U S A *95*, 2850-2855.

Trojer, P., Cao, A.R., Gao, Z., Li, Y., Zhang, J., Xu, X., Li, G., Losson, R., Erdjument-Bromage, H., Tempst, P.*, et al.* (2011). L3MBTL2 protein acts in concert with PcG protein-mediated monoubiquitination of H2A to establish a repressive chromatin structure. Mol Cell *42*, 438-450.

Trojer, P., and Reinberg, D. (2008). Beyond histone methyl-lysine binding: how malignant brain tumor (MBT) protein L3MBTL1 impacts chromatin structure. Cell Cycle *7*, 578-585.

Trumpp, A., Refaeli, Y., Oskarsson, T., Gasser, S., Murphy, M., Martin, G.R., and Bishop, J.M. (2001). c-Myc regulates mammalian body size by controlling cell number but not cell size. Nature *414*, 768-773.

Vallespinos, M., Fernandez, D., Rodriguez, L., Alvaro-Blanco, J., Baena, E., Ortiz, M., Dukovska, D., Martinez, D., Rojas, A., Campanero, M.R.*, et al.* (2011). B Lymphocyte commitment program is driven by the proto-oncogene c-Myc. J Immunol *186*, 6726-6736.

Valovka, T., Schonfeld, M., Raffeiner, P., Breuker, K., Dunzendorfer-Matt, T., Hartl, M., and Bister, K. (2013). Transcriptional control of DNA replication licensing by Myc. Sci Rep-Uk *3*.

Vennstrom, B., Sheiness, D., Zabielski, J., and Bishop, J.M. (1982). Isolation and characterization of c-myc, a cellular homolog of the oncogene (v-myc) of avian myelocytomatosis virus strain 29. J Virol *42*, 773-779.

Vervoorts, J., Luscher-Firzlaff, J., and Luscher, B. (2006). The ins and outs of MYC regulation by posttranslational mechanisms. J Biol Chem *281*, 34725-34729.

Vervoorts, J., Luscher-Firzlaff, J.M., Rottmann, S., Lilischkis, R., Walsemann, G., Dohmann, K., Austen, M., and Luscher, B. (2003). Stimulation of c-MYC transcriptional activity and acetylation by recruitment of the cofactor CBP. EMBO Rep *4*, 484-490.

Vidal, M., and Starowicz, K. (2017). Polycomb complexes PRC1 and their function in hematopoiesis. Exp Hematol *48*, 12-31.

Vlach, J., Hennecke, S., Alevizopoulos, K., Conti, D., and Amati, B. (1996). Growth arrest by the cyclin-dependent kinase inhibitor p27Kip1 is abrogated by c-Myc. EMBO J *15*, 6595-6604.

Voncken, J.W., Roelen, B.A., Roefs, M., de Vries, S., Verhoeven, E., Marino, S., Deschamps, J., and van Lohuizen, M. (2003). Rnf2 (Ring1b) deficiency causes gastrulation arrest and cell cycle inhibition. Proc Natl Acad Sci U S A *100*, 2468-2473.

Walz, S., Lorenzin, F., Morton, J., Wiese, K.E., von Eyss, B., Herold, S., Rycak, L., Dumay-Odelot, H., Karim, S., Bartkuhn, M.*, et al.* (2014). Activation and repression by oncogenic MYC shape tumour-specific gene expression profiles. Nature *511*, 483-487.

Wang, L., Brown, J.L., Cao, R., Zhang, Y., Kassis, J.A., and Jones, R.S. (2004). Hierarchical recruitment of polycomb group silencing complexes. Mol Cell *14*, 637-646.

Wang, R., Dillon, C.P., Shi, L.Z., Milasta, S., Carter, R., Finkelstein, D., McCormick, L.L., Fitzgerald, P., Chi, H., Munger, J.*, et al.* (2011). The transcription factor Myc controls metabolic reprogramming upon T lymphocyte activation. Immunity *35*, 871-882.

Wang, W.K., Tereshko, V., Boccuni, P., MacGrogan, D., Nimer, S.D., and Patel, D.J. (2003). Malignant brain tumor repeats: a three-leaved propeller architecture with ligand/peptide binding pockets. Structure *11*, 775-789.

Washkowitz, A.J., Schall, C., Zhang, K., Wurst, W., Floss, T., Mager, J., and Papaioannou, V.E. (2015). Mga is essential for the survival of pluripotent cells during peri-implantation development. Development *142*, 31-40.

Weber, J.D., Taylor, L.J., Roussel, M.F., Sherr, C.J., and Bar-Sagi, D. (1999). Nucleolar Arf sequesters Mdm2 and activates p53. Nat Cell Biol *1*, 20-26.

Welcker, M., Orian, A., Grim, J.E., Eisenman, R.N., and Clurman, B.E. (2004). A nucleolar isoform of the Fbw7 ubiquitin ligase regulates c-Myc and cell size. Curr Biol *14*, 1852-1857.

Welm, A.L., Kim, S., Welm, B.E., and Bishop, J.M. (2005). MET and MYC cooperate in mammary tumorigenesis. Proc Natl Acad Sci U S A *102*, 4324-4329.

Weng, A.P., Millholland, J.M., Yashiro-Ohtani, Y., Arcangeli, M.L., Lau, A., Wai, C., Del Bianco, C., Rodriguez, C.G., Sai, H., Tobias, J.*, et al.* (2006). c-Myc is an important direct target of Notch1 in T-cell acute lymphoblastic leukemia/lymphoma. Genes Dev *20*, 2096-2109.

West, M.J., Sullivan, N.F., and Willis, A.E. (1995). Translational upregulation of the c-myc oncogene in Bloom's syndrome cell lines. Oncogene *11*, 2515-2524.

Wu, C.H., Sahoo, D., Arvanitis, C., Bradon, N., Dill, D.L., and Felsher, D.W. (2008). Combined analysis of murine and human microarrays and ChIP analysis reveals genes associated with the ability of MYC to maintain tumorigenesis. PLoS Genet *4*, e1000090.

Xie, H., Xu, J., Hsu, J.H., Nguyen, M., Fujiwara, Y., Peng, C., and Orkin, S.H. (2014). Polycomb repressive complex 2 regulates normal hematopoietic stem cell function in a developmental-stage-specific manner. Cell Stem Cell *14*, 68-80.

Xu, L., Morgenbesser, S.D., and DePinho, R.A. (1991). Complex transcriptional regulation of myc family gene expression in the developing mouse brain and liver. Mol Cell Biol *11*, 6007-6015.

Xu, Y., Poggio, M., Jin, H.Y., Shi, Z., Forester, C.M., Wang, Y., Stumpf, C.R., Xue, L., Devericks, E., So, L.*, et al.* (2019). Translation control of the immune checkpoint in cancer and its therapeutic targeting. Nat Med *25*, 301-311.

Yada, M., Hatakeyama, S., Kamura, T., Nishiyama, M., Tsunematsu, R., Imaki, H., Ishida, N., Okumura, F., Nakayama, K., and Nakayama, K.I. (2004). Phosphorylation-dependent degradation of c-Myc is mediated by the F-box protein Fbw7. EMBO J *23*, 2116-2125.

Yang, C.S., Chang, K.Y., Dang, J., and Rana, T.M. (2016). Polycomb Group Protein Pcgf6 Acts as a Master Regulator to Maintain Embryonic Stem Cell Identity. Sci Rep *6*, 26899.

Yeh, E., Cunningham, M., Arnold, H., Chasse, D., Monteith, T., Ivaldi, G., Hahn, W.C., Stukenberg, P.T., Shenolikar, S., Uchida, T.*, et al.* (2004). A signalling pathway controlling c-Myc degradation that impacts oncogenic transformation of human cells. Nature Cell Biology *6*, 308-318.

Yoon, S.I., Logsdon, N.J., Sheikh, F., Donnelly, R.P., and Walter, M.R. (2006). Conformational changes mediate interleukin-10 receptor 2 (IL-10R2) binding to IL-10 and assembly of the signaling complex. J Biol Chem *281*, 35088-35096.

Yu, Q., Ciemerych, M.A., and Sicinski, P. (2005). Ras and Myc can drive oncogenic cell proliferation through individual D-cyclins. Oncogene *24*, 7114-7119.

Zdzieblo, D., Li, X., Lin, Q., Zenke, M., Illich, D.J., Becker, M., and Muller, A.M. (2014). Pcgf6, a polycomb group protein, regulates mesodermal lineage differentiation in murine ESCs and functions in iPS reprogramming. Stem Cells *32*, 3112-3125.

Zeller, K.I., Haggerty, T.J., Barrett, J.F., Guo, Q., Wonsey, D.R., and Dang, C.V. (2001). Characterization of nucleophosmin (B23) as a Myc target by scanning chromatin immunoprecipitation. J Biol Chem *276*, 48285-48291.

Zeller, K.I., Zhao, X., Lee, C.W., Chiu, K.P., Yao, F., Yustein, J.T., Ooi, H.S., Orlov, Y.L., Shahab, A., Yong, H.C.*, et al.* (2006). Global mapping of c-Myc binding sites and target gene networks in human B cells. Proc Natl Acad Sci U S A *103*, 17834-17839.

Zervos, A.S., Gyuris, J., and Brent, R. (1993). Mxi1, a protein that specifically interacts with Max to bind Myc-Max recognition sites. Cell *72*, 223-232.

Zhang, H., Gao, P., Fukuda, R., Kumar, G., Krishnamachary, B., Zeller, K.I., Dang, C.V., and Semenza, G.L. (2007). HIF-1 inhibits mitochondrial biogenesis and cellular respiration in VHL-deficient renal cell carcinoma by repression of C-MYC activity. Cancer Cell *11*, 407-420.

Zhang, Y., Iratni, R., Erdjument-Bromage, H., Tempst, P., and Reinberg, D. (1997). Histone deacetylases and SAP18, a novel polypeptide, are components of a human Sin3 complex. Cell *89*, 357-364.

Zhang, Y., Liu, T., Meyer, C.A., Eeckhoute, J., Johnson, D.S., Bernstein, B.E., Nusbaum, C., Myers, R.M., Brown, M., Li, W.*, et al.* (2008). Model-based analysis of ChIP-Seq (MACS). Genome Biol *9*, R137.

Zhang, Z., Jones, A., Sun, C.W., Li, C., Chang, C.W., Joo, H.Y., Dai, Q., Mysliwiec, M.R., Wu, L.C., Guo, Y.*, et al.* (2011). PRC2 complexes with JARID2, MTF2, and esPRC2p48 in ES cells to modulate ES cell pluripotency and somatic cell reprogramming. Stem Cells *29*, 229-240.

Zhao, W., Tong, H., Huang, Y., Yan, Y., Teng, H., Xia, Y., Jiang, Q., and Qin, J. (2017). Essential Role for Polycomb Group Protein Pcgf6 in Embryonic Stem Cell Maintenance and a Noncanonical Polycomb Repressive Complex 1 (PRC1) Integrity. J Biol Chem *292*, 2773-2784.

Zhou, L.J., Ord, D.C., Omori, S.A., and Tedder, T.F. (1992). Structure of the genes encoding the CD19 antigen of human and mouse B lymphocytes. Immunogenetics *35*, 102-111.

Zhou, V.W., Goren, A., and Bernstein, B.E. (2011). Charting histone modifications and the functional organization of mammalian genomes. Nat Rev Genet *12*, 7-18.

Zimmerman, K.A., Yancopoulos, G.D., Collum, R.G., Smith, R.K., Kohl, N.E., Denis, K.A., Nau, M.M., Witte, O.N., Toran-Allerand, D., Gee, C.E*., et al.* (1986). Differential expression of myc family genes during murine development. Nature *319*, 780-783.

Zindy, F., Eischen, C.M., Randle, D.H., Kamijo, T., Cleveland, J.L., Sherr, C.J., and Roussel, M.F. (1998). Myc signaling via the ARF tumor suppressor regulates p53-dependent apoptosis and immortalization. Genes Dev *12*, 2424-2433.

ACKNOWLEDGMENTS

I would like to thank to my supervisor, Dr. Bruno Amati, for giving me the opportunity to work in his laboratory on this exciting project, for the scientific discussions and for his supervision through my PhD years.

I would like to give thanks also to my added supervisor, Dr. Andrea Bisso, for his close supervision throughout these four years, and for his continuous effort to pass on his knowledge selflessly.

I would also like to thank to my internal and external advisors, Dr. Gioaccino Natoli and Dr. Kristian Helin, for their constructive comments and suggestions that contributed to my thesis work.

To all the friends that supported me during my PhD, both inside and outside of the lab, especially to Giorgia Ceccotti for being by my side always, even if I was wrong.

To my sister Olga, for surviving me during all my breakdowns and throughout life in general.

My parents for always being there for me. Your love and support mean the world to me.

To Mirko, for always being there for me.